SynaptoTagMe: A Toolkit for *In Vivo* Mapping and Modulating Neurotransmission at Single-Cell Resolution

Authors: Andrea Cuentas-Condori[1], Patricia Chanabá-López[1], Matthew Thomas[1], Likui Feng[2], Aaron Wolfe[1], Peter Agoba[1], Matthew L. Schwartz[3], Maximillian Brown[2], Margaret Ebert[2,4], Erik Jorgensen[3], Cornelia I. Bargmann[2], Daniel Colón-Ramos[1, 5, 6 *]

Affiliations:

[1] Department of Neuroscience and Department of Cell Biology, Yale University School of Medicine; New Haven, CT 06536, USA.

[2] Lulu and Anthony Wang Laboratory of Neural Circuits and Behavior, The Rockefeller University. New York, NY 10065, USA.

[3] Howard Hughes Medical Institute and School of Biological Sciences, University of Utah, Salt Lake City, UT 84112, USA.

[4] Current address: Omenn-Darling Bioengineering Institute, Princeton University, Princeton, NJ 08540, USA.

[5] Wu Tsai Institute, Yale University; New Haven, CT 06510, USA.

[6] Instituto de Neurobiología, Recinto de Ciencias Médicas, Universidad de Puerto Rico, San Juan 00901, Puerto Rico.

*Corresponding author and Lead Contact. Email: daniel.colon-ramos@yale.edu

ABSTRACT

Understanding the organization and regulation of neurotransmission at the level of individual neurons and synapses requires tools that can track and manipulate transmitter-specific vesicles *in vivo*. Here, we present SynaptoTagMe, a suite of genetic tools in *Caenorhabditis elegans* to fluorescently label and conditionally ablate the vesicular transporters for glutamate, GABA, acetylcholine, and monoamines. Using a structure-guided approach informed by protein topology and evolutionary conservation, we engineered endogenously tagged versions for each transporter that maintain their physiological function while allowing for cell-specific, bright, and stable visualization. We also developed conditional knockout strains that enable targeted disruption of neurotransmitter synthesis or packaging in single neurons. We applied this toolkit to map co-expression of vesicular transporters across the *C. elegans* nervous system, revealing that over 10% of neurons exhibit co-transmission. Using the ADF sensory neuron as a case study, we demonstrate that serotonin and acetylcholine are trafficked in partially distinct vesicle pools. Our approach provides a powerful platform for mapping, monitoring, and manipulating neurotransmitter identity and use *in vivo*. The molecular strategies described here are likely applicable across species, offering a generalizable approach to dissect synaptic communication *in vivo*.

INTRODUCTION

Understanding how the nervous system generates behavior requires tools that can resolve the molecular identity, spatial localization, and functional contribution of neurotransmitters *in vivo*. Neurotransmitters are the primary means by which neurons communicate, and their synthesis, packaging, and release are governed by evolutionarily conserved molecular pathways shared from *Caenorhabditis elegans* to vertebrates (Südhof, 2021). These transmitters shape the strength, kinetics (tonic vs. phasic), and polarity (excitatory vs inhibitory) of synaptic transmission, thereby influencing how information is processed and how behavior is regulated (Crawford & Kavalali, 2015; Gouwens et al., 2020; Kamalova & Nakagawa, 2021; Liu et al., 2021). Because neurotransmitters are central to defining the functional properties of synapses, understanding their identity and dynamics is essential for interpreting circuit function. Even in organisms with complete connectomes—such as *C. elegans* (White et al., 1986) and *Drosophila melanogaster* (Scheffer et al., 2020; Seggewisse & Winding, 2024; Yi et al., 2024) anatomical connectivity alone cannot explain how neural circuits generate behaviors. To build accurate, testable models of

circuit function, it is necessary to also determine which neurotransmitters are used at specific synapses and how their release is spatiotemporally organized and regulated *in vivo*. Yet, despite the centrality of neurotransmitters to circuit logic, the field still lacks broadly applicable tools to visualize and manipulate transmitter-specific vesicle pools with the precision needed to study their roles in intact, living animals.

Traditional approaches—such as in situ hybridization, immunohistochemistry, and transcriptomics—have been instrumental in mapping neurotransmitter identity. These methods, however, often lack cell-specific control, temporal resolution, or the ability to monitor transmitter usage dynamically within intact circuits. Moreover, neurotransmitter identity can change in response to environmental or physiological cues. For example, neurons may co-release multiple transmitters or modulate transmitter usage depending on stress, activity, or developmental stage, and these changes have consequences in animal behavior and circuit function (Chen et al., 2023; Li et al., 2024; Maddaloni et al., 2024; Sitko et al., 2025; Wu et al., 2020). Tracking and manipulating these physiological changes require new tools that allow endogenous, live imaging and functional interrogation of neurotransmitters in single neurons.

Vesicular transporters offer a strategic entry point for such investigations. These multi-pass membrane proteins package specific neurotransmitters—such as glutamate, GABA, acetylcholine, and monoamines—into synaptic vesicles and are necessary and sometimes sufficient for defining a neuron's transmitter phenotype (Edwards, 2007). Because they are genetically encoded and highly conserved (Alfonso et al., 1993; Bellocchio et al., 1998; Chaudhry et al., 1998; Lee et al., 1999; McIntire, Jorgensen, & Horvitz, 1993; McIntire et al., 1997; Roghani et al., 1994), vesicular transporters provide a powerful molecular handle for developing generalizable tools that probe synaptic identity and function across species. Tagging these transporters can offer direct, real-time readouts of presynaptic signaling and enable manipulations that dissect the functional contribution of specific neurotransmitters *in vivo* (Li et al., 2020). Yet for these tools to be broadly useful, it is essential that tagging does not disrupt the localization or function of the transporter. If appropriate insertion sites can be identified and validated functionally, the evolutionary conservation of vesicular transporters suggests that such designs could serve as generalizable platforms across systems and species.

Here, we present SynaptoTagMe, a comprehensive toolkit for tracking and manipulating transmitter-specific vesicles in *C. elegans*. Using a structure-guided approach informed by predicted protein topology and sequence conservation, we engineered endogenously tagged

versions of the vesicular transporters for glutamate (EAT-4/VGLUT), GABA (UNC-47/VGAT), acetylcholine (UNC-17/VAChT), and monoamines (CAT-1/VMAT). We validated *in vivo* that the tagged transporters retain functionality and enables bright, cell-specific imaging. In parallel, we developed conditional knockout strains that enabled spatiotemporal access to the ablation of the packaging or synthesis of specific neurotransmitters in defined neurons, allowing causal tests of neurotransmitter function at the single-cell level within behaving animals.

We applied this toolkit to identify neurons that co-express multiple vesicular transporters, revealing that 10% of *C. elegans* neurons contain the machinery for co-transmission. Focusing then on the ADF sensory neuron, we validate that ADF expresses the machinery for co-transmission of serotonin and acetylcholine. We demonstrate that serotonin and acetylcholine are packaged in partially distinct vesicle populations. Together, our observations suggest that co-transmission can be spatially organized, offering a refined view of how individual neurons diversify their signaling output *in vivo*. Our discoveries also highlight co-transmission as a widespread and previously underappreciated feature of nervous system organization, rather than a rare or specialized exception. Co-transmission is not unique to *C. elegans*; in *Drosophila* the VAChT protein can be modulated in GABAergic and glutamatergic neurons by microRNAs (Chen et al., 2023); in mammals, serotonergic neurons in the dorsal raphe co-release glutamate or GABA depending on context (Li et al., 2024), while starburst amacrine cells in the retina release both acetylcholine and GABA with distinct calcium sensitivities (Lee et al., 2010; Morrie & Feller, 2015). These examples, along with our findings, underscore the evolutionary conservation of co-transmission as a mechanism for expanding the functional repertoire of single neurons.

By enabling simultaneous visualization of different transmitter-specific vesicle pools within the same neuron, our tools uncover molecular heterogeneity at individual synapses and reveal new layers of synaptic plasticity. More broadly, our findings establish a functional framework for probing neurotransmitter dynamics, synaptic architecture, and co-transmission *in vivo*. The strategies developed here are generalizable to other model systems and open new avenues for dissecting neural circuit logic with molecular and cellular precision.

RESULTS

A systematic strategy for tagging and manipulating transmitter-specific vesicles *in vivo*

120 All synaptic vesicle transporters are multi-pass transmembrane proteins with structural loops
121 facing either the cytosolic or luminal space. To visualize transmitter-specific vesicle pools *in vivo*,
122 we developed a suite of fluorescently tagged, functional versions of the vesicular transporters for
123 glutamate (EAT-4/VGLUT), GABA (UNC-47/VGAT), acetylcholine (UNC-17/VAChT), and
124 monoamines (CAT-1/VMAT) in *C. elegans*. We chose these four neurotransmitter classes
125 because they are used by more than 90% of the neurons in *C. elegans* (Wang et al., 2024). We
126 used a systematic design pipeline that integrated (1) protein topology predictions, (2) evolutionary
127 conservation, and (3) structure-guided fluorophore placement to identify regions of each
128 transporter suitable for tagging without disrupting function. These approaches were used to
129 generate endogenous knock-in alleles with bright, cell-specific labeling through Flippase
130 recombinase systems (Schwartz & Jorgensen, 2016) or self-assembling split-GFP tags (He et al.,
131 2019) (Figure 1). When possible, tools were developed for both green and red-based fluorophores
132 to allow for multi-color imaging. For each transporter, we also created matched conditional
133 knockout strains by inserting FRT-flanked cassettes to disrupt neurotransmitter packaging or
134 synthesis in defined cells, adding to the existing cell-specific knockout tools available in the field
135 (Huang et al., 2023; Lopez-Cruz et al., 2019) (Figure 1). To drive expression of Flippase in
136 GABAergic and Cholinergic neurons we inserted Flippase into the *unc-47* and *unc-17* locus after
137 a self-cleaving 2A peptide sequence (Ahier & Jarriault, 2014), and used available Flippase drivers
138 for Serotonergic and Dopaminergic neurons (Muñoz-Jiménez et al., 2017). Together, these new
139 tools allow precise labeling and *loss-of-function* analysis of transmitter-specific vesicles in intact
140 circuits and behaving animals (summarized in Table 1). All strains created in this study are
141 accessible upon request from the Caenorhabditis Genetics Center (CGC) and the respective
142 sequences are available at https://www.intralab.app/research-papers/cuentas-condori_etal-2026.

143 **Table 1. Cellular, genetic and molecular tools to probe neurotransmission in single cells**

Genotype	**Purpose**
Toolkit for examining Glutamatergic transmission	
eat-4::gfp FLP-on(syb8568)	Cell-specific GFP knock-in (C-terminus end)
eat-4::mRuby3 FLP-on(syb9139)	Cell-specific mRuby3 knock-in (C-terminus end)
eat-4 (kySi76 kySi77)	Cell-specific knockout
Toolkit for examining GABAergic transmission	
unc-47::gfp (syb6990)	Endogenous full body GFP tagging
unc-47::mKate2 (syb7358)	Endogenous full body mKate2 tagging

unc-47::gfp11 (syb7313)	Endogenous and cell-specific GFP labeling
unc-47::gfp11x3 (syb7849)	Endogenous and cell-specific GFPx3 labeling
unc-25 (syb5949 syb6275)	Cell-specific knockout
Toolkit for examining Cholinergic transmission	
unc-17::mKate2 (ot907)	Endogenous full body mKate2 tagging
unc-17::GFP FLP-on (ola503)	Cell-specific GFP knock-in (C-terminus end)
unc-17::mRuby3 FLP-on (syb7882)	Cell-specific mRuby3 knock-in (C-terminus end)
GFP FLP-on::unc-17 (syb7251)	Cell-specific GFP knock-in (N-terminus end)
unc-17 (syb5779 syb5987)	Cell-specific knockout
Toolkit for examining Monoaminergic transmission	
cat-1::gfp11x3 (syb7239)	Endogenous and cell-specific GFPx3 labeling
cat-1 (ky1101 ky1118)	Cell-specific knockout
Flippase drivers	
P*eft-3*::Flippase (*sybIs9614)*	Flippase expression in all cells
unc-47::T2A::Flippase*(syb8125)*	Flippase expression in GABAergic neurons
unc-17::T2A::Flippase *(syb8059)*	Flippase expression in Cholinergic neurons
P*tph-1*::Flippase (*bqSi488)*	Flippase expression in Serotonergic neurons
P*dat-1*::Flippase (*bqSi614)*	Flippase expression in Dopaminergic neurons

Functional labeling of glutamatergic vesicles via EAT-4/VGLUT

Glutamate functions as a key excitatory neurotransmitter in the nervous system, and its packaging into synaptic vesicles requires the conserved Vesicular Glutamate Transporter (VGLUT) (Bellocchio et al., 1998; Lee et al., 1999), which is sufficient to confer glutamatergic identity to a neuron. In *C. elegans*, the VGLUT homolog EAT-4 is expressed in 43 of the 118 neuronal classes catalogued (Wang et al., 2024). EAT-4/VGLUT is predicted to have 12 transmembrane domains (Figure 2A), and prior tools have allowed for cell-specific knockout of its full coding sequence (Lopez-Cruz et al., 2019). A previously reported transgene with EAT-4/VGLUT fused to GFP demonstrated localization to synapses (Yu & Chang, 2022); here we extend this approach to an endogenously tagged allele.

155

156 To generate a bright, functional reporter that reflects endogenous EAT-4/VGLUT localization *in*
157 *vivo*, we inserted a GFP tag into the protein C-terminal cytoplasmic domain using a FLP-on
158 cassette (Schwartz & Jorgensen, 2016). The C-terminus was chosen based on conservation
159 analysis and AlphaFold structural predictions (Jumper et al., 2021; Pei & Grishin, 2001), which
160 identified it as a cytosolic and weakly conserved region, minimizing the risk of disrupting
161 conserved protein functions (Figure S1A-B). GFP was inserted just before the STOP codon
162 (Figure 2B). To examine if introduction of GFP into the endogenous EAT-4/VGLUT gene affected
163 function, we assessed NaCl chemotaxis (Figure S1C) —an EAT-4–dependent learning behavior
164 mediated by the ASE neurons (Figure S1C-D) (Bargmann & Horvitz, 1991; Sato et al., 2021;
165 Uchida et al., 2003). EAT-4::GFP FLP-on strains, with or without Flippase expression in all
166 neurons or selectively in ASE neurons, displayed normal chemotaxis behavior (Figure 2C and
167 S1D), in contrast to *eat-4(ky5)* loss-of-function mutants or mutant animals with defects in
168 chemosensory neurons, including ASE (*che-1* mutants; Figure 2C, S1C-D). Our findings suggest
169 that the tagged protein remains functional and capable of sustaining known glutamate-dependent
170 behaviors in the organism.

171

172 The insertion of the FLP-on cassette enables expression of EAT-4/VGLUT::GFP upon cell-
173 specific expression on the FLP recombinase. To validate its use, we expressed pan-cellular
174 flippase via the *eft-3* promoter (Seydoux & Fire, 1994) in the worms engineered with the EAT-
175 4::GFP FLP-on cassette. We observed bright EAT-4::GFP signal throughout the nervous system,
176 especially in the nerve ring and sensory neurons (Figure 2D), consistent with earlier
177 transcriptional reporters of the *eat-4* gene (Lee et al., 1999; Serrano-Saiz et al., 2013). Moreover,
178 when Flippase was driven specifically in ASE neurons (using the ASE-specific promoter, P*flp-6*),
179 we observed punctate labeling along ASE axons, matching the distribution of presynaptic sites
180 identified by serial electron microscopy (Figure 2E), and cataloged in NeuroSC (Koonce et al.,
181 2024; White et al., 1986). Consistent with this, we observed that endogenous GFP::RAB-3 in ASE
182 similarly localizes in a punctate pattern along the axons in a pattern that is reminiscent to that
183 seen for endogenous EAT-4::GFP (Figure S2 and Figure 2E).

184

185 To expand the utility of this tool for multicolor imaging, we also generated a red-shifted FLP-on
186 reporter for the *eat-4/VGLUT* gene by inserting mRuby3 (Bajar et al., 2016) with a *C. elegans*-
187 optimized sequence at the same C-terminal site (Figure 1B). These spectrally distinct reporters,
188 when combined with the previously developed *eat-4* conditional knockout (Lopez-Cruz et al.,

189 2019) provide a comprehensive toolkit for dissecting glutamatergic transmission in a cell-specific
190 manner *in vivo*.

191 **Cell-specific imaging and silencing of GABAergic neurotransmission**

192 GABAergic neurons package GABA into synaptic vesicles via the conserved vesicular GABA
193 transporter VGAT(Chaudhry et al., 1998; McIntire et al., 1997). In *C. elegans*, the VGAT homolog
194 UNC-47 is expressed in 11 of the 118 neuronal classes (Gendrel et al., 2016; Wang et al., 2024).
195 Based on *in vivo* data, the N-terminus of VGAT is cytoplasmic while the C-terminus is luminal
196 (Martens et al., 2008). The N-terminus contains dileucine motifs critical for proper trafficking
197 (Santos et al., 2013), and to preserve transporter function we focused on tagging long cytoplasmic
198 loops. Structural predictions from AlphaFold indicate that UNC-47 has 11 transmembrane
199 domains (Figure 3A), and we identified the cytosolic loop between transmembrane domains 2
200 and 3— a long (13 amino acids) region (Figure S3A-B)—as an optimal tagging site.
201
202 Within this loop, AlphaFold predicts two beta-sheet regions with high confidence. We inserted
203 GFP between amino acids E145 and N146, immediately following the first predicted beta sheet,
204 to avoid disrupting secondary structures (Figure 3A, S3A-B). To assess functionality of the newly
205 engineered UNC-47/VGAT::GFP strain, we performed thrashing assays on *unc-47 (e307)*
206 mutants, which show impaired locomotion due to loss of GABA signaling at neuromuscular
207 junctions (McIntire, Jorgensen, Kaplan, et al., 1993). Expression of UNC-47::GFP from an
208 extrachromosomal array rescued the thrashing defect to wild-type levels (Figure S3C and D), as
209 expected. We next generated endogenous knock-ins of GFP and mKate2 at the same site but in
210 the endogenous *unc-47* locus, and observed wild-type locomotion for these strains, consistent
211 with the insertion of the fluorophores not affecting endogenous function of the transporter (Figure
212 S3D). These strains showed bright, punctate fluorescence in the nerve ring and along the dorsal
213 and ventral nerve cords (Figure S3E-F), consistent with previously reported *unc-47* expression
214 patterns (McIntire et al., 1997). Together, these results demonstrate that inserting a fluorescent
215 protein at position E145 results in a functionally tagged UNC-47/VGAT reporter that enables
216 endogenous visualization of the protein.
217
218 To enable *in vivo* visualization of GABAergic vesicles in single-cells, we next generated two UNC-
219 47::splitGFP alleles by inserting either one or three tandem copies of GFP11 at the E145 position
220 (Figure 3B). We used the splitGFP approach to avoid disruptions of the protein structures due to
221 the introduction of the FRT-cassettes at an internal sequence site. By leveraging the self-

222 assembling property of the GFP beta barrel, knock-in of the eleventh beta strand (GFP11) results
223 in labeling of a protein that is only visible when the complementary GFP1-10 is expressed in the
224 same cell. This property results in a combinatorial labeling strategy, in which cell-specific labeling
225 is achieved only in those cells that express both the GFP11 and the GFP 1-10 (He et al., 2019).
226 To validate these tools, we first achieved pan-cellular expression of GFP1-10 (*eft-3* promoter)
227 (Seydoux & Fire, 1994) in animals carrying the UNC-47::GFP11x3 *(syb7849)* allele. We observed
228 GABAergic synapses throughout the nerve ring and nerve cords (Figure 3C), similar to full-body
229 knock-in strains (Figure S3E-F). To then visualize GABAergic vesicles in subsets of cells, we
230 expressed GFP1-10 in the GABAergic DD motor neurons using the *flp-13* promoter and in animals
231 carrying the GFP11 (*syb7313*) or UNC-47::GFP11x3 *(syb7849)* alleles. We observed punctate
232 reconstituted signal in the dorsal nerve cord of both GFP11 and GFP11x3 strains, consistent with
233 the known distribution of DD synapses (Figure S4E). The triple GFP11 version produced
234 significantly brighter signal (Figure S4E-G), in line with reports of enhanced fluorescence from
235 multimerized tags (He et al., 2019).
236
237 To then visualize GABAergic synapses in single cells, we expressed GFP1-10 under an RIB-
238 interneuron, cell-specific promoter. We selected RIB because it is a GABAergic interneuron
239 embedded in the nerve ring and proximal to three other GABAergic interneurons with overlapping
240 neurites that impede visualization of RIB-specific synapses *in vivo* when using traditional
241 approaches (Figure S4A-C). Reconstituted fluorescence using our tools enabled visualization of
242 RIB-specific synapses, and the observed synaptic pattern was consistent with the pattern
243 expected from electron microscopy reconstructions (Figure 3D) (Koonce et al., 2024; White et al.,
244 1986) and from expression of endogenous mScarlet::RAB-3 in RIB neurons (Figure S4D). These
245 findings underscore the value of the tool in labeling GABAergic synapses in individual cells *in*
246 *vivo*.
247
248 To functionally dissect GABAergic transmission, we developed a conditional knockout of *unc-25*,
249 the gene encoding Glutamic Acid Decarboxylase (GAD), which catalyzes GABA synthesis. We
250 decided to target *unc-25*/GAD because it results in the elimination of GABA from neurons
251 (Gendrel et al., 2016). We flanked the *unc-25* coding sequence with FRT sites and inserted a
252 nuclear mCherry reporter downstream to indicate successful recombination (Figure 3B). We then
253 validated the tool by using thrashing assays. Consistent with previous findings, *unc-25* null
254 mutants show severely reduced locomotion in the thrashing assays (McIntire, Jorgensen, Kaplan,
255 et al., 1993) (Figure 3E). We observed that animals carrying the conditional knockout allele

behaved normally in the absence of Flippase, but that pan-cellular Flippase expression in all GABAergic neurons (*unc-47* promoter), which is expected to result in loss of GABAergic neurotransmission, phenocopied the thrashing defect of *unc-25* mutants (Figure 3E). These results confirm that this tool effectively eliminates *unc-25/*GAD activity, with the capacity to be activated in a cell-specific manner and allows investigation of how GABAergic transmission contributes to neural function and behavior.

Functional labeling of cholinergic vesicles via UNC-17/VAChT

The cholinergic identity of neurons is defined by the expression of a conserved gene locus, shared from nematodes to vertebrates, that includes both the acetylcholine synthesis enzyme Choline Acetyltransferase (ChAT) and the Vesicular Acetylcholine Transporter (VAChT) (Eiden, 1998). In *C. elegans*, the VAChT homolog UNC-17 is expressed in 57 of the 118 neuronal classes (Wang et al., 2024). Based on prior studies, both the N- and C-termini of VAChT face the cytosol and contain regulatory motifs important for trafficking (Fei et al., 2008). AlphaFold predicts UNC-17 has 12 transmembrane domains, but most cytosolic loops are very short (<5 amino acids), except for the third cytoplasmic loop, which contains 28 amino acids and exhibits relatively high sequence conservation (Figure S5A-B).

To determine suitable tagging sites for imaging UNC-17 without disrupting function, we tested three locations: the conserved third cytosolic loop (site 1), the N-terminus (site 2), and the C-terminus (site 3) (Figure S5B-C and S5E). We used a thrashing assay to assess function, as *unc-17(e245)* null mutants fail to thrash in liquid and are rescued by the re-expression of untagged UNC-17 under its own promoter (Figure S5F). We generated transgenic strains with a rescue array containing the *unc-17* gene with GFP inserted into these three sites. We observed that GFP insertion into site 1 failed to rescue the phenotype, suggesting disruption of UNC-17 function. In contrast, tagging either the N-terminus or C-terminus restored normal thrashing (Figure S5E–F), indicating that these positions tolerate modification. Informed by these rescue experiments, we then generated two FLP-on conditional knockout alleles (Schwartz & Jorgensen, 2016) with GFP inserted at either the N-terminus (*syb7251*) or C-terminus (*ola503*) (Figure 4A-B). To test whether the FLP-on cassettes affected protein function, we examined behavior before Flippase expression and found that both alleles behaved like wild-type animals (Figure S5F). Because splicing regulatory elements are located near the 5' end of the *unc-17* gene and are required for successful splicing of the cholinergic locus (both *unc-17* and *cha-1* transcripts) (Mathews et al., 2015), we

288 proceeded with the C-terminally tagged *ola503* allele, which leaves the 5' region intact. We tested
289 whether pan-cellular expression of Flippase in this strain impairs behavior. Animals with global
290 GFP-tagged UNC-17 showed wild-type thrashing in liquid (Figure 4C), confirming that the tagged
291 transporter is functional and validating this approach for cell-specific labeling of cholinergic vesicle
292 pools.
293
294 At the cellular level, GFP labeling of UNC-17/VAChT using the *ola503* allele and pan-cellular
295 Flippase expression (driven by the *eft-3* promoter) (Seydoux & Fire, 1994) resulted in
296 fluorescence in the nerve ring, dorsal cord, ventral cord, and sublateral cords (Figure 4D). This
297 expression pattern matched that of a full-body mKate2 knock-in of endogenous UNC-17/VAChT
298 (Figure S5D) (Pereira et al., 2019) and was consistent with prior transcriptional reporters (Pereira
299 et al., 2015) and anti-UNC-17 antibody staining (Duerr et al., 2008). The *ola503* allele also enables
300 cell-specific labeling. When Flippase was expressed specifically in ADF neurons using the P*srh-*
301 *142* promoter (Maicas et al., 2021), we observed UNC-17::GFP puncta along the ADF axon
302 (Figure 4E). This punctate pattern aligned with known ADF presynaptic sites from electron
303 microscopy reconstructions of L4 animals (Koonce et al., 2024; White et al., 1986). Together,
304 these results demonstrate that the UNC-17::GFP FLP-on allele provides a reliable tool to label
305 cholinergic vesicles in individual neurons *in vivo*, and that this labeling does not affect function in
306 our assays. To enable multicolor imaging, we generated a red, fluorescent version of the UNC-
307 17/VAChT tool by replacing GFP with *C. elegans*-optimized mRuby3 (Figure 4B). This mRuby-
308 tagged allele performs as wild type animals in a thrashing assay and labels synaptic structures
309 along the nerve ring and nerve cords (Figure S6). Combined with the previously described cell-
310 specific *unc-17* knockout strain (Huang et al., 2023) (Figure 4B), these tools allow precise tracking
311 and manipulation of cholinergic neurotransmission *in vivo*.

312 **Probing Monoaminergic Transmission**

313 Monoamines such as serotonin, dopamine, norepinephrine, epinephrin, octopamine, and
314 tyramine are transported into vesicles by the conserved Vesicular Monoamine transporter (Duerr
315 et al., 1999; Erickson et al., 1992). In *C. elegans*, the VMAT homolog CAT-1 is expressed in 16
316 of the 118 neuronal classes (Wang et al., 2024). Recently, CAT-1 was tagged at its C-terminus
317 with a split GFP11x3 reporter (Figure 5A–B) (Huang et al., 2023). When GFP is reconstituted
318 pan-cellularly, this fusion produces a punctate signal enriched in the nerve ring—including the
319 characteristic and well-known serotonergic neuron NSM—and in serotonergic neurons that are
320 part of the reproductive organs (Figure 5C).

321 To determine whether the CAT-1::GFP11x3 fusion maintains protein function, we used a
322 behavioral assay based on the role of serotonin to prevent animal exploration on a lawn of bacteria
323 (Flavell et al., 2013). Since serotonin is packaged into vesicles by CAT-1/VMAT, similar to mutants
324 of serotonin production (Flavell et al., 2013), *cat-1* mutants display increased exploration behavior
325 compared to wild-type animals (Figure 5D). We found that animals with reconstituted CAT-
326 1::GFP11x3 explore bacterial lawns at levels comparable to wild-type (Figure 5D), indicating that
327 the GFP11x3 tag nor its reconstitution impair CAT-1 function. To complement this tool, we also
328 developed a cell-specific *cat-1* knockout allele in which the full coding sequence is excised upon
329 Flippase expression (Figure 5B). Removal of serotonin production (*tph-1*) specifically from ADF
330 neurons result in increased aversion from wild type *E. coli* bacteria lawns (Feng et al., 2025).
331 Consistent with this, cell-specific KO of *cat-1* in ADF neurons (via expression of ADF::Flippase)
332 results in increased *E. coli* aversion (Figure 5E). Together, these tools now enable the cell-specific
333 tracking and silencing of monoaminergic synapses in living animals.

334 ***In-Vivo* Identification of Co-Transmitter Neurons**

335 Co-transmission is a conserved feature of neurons across the animal kingdom (Granger et al.,
336 2017; Trudeau & El Mestikawy., 2018; Vaaga et al., 2014), including *C. elegans* (Duerr et al.,
337 2008; Gendrel et al., 2016; Pereira et al., 2015; Pocock & Hobert, 2010; Serrano-Saiz et al., 2017;
338 Serrano-Saiz et al., 2013; Taylor et al., 2021; Wang et al., 2024), but the prevalence of co-
339 transmission *in vivo* for any given organism is not well understood. To validate the utility of our
340 tools and to map the architecture of co-transmission in *C. elegans*, we developed an intersectional
341 genetic strategy using Flippase recombinase and FRT-flanked fluorescent reporters (Figure 6A).
342 We focused on identifying neurons that co-transmit glutamate or acetylcholine—the two most
343 abundant excitatory neurotransmitters in *C. elegans*—in combination with other transmitters
344 (Figure 6B).

345 We reasoned that if two neurotransmitters were co-expressed in the same neuron, driving
346 Flippase under the promoter of one transmitter would activate the conditional reporter—resulting
347 in fluorescence—only in cells also expressing a second neurotransmitter identity (Figure 6A-B).
348 To achieve this, we used the engineered alleles for each vesicular transporter that we developed
349 (Figures 2B, 3B, 4B, and 5B) (Table 1) and developed additional Flippase driver by modifying the
350 locus of genes involved in the packaging of acetylcholine (*unc-17*) and GABA (*unc-47*) (Table 1).
351 Additionally, we used available Flippase driver lines for serotonin and dopamine (Figures S7A–B,
352 Table 1) (Muñoz-Jiménez et al., 2017).

353 We first used a conditional *eat-4/VGLUT* reporter strain in which cytosolic mCherry is expressed
354 upon Flippase-mediated recombination (Lopez-Cruz et al., 2019). When Flippase was driven by
355 the *unc-17/VAChT* promoter (cholinergic), we observed five mCherry-positive neurons in the head
356 and tail, consistent with co-expression of *unc-17/VAChT* and *eat-4/VGLUT*. Based on cell
357 position, neurite morphology, transcriptomic data (Taylor et al., 2021), and anatomical maps
358 (Wang et al., 2024), we identified these neurons as AFDL, AFDR, M5, DVA, and PVN (Figure
359 6C–D).

360 Flippase expression from the GABAergic *unc-47* promoter activated *eat-4*-driven mCherry
361 expression in a single pharyngeal neuron, identified as I2L (Figure 6E, S8A). Driving Flippase
362 from the dopaminergic *dat-1* promoter labeled the PDE neuron (Figure 6F, S8B), while
363 serotonergic *tph-1*-driven Flippase did not produce any mCherry-positive neurons. These results
364 are summarized in Figure S7C.

365 We applied a similar strategy by using our Flippase-dependent *unc-17*::GFP reporter to identify
366 candidate neurons that co-release acetylcholine with other neurotransmitters. In this context,
367 when Flippase was driven from the GABAergic *unc-47* locus, we observed GFP expression in the
368 M4, SDQR, and SMD neurons (Figure 6G, S8D). Flippase expression from the serotonergic *tph-*
369 *1* promoter revealed previously described acetylcholine/serotonin co-transmitting neurons,
370 including ADF, HSN, and VC4/VC5 (Figure 6H, S8C), consistent with prior findings (Pereira et al.,
371 2015). All neurons identified through this dual-reporter approach are summarized in Figure S7C.

372 We compared our findings with previous reports and have compiled a list of potential co-
373 transmitter neurons that are consistently identified across independent studies (Figure S9),
374 suggesting these are likely *bona fide* co-transmitter neurons. Together, we observe that *C.*
375 *elegans* has 35 neurons exhibiting molecular signatures of co-transmission (Table 2)—
376 representing ~ 10% of the *C. elegans* nervous system (Figure S9 and Table 3). Strikingly, the
377 pharyngeal nervous system—analogous to the vertebrate enteric nervous system (Albertson &
378 Thomson, 1976)—had the highest density of co-transmitter neurons: 30% (6 of 20 neurons)
379 displayed co-expression of multiple vesicular transporters. Across the entire nervous system, co-
380 transmission was prevalent among sensory neurons, with 12% (10 of 83), compared to 11% of
381 interneurons (9 of 81) and 7% of motor neurons (8 of 116) (Table 2). We also compiled a list of
382 neurons that were suggested to be co-transmitters (RIB, AVA, AVB) (Gendrel et al., 2016), but
383 that are not supported by other expression studies (Taylor et al., 2021) (Table 4).

384

385 ***In-vivo* visualization of co-transmitter synapses in the ADF chemosensory neuron**

386 We next used our toolkit to investigate the subcellular localization of vesicular transporters in a
387 co-transmitting neuron, ADF. The ADF neurons are a bilaterally symmetric pair of sensory
388 neurons in *C. elegans* known to regulate food exploration, chemotaxis and entry into the lethargic-
389 like dauer state (Bargmann & Horvitz, 1991). While ADF has long been known to use serotonergic
390 neurotransmission, our findings indicate that it is also capable of acetylcholine synthesis and
391 packaging (Figure 6H, S7C and S10A-B). Our findings are consistent with recent transcriptomic
392 and reporter-based studies (Pereira et al., 2015; Taylor et al., 2021; Wang et al., 2024).

393 To examine the subcellular distribution of serotonin or acetylcholine vesicular transporters in ADF,
394 we used previously developed tools to endogenously label the serotonin vesicular transporter
395 CAT-1/VMAT (Huang et al., 2023), and the acetylcholine vesicular transporter UNC-17/VAChT
396 with GFP (Figures 4 and 5). To label these vesicular transporters specifically in ADF, we drove
397 Flippase and GFP1-10 expression using the AFD-specific promoter, *srh-142* promoter (Maicas et
398 al., 2021). Both UNC-17/VAChT and CAT-1/VMAT displayed punctate fluorescence along the
399 ADF axon, consistent with the location of presynaptic sites expected from electron microscopy-
400 based 3D reconstructions (Figure S10C) (Koonce et al., 2024; White et al., 1986).

401 To then visualize the spatial relationship between these two vesicular transporters, we generated
402 a strain in which UNC-17/VAChT was tagged with mRuby and CAT-1/VMAT with GFP at their
403 respective endogenous loci, cell-specifically in ADF neurons (Figure 7A). *In vivo i*maging using a
404 spinning disk confocal microscope revealed that these transporters frequently co-localize within
405 the same synaptic boutons (Figure 7B and 7B'). Interestingly, we also found instances in which
406 the UNC-17/VAChT::mRuby and CAT-1/VMAT::GFP signals partially segregate into separate
407 boutons along the same axon (Figure 7C and 7C'), suggesting that these vesicular transporters
408 can be sorted into distinct vesicle populations. Consistent with the idea that UNC-17 and CAT-1
409 localizes to synaptic vesicles along the axon, we observed that UNC-17 and CAT-1 localization
410 was disrupted in a Kif1A/*unc-104* (*e1265*) mutant animal (Hall & Hedgecock, 1991), absent in the
411 axon and accumulated in the cell body (Figure 7D-D').
412

413 To test whether both transporters are present at all ADF synapses, we endogenously tagged the
414 active zone protein UNC-13/Munc13 with mScarlet and examined its spatial relationship to UNC-
415 17/VAChT::GFP and CAT-1/VMAT::GFP (Figure 7E). We observed active zone UNC-

416 13::mScarlet puncta that lacked either CAT-1/VMAT::GFP (Figure 7F) or UNC-17/VAChT::GFP
417 labeling (Figure 7G). These findings are consistent with the idea that, while these two vesicular
418 transporters display co-localization in synaptic varicosities, they also independently localize to
419 distinct subcellular compartments.
420
421 Synaptic varicosities in *C. elegans* can be within the diffraction limits of light microscopy,
422 preventing differentiation of co-localizing vesicular populations. To better understand the relative
423 distribution of these vesicular transporters, we next visualized ADF synapses with increased
424 resolution, using AiryScan imaging, which can achieve differentiation of fluorophores up to 120
425 nm apart (Wu & Hammer, 2021). We observed that, even in synaptic boutons in which the
426 vesicular transporters were observed to co-localize with traditional light microscopy methods,
427 UNC-17/VAChT::mRuby and CAT-1/VMAT::GFP differentially segregated when imaged using
428 AiryScan microscopy (Figure 7H).
429
430 Together these results suggest that acetylcholine and serotonin co-localize to synapses, but might
431 be packaged into distinct vesicles with specific synaptic subcellular localization that is detectable
432 upon super-resolution microscopy. Our findings underscore the importance of endogenous
433 labeling in determining the specific localization of these vesicular transporters and their use with
434 higher-resolution imaging methods, highlighting the value of the tools developed in this study to
435 understand the cell-biological organization of synapses *in vivo*, particularly for neurons using more
436 than one neurotransmitter.
437
438 **DISCUSSION**
439
440 The integration of anatomical connectivity, molecular identity, neural activity, and transmitter
441 usage provides a powerful framework for building models of neural circuit function. The *C.*
442 *elegans* community has access to a complete connectome (White et al., 1986); the cellular identity
443 of all neurons (Sulston & Horvitz, 1977; Sulston et al., 1983); whole-brain calcium imaging
444 (Nguyen et al., 2016; Prevedel et al., 2014; Schrödel et al., 2013); single-cell transcriptomic
445 profiles (Taylor et al., 2021); and a full neurotransmitter identity map for all neurons (Wang et al.,
446 2024). These datasets have inspired models describing how specific circuits may give rise to
447 behavior. However, validating these models *in vivo* requires tools that can precisely manipulate
448 the molecular components of individual synaptic connections (Dag et al., 2023; Hawk et al., 2018;
449 Kumar et al., 2024). SynaptoTagMe provides that missing capability (Table 1) for the

neurotransmitter systems that cover approximately 90% of the *C. elegans* nervous system (GABA, glutamate, acetylcholine, and the monoamines). By enabling cell-specific labeling and conditional knockout of vesicular transporters, we can now directly test the contribution of individual neurotransmitters within defined circuits and link those changes to behavioral outcomes. Moreover, due to the evolutionary conservation of vesicular transporters, the *in vivo* validation of tagging strategies will help identify suitable labeling strategies for other organisms, providing a path toward comparative and cross-species studies of synaptic dynamics based on neurotransmitter identity.

Co-transmission is a conserved feature of neural systems across the animal kingdom (Granger et al., 2017; Lacin et al., 2019; Vaaga et al., 2014), but its preponderance *in vivo*, its regulation and its functional significance is still an area of active research. Using *in-vivo* reporters subject to endogenous regulation, and contrasting our results with previous studies, we determine that more than 10% of *C. elegans* neurons have co-transmission potential (Figure S9) (Tables 2 and 3). Our *in vivo* characterization of co-transmitting neurons confirm and expand findings reported for the latest neurotransmitter atlas of *C. elegans* (Wang et al., 2024) and yield three key insights. First, co-transmission occurs throughout the nervous system of *C. elegans*, including both the pharyngeal (enteric-like) and more central nervous systems, like the nerve ring and nerve cords (Table 2). Second, neurons can co-transmit multiple neurotransmitters in specific combinations that are conserved from nematodes to mammals (Figure 6 and S9) (Granger et al., 2017; Lacin et al., 2019; Trudeau & El Mestikawy., 2018; Vaaga et al., 2014; Wang et al., 2024). Importantly, the same neurons consistently exhibit co-transmission of the same neurotransmitter identities across individual animals, consistent with co-transmitter identity mapping to neuronal identity (Figure 6D-H). Third, co-transmission is part of every layer of a circuit, from sensory neurons to interneurons and motor neurons (Table 2). This is especially interesting in light of recent studies showing that co-transmission in sensory and motor circuits can be modulated by environmental cues such as stress (Bertuzzi et al., 2018; Li et al., 2024; Pocock & Hobert, 2010) or light-dark cycles (Chen et al., 2023; Maddaloni et al., 2024). With the tools developed here - based on endogenously tagged vesicular transporters – it is now possible to monitor the dynamic expression and subcellular distribution of specific vesicle populations *in vivo* and what molecular mechanisms drive those changes.

Our conclusions are supported by independent and convergent lines of evidence, and the toolkit developed here enables direct empirical interrogation of both the existence and functional

484 relevance of co-transmission *in vivo*. While expression of vesicular transporters represents one
485 line of evidence for co-transmission potential, it does not by itself establish functional co-release,
486 which additionally depends on neurotransmitter biogenesis, release competence, and activity-
487 dependent regulatory mechanisms. SynaptoTagMe now make it possible to systematically test
488 these requirements.
489
490 We note that the current characterization of co-transmitting neurons might be an under-estimate
491 of the total number of neurons which use co-transmission. For example, it has been proposed
492 that additional neurotransmitters, like betaine, may function in the *C. elegans* nervous system
493 (Wang et al., 2024). Accounting for neurons that express proteins capable of synthesizing or
494 packaging betaine, the proportion of potential co-transmitter neurons may exceed 20% of the
495 whole nervous system of *C. elegans*. Our characterization of co-transmission focused on the *C.*
496 *elegans* adult hermaphrodite, and co-transmitting neuron identities could be developmentally
497 regulated, or modulated based on prior experience. Consistent with this, it has been observed
498 that the identity of co-transmitting neurons is different between males and hermaphrodites
499 (Serrano-Saiz et al., 2017), underscoring the importance of future examination of the plasticity
500 and developmental regulation (Pereira et al., 2019; Pereira et al., 2015) of co-transmitting capacity
501 for individual neurons.
502
503 Expression of a vesicular transporter, while consistent with co-transmitting capacity, is not
504 conclusive for the existence of co-transmission for that neuron. For example, we identified co-
505 expression of the GABA and Glutamate vesicular transporters in the pharyngeal neurons I2
506 (Figure S8A). Notably, I2 does not express the GABA synthesis enzyme, *unc-25*/GAD (McIntire,
507 Jorgensen, & Horvitz, 1993) or the GABA re-uptake transporter, *snf-11* (Mullen et al., 2006). Thus,
508 it is unlikely that it produces GABA or uptakes it from the extracellular space. VGAT/UNC-47 has
509 also been reported to transport neurotransmitters such as glycine (Aubrey et al., 2007) and beta-
510 alanine (Juge et al., 2013), raising the possibility that I2 could co-transmit glutamate with an
511 unconventional neurotransmitter. Additionally, it is important to mention that the identification of
512 *eat-4*-positive neurons through the replacement of the *eat-4* coding sequence and introns (Figure
513 S7A) could result in the elimination of regulatory sequences. Thus, we conceptualize the list of
514 co-transmitting neurons as a hypothesis-generating framework to be further examined with the
515 tools developed in this study.
516

517 Our observations of the identity of co-transmitting neurons, and the specific combinations
518 represented in the neurons, suggest that there may be transmitter-specific rules of synaptic
519 biology important for circuit function (Silm et al., 2019; Trudeau & El Mestikawy., 2018). This is
520 consistent with findings in vertebrates, in which specific neurotransmitter combinations and their
521 distributions could underpin specific features of circuit function. For example, in Starburst
522 Amacrine cells in the mammalian retina, acetylcholine and GABA (O'Malley et al., 1992) are
523 packaged into distinct vesicle pools that exhibit different calcium sensitivities for release (Lee et
524 al., 2010). The distribution of specific vesicular populations and their release probabilities might
525 constitute an architecture that helps encode the sensory signals processed by Starburst Amacrine
526 cells. We similarly hypothesize that the specific distribution of co-transmitting synapses across
527 the *C. elegans* connectome, and the identities of the neurotransmitters used, might help encode
528 features important for circuit function and animal behavior. By allowing longitudinal, cell-specific
529 monitoring of the expression, regulation, and subsynaptic distribution of distinct vesicle
530 populations in living animals, this toolkit provides a platform for probing when, where, and how
531 co-transmission is deployed, and for defining the molecular and circuit-level mechanisms that
532 govern its use under different physiological and environmental conditions.
533
534 **METHODS**
535
536 **Strains**
537 Worms were maintained at 20°C using standard techniques (Brenner, 1973). Strains were
538 maintained on NGM plates seeded with *E. coli* (OP-50). The wild type (WT) is N2, and only
539 hermaphrodite worms were used for this study. A complete list of strains appears below. Strains
540 that were developed in this study as part of the SynaptoTagMe toolkit and appear in Table 1 can
541 be requested through CGC. The necessary sequencing information can be found at:
542 https://www.intralab.app/research-papers/cuentas-condori_etal-2026.
543
544 **Generation of new alleles**
545 For the strains engineered by Sunybiotech, as described below, strain design was
546 performed in the Colón-Ramos lab by Andrea Cuentas-Condori.
547 Sunybiotech used CRISPR/Cas9 to insert GFP FLP-on cassettes (Schwartz & Jorgensen,
548 2016) at either the N-termini of the *unc-17* locus (*syb7251*) or C-termini end of the *unc-17*
549 *(ola503),* or *eat-4 (syb8568)* locus, according to sequence design. mRuby FLP-on cassettes were
550 inserted similarly at the C-termini end of *eat-4* (*syb9193*) and *unc-17* (*syb7882*) locus. To visualize

551 the fluorescent signal tagged to the protein of interest, Sunybiotech generated single-copy MosCI
552 strains.
553 Sunybiotech used CRISPR/Cas9 to add full length GFP (*syb6990*), full length mKate
554 (*syb7358*) or split GFP (one (*syb7313*) or three (*syb7849*) copies of GFP11) to the *unc-47* locus
555 at the +893bp position. To visualize the reconstituted GFP signal in RIB neurons, complementary
556 GFP1-10 was driven with the P*sto-3b* promoter; and to visualize the GFP-reconstituted signal in
557 DD neurons, GFP1-10 was driven with the P*flp-13* promoter.
558 Sunybiotech used CRISPR/Cas9 to introduce an FRT site before the +1bp in the *unc-25*
559 gene locus (*syb5949*). In a second round of CRISPR editing, they introduced *let-858* 3' UTR
560 followed by a second FRT and nuclear mCherry (*syb6275)*.
561 *cat-1* (*ky1101 ky1118*) cell-specific knock out strain was created using CRISPR/Cas9 to
562 introduce an FRT site immediately before the ATG in the *cat-1* gene locus (*ky1101*). A second
563 round of CRISPR editing in that strain introduced the *let-858* 3' UTR followed by a second FRT
564 and the mCherry coding region immediately after the stop codon of *cat-1* to generate *ky1118*.
565 Sunybiotech used CRISPR/Cas9 to introduce a T2A::Flippase sequence before the STOP
566 codon of *unc-47(syb8125)* and *unc-17(syb8059)*. All strains generated using CRISPR/Cas9 were
567 outcrossed twice before use.
568

569 **Molecular Biology**

570 Plasmids were constructed using Gibson cloning. First, Snapgene (Version 7.0.3)
571 software was used to design primers targeting the desired DNA vector backbone and DNA insert.
572 The vector backbone and DNA insert were PCR linearized and amplified using "CloneAmp HiFi
573 PCR Premix." To assemble the desired plasmid, the purified vector backbone DNA and insert
574 DNA were combined and incubated in solution with "2x Gibson Assembly Enzyme Premix."
575 Following incubation, the reaction mixture was used to transform Stellar Competent Cells, which
576 were subsequently plated and grown overnight on LB-Amp plates. All plasmids were verified with
577 Sanger sequencing.
578

579 **Protein alignment and structure visualization**

580 For each gene under study, NCBI BLAST was used to generate a protein sequence
581 alignment of the *C. elegans* gene with the closest orthologs from the other model organisms *M.*
582 *musculus*, *D. rerio*, *D. melanogaster*, and *H. sapiens*. Protein structure models for the C. elegans
583 genes were downloaded from the AlphaFold database (Jumper et al., 2021) and predicted models

584 for the CRISPR-Cas9 modified genes including fluorophores were generated by the Alphafold3
585 online server (Abramson et al., 2024). Visualization and image generation of protein structures
586 was done using the ChimeraX software (Pettersen et al., 2021). To color the structures by
587 sequence conservation, the alignments per gene were overlaid onto the structures with ChimeraX
588 and colored by resulting sequence conservation Z-scores as calculated by the AL2CO algorithm
589 (Pei & Grishin, 2001) within the software.
590
591 **Table 5 – List of all molecular locations tested for labeling each synaptic vesicle**
592 **transporter**

Gene	AA tested for fluorescent protein insertion	Functional tag?
eat-4	N-terminus (After START codon)	yes
unc-47	Between E145 – N146	yes
unc-17	Between AA P6-V7	yes
unc-17	Between AA N242 - P243	no
unc-17	C-terminus (Before STOP codon)	yes

593
594 **Microscopy**
595 Larval or young adult animals were immobilized on 2-10% agarose pads with 10mM
596 levamisole. A Nikon Ti2 microscope equipped with a CSU-W1 spinning disk head, ORCA-Fusion
597 BT SCMOS camera, high-speed piezo stage motor, 60X/1.40 Apo Lambda oil objective lens was
598 used for live imaging. Z-stack images were collected (0.3-0.5 µm/step), spanning the focal depth
599 of the nerve cord and nerve ring synapses. A Zeiss LSM880 microscope equipped with an
600 AiryScan detector and 63X NA 1.4 oil objective was used for AiryScan imaging. FIJI (Schindelin
601 et al., 2012) or NIS Elements AR analysis software (version 6.10.01) were used to create
602 maximum intensity projections and 2D renderings.
603
604 **Thrashing Assay**
605 *C. elegans* were raised at 20°C under standard laboratory conditions on agar plates
606 seeded with a lawn of *E. coli* (OP50). Worms were synchronously grown to L4-stage and placed
607 in individual wells of a Corning™ PYREX™ Spot Plate (Catalogue #722085) containing 1000 µl
608 of M9 buffer, ensuring the buffer remained within the well's borders. After a 30-second acclimation
609 period to M9, thrashes were manually counted for 1 min. A single thrash was defined as a change
610 in the direction of the worm's midbody bending, counting each time the worm's body flexed to one
611 side. Following each trial, the worm was removed using a pipette and disposed of, and the M9
612 buffer was absorbed and discarded. The well was then cleaned with 70% ethanol and wiped dry.
613 To avoid bias, the counter was blinded to each genotype. Each worm was tested only once, with

614 assays conducted on 10 worms per genotype per day, and repeated over 2–3 days to account
615 for potential day-to-day environmental variations.
616
617 **Chemotaxis Assay**
618 Worms were maintained at 20°C for at least two generations on Nematode Growth
619 Medium (NGM) seeded with OP50 *Escherichia coli* bacteria. The concentration of our attractant
620 (NaCl) is approximately 50 mM in NGM plates. "Training" plates were produced using NGM with
621 the further addition of 50 mM NaCl to a total concentration of 100 mM, then also seeded with
622 OP50.
623 Chemotaxis assay was modified from standard procedure (Ward, 1973). All assays were
624 performed on 50 mm diameter plates. Unseeded NGM plates were marked at the center and one
625 point 12.5 mm away from the center. A ~60-85 mM gradient of NaCl was created between the
626 center and outer point by adding 5 M NaCl at the outer point as drops of 4μL (20-24 hours before
627 the assay), 4μL (5 hours before), and 1.6μL (2 hours before); a sham gradient was created using
628 only water. Gradient prediction was determined as previously described (Crank, 1956; Pierce-
629 Shimomura et al., 1999); briefly, for every point some distance *r* in cm from the salt peak, the
630 concentration *C* in mM at any point in time was calculated as:
631 $$C(t_i, r) = C_o + \sum_{i=1}^{n} c(t_i, r) \quad (1)$$
632 where C_o is the initial concentration of NaCl in the agar (50 mM), *n* is the drop number, and t_i is
633 the time in seconds since the drop had been applied; the contribution from each drop, in turn,
634 was calculated as:
635 $$c(t_i, r) = 10^6 \frac{N_i}{\sqrt{4\pi d D(t_i)}} e^{-\left(\frac{r^2}{4D(t_i)}\right)} \quad (2)$$
636 where N_i is the moles of NaCl added per drop; *d* is the depth (cm) of the agar; and *D* is 1.590 ×
637 10^{-5} cm^2/s, the diffusion coefficient for 5 M NaCl through an aqueous medium (Robinson RA,
638 1959). The resulting gradients were validated by electrical conductivity measurements using an
639 Oakton CON 6+ Handheld Conductivity Meter with a custom conductivity probe with 1 mm
640 insertion depth (Micro-electrodes, Inc, Bedford, NH). The conductivity readings from 50 mM and
641 100 mM NaCl NGM plates were used for calibration at specific room temperatures.
642 The day before experiments, L4 animals were transferred to a seeded NGM plate to
643 synchronize worms by developmental stage. At 5 hours before each assay, worms were
644 transferred to a training plate using standard NGM plate recipe adjusted to 100 mM NaCl. After
645 training, 8 worms were picked, with preference to those on the bacterial lawn, washed sequentially
646 in two 100 μL drops of liquid NGM buffer (25 mM potassium phosphate pH 6, 1 mM CaCl2, 1 mM

647 MgSO4, 50 mM NaCl) to remove adherent OP50, and transferred to a single 2 µL drop of NGM
648 buffer at the center of the assay plate with prepared NaCl gradient as described. Data collection
649 began when the water drop was fully absorbed into the assay plate and the first worm began to
650 migrate from its starting point. Six assay plates were imaged for each strain across two separate
651 days, yielding a total of 48 worms imaged per strain.
652 Images of chemotaxis behavior were acquired at 3.75 fps for 7 minutes using a Basler acA2440-
653 35mm monochromatic sensor with an infrared filter on a commercially available WormLab
654 imaging system and computer running WormLab 2023.1.1 software (MBF Bioscience LLC,
655 Williston, VT USA). Individual worm position data was obtained by constructing tracks in
656 WormLab software, then analyzed using custom scripts in R 4.4.1 (can be accessed through
657 GitHub (https://github.com/colonramoslab/Cuentas-Condori-et-al.-2025-Toolkit-). The assay
658 outcome was defined as the mean distance from the peak of the salt gradient for each worm,
659 averaged over every available frame in the last minute of the assay. When a worm track was
660 interrupted, e.g. by a worm exiting the camera field of view or by two worms intersecting, the last
661 available position for the worm was repeated until the worm was re-detected.
662
663 **Roaming Assay**
664 Roaming assay plates were prepared 3-5 days prior to the experiment by seeding NGM
665 agar plates with *E. coli* (OP50) culture no older than 2 days. Plates were seeded using a sterile
666 glass rod to spread the bacteria evenly across each plate. Plates were left to dry completely
667 between 3-5 days at room temperature to ensure the bacteria layer was fully dry, thereby allowing
668 for visible worm tracks during the assay. *C. elegans* were raised at 20°C under standard
669 laboratory conditions on agar plates seeded with a lawn of *E. coli* (OP50). On the day before the
670 assay, worms synchronously grown to L4-stage were transferred to regular seeded plates and
671 stored at 20°C. After approximately 10 hours, worms were transferred to individual assay plates
672 and incubated at 20°C for 16 hours. After this time, worms were removed and a grid overlay (3
673 mm x 3 mm squares) covering the assay plate was used to count the number of squares the
674 worms had traversed during the incubation period. The number of squares crossed provided a
675 quantifiable measure of roaming activity. To avoid bias, the counter was blinded to each genotype.
676 Each worm was tested only once, with assays conducted on 10 worms per genotype per day and
677 repeated over 2–3 days to account for potential day-to-day environmental variations.
678
679 **Aversion behavior Assay**

680 Aversion behavior assay were performed as previously described (Feng et al.,
681 2025). Animals were fed on *E. coli* BW25113 for at least three generations before the behavioral
682 assay. 12.5 μL of overnight BW25113 cultures were seeded onto standard NGM agar plates,
683 grown at 37˚C incubator for 24 hours and then left at room temperature for another 24
684 hours. 15~20 animals at L4 stages from each genotype were transferred onto behavioral assay
685 plate and recorded at 21˚C for 20 hours, at a recording rate of 1 frame per minute. Biological
686 replicates across two different days were conducted. Videos were cropped and analyzed using
687 standard MatLab codes (Marquina-Solis et al., 2024). Aversion ratio was defined by the number
688 of worms outside the bacterial lawn over total number of worms on assay plates.
689
690 **Statistical Analysis**
691 We used the Shapiro-Wilk test to determine sample distribution. For comparisons between
692 2 normally distributed groups, Student's T-test was used and $p<0.05$ was considered significant.
693 ANOVA was used to compare between 3 or more normally distributed groups followed by
694 Dunnett's multiple-comparison test. If the samples were not normally distributed, we used a Mann-
695 Whitney test to compare two groups and a Kruskal-Wallis test to compare three or more groups.
696 Specific post-hoc statistical tests are listed in the figure legend of each experiment. Prism 10.4.2
697 was used to graph the data and for all statistical analysis.
698
699 **List of strains**

Strain name	**Genotype**
PHX8568	*eat-4::gfp FLP-on(syb8568)* III
DCR9575	*eat-4::gfp FLP-on(syb8568)* III 2X outcrossed
MT6308	*eat-4(ky5)* III
DCR9690	*Pflp-6::FLP(sybIs9606)* II
DCR9814	*Pflp-6::FLP(sybIs9606)* II 2X outcrossed
DCR9872	*eat-4::gfp FLP-on(syb8568)* III*; Peft-3::FLP (sybIs9614)* II
DCR9816	*eat-4::gfp FLP-on(syb8568)* III*; Pflp-6::FLP (sybIs9606)* II
DCR9681	*eat-4::mRuby FLP-on(syb9193)* III 2X outcrossed
DCR9963	*GFP::RAB-3 FLP-on(ox699)* III; *Pgcy-5::FLP (sybIs8828)*
DCR9965	*GFP::RAB-3 FLP-on(ox699)* III; *olaEx5706[*P*gcy-7*::Flippase::T2A::BFP*; Punc-122::RFP]*

DCR9210	*unc-47::gfp (syb6990)* III 2X outcrossed
DCR9453	*unc-47::mKate2 (syb7358)* III 2X outcrossed
CB307	*unc-47(e307)* III
DCR9269	*unc-47::gfp (syb6990)* III*; olaEx5490[Psto-3b::BFP; Punc-122::RFP]*
PHX7313	*unc-47::gfp11 (syb7313)* III
DCR9280	*unc-47::gfp11 (syb7313)* III 1X outcrossed
DCR9738	*unc-47::gfp11 (syb7313)* III*; olaEx5686[Pflp-13::GFP1-10; Pmyo-2::mCherry]*
PHX7849	*unc-47::gfp11x3 (syb7849)* III
DCR9739	*unc-47::gfp11x3 (syb7849)* III 2X outcrossed
DCR9740	*unc-47::gfp11x3 (syb7849)* III*; olaEx5686[Pflp-13::GFP1-10; Pmyo-2::mCherry]*
DCR9741	*unc-47::gfp11x3 (syb7849)* III*; olaEx5687[Psto-3b::GFP1-10; Punc-122::RFP]*
CF4587	*muIs253 [Peft-3*::GFP1-10::*unc-54* 3'UTR + *Cbr-unc-119*(+)*]* II; *unc-119(ed3)* III
DCR9838	*muIs253 [Peft-3*::GFP1-10::*unc-54* 3'UTR + *Cbr-unc-119*(+)*]* II; *unc-119(ed3)* III *unc-47::gfp11x3 (syb7849)* III recombinant
PHX6275	*unc-25 (syb5949 syb6275)* III
DCR9898	*unc-25 (syb5949 syb6275)* III; bqSi506[P*rgef-1*::Flippase D5 + unc-119(+)] IV
CB933	*unc-17(e245)* IV
DCR9891	*unc-17(e245)* IV*; olaEx5703[Punc-17::*UNC-17cDNA]
DCR9074	*unc-17(e245)* IV*; olaEx5400[Punc-17::*GFP::UNC-17 (N-terminal tag)]
DCR9892	*unc-17(e245)* IV*; olaEx5704[Punc-17::*UNC-17::GFP (between TM6-7)]
OH15568	*unc-17::mKate2 (ot907)* IV
DCR9011	*unc-17::GFP FLP-on(ola503)* IV
DCR9211	*unc-17::GFP FLP-on(ola503)* IV 1X outcrossed
PHX7251	*GFP FLP-on::unc-17 (syb7251)* IV
DCR9265	*GFP FLP-on::unc-17 (syb7251)* IV 1X outcrossed
DCR9720	*Peft-3::FLP (sybIs9614)* II
DCR9733	*Peft-3::FLP (sybIs9614)* II *2X outcrossed*

DCR9742	*unc-17::GFP FLP-on(ola503)* IV*; Peft-3::FLP (sybIs9614)* II
DCR9374	*unc-17::mRuby FLP-on(syb7882)* IV 2X outcrossed
DCR9989	*unc-17::mRuby FLP-on(syb7882)* IV; *Peft-3::FLP (sybIs9614)* II
PHX7239	*cat-1::gfp11x3(syb7239)* X
DCR9370	*cat-1::gfp11x3(syb7239)* X 2X outcrossed
DCR9338	*cat-1::gfp11x3(syb7239)* X*; olaEx5516[Psrh-142::GFP1-10; Psrh-142::BFP; Punc-122::RFP]*
RB681	*cat-1(ok411)*
DCR9837	*muIs253* [P*eft-3*::GFP1-10::*unc-54* 3'UTR + *Cbr-unc-119*(+)] II; *unc-119(ed3)* III *cat-1::GFP11x3(syb7239) X*
DCR9414	*cat-1(ky1101 ky1118)* X 2X outcrossed
DCR9736	*Psrh-142::FLP (syb9159) II* 2X outcrossed
DCR9912	*Psrh-142::FLP (syb9159) II; cat-1(ky1101 ky1118)* X
DCR9342	*unc-17::GFP FLP-on(ola503)* IV*; unc-13::mScarlet FLP-on (wy1322)* I*; vlcSi1[unc-119(+); Psrh-142::Flippase]* III
DCR9574	*unc-17::mRuby FLP-on(syb7882)* IV; *cat-1::gfp11x3(syb7239)* X; *olaIs153 [Psrh-142::GFP1-10; Psrh-142::FLP; Punc-122::RFP]*
DCR9588	*unc-104(e1265)* II*; unc-17::mRuby FLP-on(syb7882)* IV; *cat-1::gfp11x3(syb7239)* X; *olaEx5548[Psrh-142::Flippase; Psrh142::GFP1-10; Punc-122::RFP]*
DCR9448	*cat-1::gfp11x3(syb7239)* X*; unc-13::mScarlet FLP-on (wy1322)* I*; olaEx5550[Psrh-142::Flippase; Psrh142::GFP1-10; Punc-122::RFP]*
DCR9583	*bas-1*(*syb5923*[*bas-1*::SL2::GFP::H2B]) III; *olaex5513* [P*srh-142*::BFP; P*unc-122*::RFP]
DCR9590	*mod-5*(*vlc47*[*mod-5*::T2A::mNeonGreen]); *olaex5513* [P*srh-142*::BFP; P*unc-122*::RFP]
DCR9577	*eat-4(kySi76 kySi77)* III [*eat-4* cell-specific KO]; *unc-17(syb8059)* IV [Flippase expression in *unc-17* locus]
DCR9584	*eat-4(kySi76 kySi77)* III [*eat-4* cell-specific KO]; *unc-47(syb8125)* III [Flippase expression in *unc-47* locus]

DCR9371	*eat-4(kySi76 kySi77)* III [*eat-4* cell-specific KO]; *bqSi614* IV [P*dat-1*::Flippase]
DCR9334	*eat-4(kySi76 kySi77)* III [*eat-4* cell-specific KO]; *bqSi488* IV [P*tph-1*::Flippase]
DCR9576	*unc-17::GFP FLP-on(ola503)* IV [*unc-17* cell-specific GFP knock-in]; *unc-47(syb8125)* III [Flippase expression in *unc-47* locus]
DCR9344	*unc-17::GFP FLP-on(ola503)* IV [*unc-17* cell-specific GFP knock-in]; *bqSi488* IV [P*tph-1*::Flippase] recombinant
DCR9897	*unc-17::GFP FLP-on(ola503)* IV [*unc-17* cell-specific GFP knock-in]; *bqSi614* IV [P*dat-1*::Flippase]

List of plasmids

Plasmid name	**Genotype**
DACR218	P*unc-122::RFP*
DACR704	P*myo-2*::mCherry
DACR4016	P*sto-3b::BFP*
DACR4027	P*unc-17*::UNC-17cDNA
DACR4033	P*unc-17*::UNC-17cDNA::GFP in TM6-7
DACR4038	P*unc-17*::GFP::UNC-17cDNA
DACR4064	P*sto-3b::GFP1-10*
DACR4078	*Psrh-142::*BFP
DACR4083	*Psrh-142::*Flippase
DCR4092	P*srh-142*::GFP1-10
pSH87	P*flp-13::*GFP1-10

ACKNOWLEDGEMENTS

We thank Nuria Flames Bonilla (Instituto de Biomedicina de Valencia, Spain), Rafa Alis (Instituto de Biomedicina de Valencia, Spain), Steven Flavell (MIT), and Yung-Chi Huang (MIT) for sharing reagents and constructs. We thank James Rand, Oliver Hobert (Columbia University) and Chen Wang (Columbia University) for sharing unpublished observations. We thank Ian Gonzalez for the creation of the name for this toolkit. We thank members of the Colón-Ramos Lab for feedback on figures and the manuscript. We also thank Stacy Wilson for technical support and training using

the AiryScan imaging set-up as part of the Yale Neuroscience Imaging Core Facility. We also thank Emerson Santiago, member of the Koelle Lab (Yale University), for expert advice on assays of serotonin function. Some strains were provided by the CGC, which is funded by NIH Office of Research Infrastructure Programs (P40 OD010440). Some figures were created in https://BioRender.com. This work was supported by National Institutes of Health grants to DC-R (R35NS132156 and R01NS076558) and to AW (K99AG083129), to EMJ (R01 NS034307), and to MLS (F32GM133139). The Pew Latin American Fellowship to ACC (AWD0006561), the Jane Coffin Childs Fellowship to ACC (AWD0006564), the HHMI Hanna Gray Fellowship to ACC (GT15993), and the Chan Zuckerberg Initiative to CIB.

FUNDING

ACC was supported by The Pew Foundation, the Jane Coffins Child, HHMI-HGF
AW was supported by K99AG083129
DC-R, PC-L and MT were supported by R35NS132156 and R01NS076558
MLS was supported by F32GM133139
EMJ was supported by R01 NS034307, R01 GM095817, and HHMI
MB, MSE, LF and CB were supported by a grant from the Chan Zuckerberg Initiative.

ORCID

Cuentas-Condori: 0000-0002-4847-0031
Feng: 0000-0003-4601-4224
Wolfe: 0000-0002-4926-5064
Schwartz: 0000-0002-5542-9109
Brown: 0000-0003-0547-6545
Ebert: 0000-0002-9122-7854
Jorgensen: 0000-0002-2978-8028
Bargmann: 0000-0002-8484-0618
Colón-Ramos: 0000-0003-0223-7717

REFERENCES

Abramson, J., Adler, J., Dunger, J., Evans, R., Green, T., Pritzel, A.,...Jumper, J. M. (2024). Accurate structure prediction of biomolecular interactions with AlphaFold 3. *Nature*, *630*(8016), 493-500. https://doi.org/10.1038/s41586-024-07487-w

Ahier, A., & Jarriault, S. (2014). Simultaneous expression of multiple proteins under a single promoter in Caenorhabditis elegans via a versatile 2A-based toolkit. *Genetics*, *196*(3), 605-613. https://doi.org/10.1534/genetics.113.160846

Albertson, D. G., & Thomson, J. N. (1976). The pharynx of Caenorhabditis elegans. *Philos Trans R Soc Lond B Biol Sci*, *275*(938), 299-325. https://doi.org/10.1098/rstb.1976.0085

Alfonso, A., Grundahl, K., Duerr, J. S., Han, H.-P., & Rand, J. B. (1993). The Caenorhabditis unc-17 gene: A putative vesicular acetylcholine transporter. *Science*, *261*.

Aubrey, K. R., Rossi, F. M., Ruivo, R., Alboni, S., Bellenchi, G. C., Le Goff, A.,...Supplisson, S. (2007). The transporters GlyT2 and VIAAT cooperate to determine the vesicular glycinergic phenotype. *J Neurosci*, *27*(23), 6273-6281. https://doi.org/10.1523/JNEUROSCI.1024-07.2007

Bajar, B. T., Wang, E. S., Lam, A. J., Kim, B. B., Jacobs, C. L., Howe, E. S.,...Chu, J. (2016). Improving brightness and photostability of green and red fluorescent proteins for live cell imaging and FRET reporting. *Sci Rep*, *6*, 20889. https://doi.org/10.1038/srep20889

Bargmann, C. I., & Horvitz, R. H. (1991). Chemosensory neurons with overlapping functions direc chemotaxis to multiple chemicals in C. elegans. *Neuron*, *7*.

Bellocchio, E. E., Hu, H., Pohorille, A., Chan, J., Pickel, V. M., & Edwards, R. H. (1998). The localization of the brain-specific inorganic phosphate transporter suggests a specific presynaptic role in glutamatergic transmission. *The journal of neuroscience*, *18*.

Bertuzzi, M., Chang, W., & Ampatzis, K. (2018). Adult spinal motoneurons change their neurotransmitter phenotype to control locomotion. *Proc Natl Acad Sci U S A*, *115*(42), E9926-E9933. https://doi.org/10.1073/pnas.1809050115

Brenner, S. (1973). The genetics of Caenorhabidits elegans. *Genetics*, *77*.

Chaudhry, F. A., Reimer, R. J., Bellocchio, E. E., Danbolt, N. C., Osen, K. K., Edwards, R. H., & Storm-Mathisen, J. (1998). The vesicular GABA transporter, VGAT, localizes to synaptic vesicles in sets of glycinergic as well as GABAergic neurons. *The journal of neuroscience*, *18*.

Chen, N., Zhang, Y., Rivera-Rodriguez, E. J., Yu, A. D., Hobin, M., Rosbash, M., & Griffith, L. C. (2023). Widespread posttranscriptional regulation of cotransmission. *Sci Adv*, *9*(22), eadg9836. https://doi.org/10.1126/sciadv.adg9836

Crank, J. (1956). *The Mathematics of Diffusion*.

Crawford, D. C., & Kavalali, E. T. (2015). Molecular underpinnings of synaptic vesicle pool heterogeneity. *Traffic*, *16*(4), 338-364. https://doi.org/10.1111/tra.12262

Dag, U., Nwabudike, I., Kang, D., Gomes, M. A., Kim, J., Atanas, A. A.,...Flavell, S. W. (2023). Dissecting the functional organization of the C. elegans serotonergic system at whole-brain scale. *Cell*, *186*(12), 2574-2592.e2520. https://doi.org/10.1016/j.cell.2023.04.023

Duerr, J. S., Frisby, D. L., Gaskin, J., Duke, A., Asermely, K., Huddleston, D.,...Rand, J. B. (1999). The cat-1 gene of Caenorhabditis elegans encodes a vesicular monoamine

transporter required for specific monoamine-dependent behaviors. *The journal of neuroscience*, *19*.

Duerr, J. S., Han, H. P., Fields, S. D., & Rand, J. B. (2008). Identification of major classes of cholinergic neurons in the nematode Caenorhabditis elegans. *J Comp Neurol*, *506*(3), 398-408. https://doi.org/10.1002/cne.21551

Edwards, R. H. (2007). The neurotransmitter cycle and quantal size. *Neuron*, *55*(6), 835-858. https://doi.org/10.1016/j.neuron.2007.09.001

Eiden, L. E. (1998). The cholinergic gene locus. *J Neurochem*, *70*(6), 2227-2240. https://doi.org/10.1046/j.1471-4159.1998.70062227.x

Erickson, J., Eiden, L. E., & Hoffman, B. J. (1992). Expression cloning of a reserpine-sensitive vesicular monoamine transporter. *Proceedings of the national academy of sciences of the United States of America*, *89*.

Fei, H., Grygoruk, A., Brooks, E. S., Chen, A., & Krantz, D. E. (2008). Trafficking of vesicular neurotransmitter transporters. *Traffic*, *9*.

Feng, L., Marquina-Solis, J., Yue, L., Harnagel, A., Greenfeld, Y., & Bargmann, C. I. (2025). *C. elegans* interprets dietary quality through context-dependent serotonergic modulation. *bioRxiv*. https://doi.org/https://doi.org/10.1101/2025.01.05.631367

Flavell, S. W., Pokala, N., Macosko, E. Z., Albrecht, D. R., Larsch, J., & Bargmann, C. I. (2013). Serotonin and the neuropeptide PDF initiates and extend opposing behavioral states in C. elegans. *Cell*, *154*.

Gendrel, M., Howell, E. G., & Hobert, O. (2016). A cellular and regulatory map of the GABAergic nervous system of C. elegans. *eLIFE*, *5*.

Gouwens, N. W., Sorensen, S. A., Baftizadeh, F., Budzillo, A., Lee, B. R., Jarsky, T.,...Zeng, H. (2020). Integrated Morphoelectric and Transcriptomic Classification of Cortical GABAergic Cells. *Cell*, *183*(4), 935-953.e919. https://doi.org/10.1016/j.cell.2020.09.057

Granger, A. J., Wallace, M. L., & Sabatini, B. L. (2017). Multi-transmitter neurons in the mammalian central nervous system. *Curr Opin Neurobiol*, *45*, 85-91. https://doi.org/10.1016/j.conb.2017.04.007

Hall, D. H., & Hedgecock, E. M. (1991). Kinesin-related gene unc-104 is required for axonal transport of synaptic vesicles in C. elegans. *Cell*, *65*.

Hawk, J. D., Calvo, A. C., Liu, P., Almoril-Porras, A., Aljobeh, A., Torruella-Suárez, M. L.,...Colón-Ramos, D. A. (2018). Integration of Plasticity Mechanisms within a Single Sensory Neuron of C. elegans Actuates a Memory. *Neuron*, *97*(2), 356-367.e354. https://doi.org/10.1016/j.neuron.2017.12.027

He, S., Cuentas-Condori, A., & Miller, D. M. (2019). NATF (Native and Tissue-specific fluorescence: A strategy for bright, tissue-specific GFP labeling of native proteins in Caenorhabditis elegans. *Genetics*, *212*.

Huang, Y.-C., Luo, J., Huang, W., Baker, C. M., Gomez, M. A., Meng, B.,...Flavell, S. W. (2023). A single neuron in C. elegans orchestrates multiple motor outputs through parallel modes of transmission. *Current Biology*, *33*.

Juge, N., Omote, H., & Moriyama, Y. (2013). Vesicular GABA transporter (VGAT) transports β-alanine. *J Neurochem*, *127*(4), 482-486. https://doi.org/10.1111/jnc.12393

Jumper, J., Evans, R., Pritzel, A., Green, T., Figurnov, M., Ronneberger, O.,...Hassabis, D. (2021). Highly accurate protein structure prediction with AlphaFold. *Nature*, *596*(7873), 583-589. https://doi.org/10.1038/s41586-021-03819-2

Kamalova, A., & Nakagawa, T. (2021). AMPA receptor structure and auxiliary subunits. *J Physiol*, *599*(2), 453-469. https://doi.org/10.1113/jp278701

Koonce, N. L., Emerson, S. E., Bhaskar, D., Kuchroo, M., Moyle, M. W., Arroyo-Morales, P.,...Colón-Ramos, D. (2025). NeuroSC: Exploring Neurodevelopment via Spatiotemporal Collation of Anatomical Networks. *bioRxiv*. https://doi.org/10.1101/2024.08.27.609993

Koonce, N. L., Emerson, S. E., Dhananjay, B., Kuchroo, M., Moyle, M. W., Arroyo-Morales, P.,...Colon-Ramos, D. (2024). NeuroSCAN: Exploring neurodevelopment via spatiotemporal collation of anatomical networks. *bioRxiv*.

Kumar, S., Sharma, A. K., & Leifer, A. M. (2024). An inhibitory acetylcholine receptor gates context-dependent mechanosensory processing in. *iScience*, *27*(10), 110776. https://doi.org/10.1016/j.isci.2024.110776

Lacin, H., Chen, H. M., Long, X., Singer, R. H., Lee, T., & Truman, J. W. (2019). Neurotransmitter identity is acquired in a lineage-restricted manner in the. *eLIFE*, *8*. https://doi.org/10.7554/eLife.43701

Lee, R. Y., Sawin, E. R., Chalfie, M., Horvitz, R. H., & Avery, L. (1999). EAT-4, homolog of a mammalian sodium-dependent inorganic phosphate co-transporter, is necessary for glutamatergic neurotransmission in Caenorhabditis elegans. *The journal of neuroscience*, *19*.

Lee, S., Kim, K., & Zhou, Z. J. (2010). Role of ACh-GABA cotransmission in detecting image motion and motion direction. *Neuron*, *68*(6), 1159-1172. https://doi.org/10.1016/j.neuron.2010.11.031

Li, H. Q., Jiang, W., Ling, L., Pratelli, M., Chen, C., Gupta, V.,...Spitzer, N. C. (2024). Generalized fear after acute stress is caused by change in neuronal cotransmitter identity. *Science*, *383*(6688), 1252-1259. https://doi.org/10.1126/science.adj5996

Li, H. Q., Pratelli, M., Godavarthi, S., Zambetti, S., & Spitzer, N. C. (2020). Decoding Neurotransmitter Switching: The Road Forward. *J Neurosci*, *40*(21), 4078-4089. https://doi.org/10.1523/JNEUROSCI.0005-20.2020

Liu, C., Goel, P., & Kaeser, P. S. (2021). Spatial and temporal scales of dopamine transmission. *Nat Rev Neurosci*, *22*(6), 345-358. https://doi.org/10.1038/s41583-021-00455-7

Lopez-Cruz, A., Sordillo, A., Pokala, N., Liu, Q., McGrath, P. T., & Bargmann, C. I. (2019). Parallel multimodal circuits control an innate foraging behavior. *Neuron*, *102*.

Maddaloni, G., Chang, Y. J., Senft, R. A., & Dymecki, S. M. (2024). Adaptation to photoperiod via dynamic neurotransmitter segregation. *Nature*, *632*(8023), 147-156. https://doi.org/10.1038/s41586-024-07692-7

Maicas, M., Jimeno-Martin, A., Millan-Trejo, A., Alkema, M. J., & Flames, N. (2021). The transcription factor LAG-1/CSL plays a Notch-independent role in controlling terminal differentiation, fate maintenance, and plasticity of serotonergic chemosensory neurons. *PLoS Biology*, *19*.

874 Marquina-Solis, J., Feng, L., Vandewyer, E., Beets, I., Hawk, J., Colon-Ramos,
875 D.,...Bargmann, C. I. (2024). Antagosnism between neuropeptides and monoamines
876 in a distributed circuit for pathogen avoidance. *Cell Reports*, *43*.
877 Martens, H., Weston, M. C., Boulland, J.-L., Gronborg, M., Grosche, J., Kacza, J.,...Hartig, W.
878 (2008). Unique luminal localization of VGAT-C terminus allows for selective labeling
879 of active cortical GABAergic synapses. *The journal of neuroscience*, *28*.
880 Mathews, E. A., Mullen, G. P., Manjarrez, J. R., & Rand, J. B. (2015). Unusual regulation of
881 splicing of the cholinergic locus in Caenorhabditis elegans. *Genetics*, *199*.
882 McIntire, S. L., Jorgensen, E., & Horvitz, R. H. (1993). Genes required for GABA function in
883 Caenorhabditis elegans. *Nature*, *364*.
884 McIntire, S. L., Jorgensen, E., Kaplan, J., & Horvitz, R. H. (1993). The GABAergic nervous
885 system of Caenorhabditis elegans. *Nature*, *364*.
886 McIntire, S. L., Reimer, R. J., Schuske, K., Edwards, R. H., & Jorgensen, E. (1997).
887 Identification and characterization of the vesicular GABA transporter. *Nature*, *389*.
888 Morrie, R. D., & Feller, M. B. (2015). An Asymmetric Increase in Inhibitory Synapse Number
889 Underlies the Development of a Direction Selective Circuit in the Retina. *J Neurosci*,
890 *35*(25), 9281-9286. https://doi.org/10.1523/JNEUROSCI.0670-15.2015
891 Mullen, G. P., Mathews, E. A., Saxena, P., Fields, S. D., McManus, J. R., Moulder, G.,...Rand,
892 J. B. (2006). The Caenorhabditis elegans snf-11 gene encodes a sodium-dependent
893 GABA transporter required for clearance of synaptic GABA. *Mol Biol Cell*, *17*(7), 3021-
894 3030. https://doi.org/10.1091/mbc.e06-02-0155
895 Muñoz-Jiménez, C., Ayuso, C., Dobrzynska, A., Torres-Mendéz, A., Ruiz, P. C., & Askjaer, P.
896 (2017). An Efficient FLP-Based Toolkit for Spatiotemporal Control of Gene Expression
897 in. *Genetics*, *206*(4), 1763-1778. https://doi.org/10.1534/genetics.117.201012
898 Nguyen, J. P., Shipley, F. B., Linder, A. N., Plummer, G. S., Liu, M., Setru, S. U.,...Leifer, A. M.
899 (2016). Whole-brain calcium imaging with cellular resolution in freely behaving
900 Caenorhabditis elegans. *Proc Natl Acad Sci U S A*, *113*(8), E1074-1081.
901 https://doi.org/10.1073/pnas.1507110112
902 O'Malley, D. M., Sandell, J. H., & Masland, R. H. (1992). Co-release of acetylcholine and
903 GABA by the starburst amacrine cells. *J Neurosci*, *12*(4), 1394-1408.
904 https://doi.org/10.1523/JNEUROSCI.12-04-01394.1992
905 Pei, J., & Grishin, N. V. (2001). AL2CO: calculation of positional conservation in a protein
906 sequence alignment. *Bioinformatics*, *17*(8), 700-712.
907 https://doi.org/10.1093/bioinformatics/17.8.700
908 Pereira, L., Aeschimann, F., Wang, C., Lawson, H., Serrano-Saiz, E., Portman, D.
909 S.,...Hobert, O. (2019). Timing mechanism of sexually dimorphic nervous system
910 differentiation. *Elife*, *8*. https://doi.org/10.7554/eLife.42078
911 Pereira, L., Kratsios, P., Serrano-Saiz, E., Sheftel, H., Mayo, A. E., H., H. D.,...Hobert, O.
912 (2015). A cellular and regulatory map of the cholinergic nervous system of C. elegans.
913 *eLIFE*, *4*.
914 Pettersen, E. F., Goddard, T. D., Huang, C. C., Meng, E. C., Couch, G. S., Croll, T. I.,...Ferrin,
915 T. E. (2021). UCSF ChimeraX: Structure visualization for researchers, educators, and
916 developers. *Protein Sci*, *30*(1), 70-82. https://doi.org/10.1002/pro.3943

Pierce-Shimomura, J. T., Morse, T. M., & Lockery, S. R. (1999). The fundamental role of pirouettes in Caenorhabditis elegans chemotaxis. *J Neurosci*, *19*(21), 9557-9569. https://doi.org/10.1523/JNEUROSCI.19-21-09557.1999

Pocock, R., & Hobert, O. (2010). Hypoxia activates a latent circuit for processing gustatory information in C. elegans. *Nat Neurosci*, *13*(5), 610-614. https://doi.org/10.1038/nn.2537

Prevedel, R., Yoon, Y. G., Hoffmann, M., Pak, N., Wetzstein, G., Kato, S.,...Vaziri, A. (2014). Simultaneous whole-animal 3D imaging of neuronal activity using light-field microscopy. *Nat Methods*, *11*(7), 727-730. https://doi.org/10.1038/nmeth.2964

Robinson RA, S. R. (1959). *Electrolyte Solutions*.

Roghani, A., Feldman, J., Kohan, S. A., Shirzadi, A., Gundersen, C. B., Brecha, N., & Edwards, R. H. (1994). Molecular cloning of a putative vesicular transporter for acetylcholine. *Proceedings of the national academy of sciences of the United States of America*, *91*.

Santos, M., Park, K. C., Foss, S. M., & Voglmaier, S. M. (2013). Sorting of the vesicular GABA transporter to functional vesicle pools by an atypical dileucine-like motif. *The journal of neuroscience*, *33*.

Sato, H., Kunitomo, H., Fei, X., Hashimoto, K., & Lino, Y. (2021). Glutamate signaling from a single sensory neuron mediates experience-dependent bidirectional behavior in Caenorhabditis elegans. *Cell Reports*, *35*.

Scheffer, L. K., Xu, C. S., Januszewski, M., Lu, Z., Takemura, S. Y., Hayworth, K. J.,...Plaza, S. M. (2020). A connectome and analysis of the adult Drosophila central brain. *Elife*, *9*. https://doi.org/10.7554/eLife.57443

Schindelin, J., Arganda-Carreras, I., Frise, E., Kaynig, V., Longair, M., Pietzsch, T.,...Cardona, A. (2012). Fiji: an open-source platform for biological-image analysis. *Nat Methods*, *9*(7), 676-682. https://doi.org/10.1038/nmeth.2019

Schrödel, T., Prevedel, R., Aumayr, K., Zimmer, M., & Vaziri, A. (2013). Brain-wide 3D imaging of neuronal activity in Caenorhabditis elegans with sculpted light. *Nat Methods*, *10*(10), 1013-1020. https://doi.org/10.1038/nmeth.2637

Schwartz, M. L., & Jorgensen, E. (2016). SapTrap, a toolkit for high-throughput CRISPR/Cas9 gene modification in Caenorhabditis elegans. *Genetics*, *202*.

Seggewisse, A., & Winding, M. (2024). Mapping the fly nerve cord. *Elife*, *13*. https://doi.org/10.7554/eLife.99804

Serrano-Saiz, E., Pereira, L., Gendrel, M., Aghayeva, U., Bhattacharya, A., Howell, K.,...Hobert, O. (2017). A neurotransmitter atlas of the Caenorhabditis elegans male nervous system reveals sexually dimorphic neurotransmitter usage. *Genetics*, *206*.

Serrano-Saiz, E., Poole, R. J., Felton, T., Zhang, F., De la Cruz, E. D., & Hobert, O. (2013). Modula control of glutamateric neuronal identity in C. elegans by distinct homeodomain proteins. *Cell*, *155*.

Seydoux, G., & Fire, A. (1994). Soma-germline asymmetry in the distributions of embryonic RNAs in Caenorhabditis elegans. *Development*, *120*(10), 2823-2834. https://doi.org/10.1242/dev.120.10.2823

Silm, K., Yang, J., Marcott, P. F., Asensio, C. S., Eriksen, J., Guthrie, D. A.,...Edwards, R. H. (2019). Synaptic Vesicle Recycling Pathway Determines Neurotransmitter Content

and Release Properties. *Neuron*, *102*(4), 786-800.e785. https://doi.org/10.1016/j.neuron.2019.03.031

Sitko, A. A., Frank, M. M., Romero, G. E., Hunt, M., & Goodrich, L. V. (2025). Lateral olivocochlear neurons modulate cochlear responses to noise exposure. *Proc Natl Acad Sci U S A*, *122*(4), e2404558122. https://doi.org/10.1073/pnas.2404558122

Sulston, J. E., & Horvitz, H. R. (1977). Post-embryonic cell lineages of the nematode, Caenorhabditis elegans. *Dev Biol*, *56*(1), 110-156. https://doi.org/10.1016/0012-1606(77)90158-0

Sulston, J. E., Schierenberg, E., White, J. G., & Thomson, J. N. (1983). The embryonic cell lineage of the nematode Caenorhabditis elegans. *Dev Biol*, *100*(1), 64-119. https://doi.org/10.1016/0012-1606(83)90201-4

Südhof, T. C. (2021). The cell biology of synapse formation. *J Cell Biol*, *220*(7). https://doi.org/10.1083/jcb.202103052

Taylor, S. R., Santpere, G., Weinreb, A., Barrett, A., Reilly, M. B., Xu, C.,...Miller, D. M., 3rd. (2021). Molecular topography of an entire nervous system. *Cell*, *184*(16), 4329-4347.e4323. https://doi.org/10.1016/j.cell.2021.06.023

Trudeau, L.-E., & El Mestikawy., S. (2018). Glutamate cotransmission in cholinergic, GABAergic and monoamine systems: Contrasts and commonalities. *Frontiers in neural circuits*, *12*.

Uchida, O., Nakano, H., Koga, M., & Ohshima, Y. (2003). The C. elegans che-1 gene encondes a zinc finger trnascription factor required for specification of the ASE chemosensory neurons. *Development*, *130*.

Vaaga, C. E., Borisovska, M., & Westbrook, G. L. (2014). Dual-transmitter neurons: functional implications of co-release and co-transmission. *Curr Opin Neurobiol*, *29*, 25-32. https://doi.org/10.1016/j.conb.2014.04.010

Wang, C., Vidal, B., Sural, S., Loer, R. G., Merritt, D. M., Toker, I. A.,...Hobert, O. (2024). A neurotransmitter atlas of C. elegans males and hermaphrodites. *eLIFE*.

Ward, S. (1973). Chemotaxis by the nematode Caenorhabditis elegans: identification of attractants and analysis of the response by use of mutants. *Proc Natl Acad Sci U S A*, *70*(3), 817-821. https://doi.org/10.1073/pnas.70.3.817

White, J. G., Southgate, E., Thomson, J. N., & Brenner, S. (1986). The structure of the nervous system of the nematode Caenorhabditis elegans. *philosophical Transactions of the Royal Society of London*, *314*.

Wu, J. S., Yi, E., Manca, M., Javaid, H., Lauer, A. M., & Glowatzki, E. (2020). Sound exposure dynamically induces dopamine synthesis in cholinergic LOC efferents for feedback to auditory nerve fibers. *eLIFE*, *9*. https://doi.org/10.7554/eLife.52419

Wu, X., & Hammer, J. A. (2021). ZEISS Airyscan: Optimizing Usage for Fast, Gentle, Super-Resolution Imaging. *Methods Mol Biol*, *2304*, 111-130. https://doi.org/10.1007/978-1-0716-1402-0_5

Yi, Y., Li, Y., Zhang, S., Men, Y., Wang, Y., Jing, D.,...Zhao, H. (2024). Mapping of individual sensory nerve axons from digits to spinal cord with the transparent embedding solvent system. *Cell Res*, *34*(2), 124-139. https://doi.org/10.1038/s41422-023-00867-3

1003 Yu, C. Y., & Chang, H. C. (2022). Glutamate signaling mediates C. elegans behavioral
1004 plasticity to pathogens. *iScience*, *25*(3), 103919.
1005 https://doi.org/10.1016/j.isci.2022.103919
1006

1007 **Table 2 – List of potential co-transmitter neurons by neuronal type**

pharyngeal neurons	sensory neurons	interneurons	motor neurons
I2L	ADFL	AIML	HSNL
I5	ADFR	AIMR	HSNR
M4	AFDL	RIH	SMDDL
M5	AFDR	PVNL	SMDDR
MI	URXL	PVNR	SMDVL
	URXR	RIML	SMDVR
	SDQR	RIMR	VC04
	DVA	RICL	VC05
	PDEL	RICM	
	PDER		

1008

1009 **Table 3 – List of potential co-transmitter neurons reported by at least more than one study**

Co-transmitter neurons	Suggested by CenGEN expression data?*	Consistent with previous reports:	Combination suggested
ADF	Yes	Pereira et al. (2015), Wang et al. (2024) & this study	Serotonin + acetylcholine
AFD	Yes	Wang et al. (2024) & this study	Acetylcholine + glutamate
AIM	No	Jafari et al. (2011), Serrano-Saiz et al. (2013), Wang et al. (2024)	Serotonin + glutamate
DVA	Yes	Wang et al. (2024) & this study	Acetylcholine + glutamate
HSN	Yes	Duerr et al. (2001), Wang et al. (2024) & this study	Serotonin + acetylcholine
I2L	No	Wang et al. (2024) & this study	glutamate + UNC-47-dependent NT
I5	No	Jafari et al. (2011), Serrano-Saiz et al. (2013), Wang et al. (2024)	Serotonin + glutamate
M4	No	Wang et al. (2024) & this study	acetylcholine + UNC-47-dependent NT
M5	Yes	Wang et al. (2024) & this study	Acetylcholine + glutamate
MI	Yes	Serrano-Saiz et al. (2013), Wang et al. (2024)	Serotonin + glutamate
PDE	No	Wang et al. (2024) & this study	dopamine + glutamate
PVN	Yes	Wang et al. (2024) & this study	Acetylcholine + glutamate

RIC	Yes	Reilly et al. (2022), Wang et al. (2024)	glutamate + octopamine
RIH	Yes	Jafari et al. (2011), Wang et al. (2024)	Serotonin + acetylcholine
RIM	Yes	Alkema et al. (2005), Serrano-Saiz et al. (2013), Wang et al. (2024)	Glutamate + tyramine
SDQR	Yes	Wang et al. (2024) & this study	acetylcholine + UNC-47-dependent NT
SMD	Yes	Gendrel et al. (2016) & this study	GABA + acetylcholine
URX	No	Jafari et al. (2011), Wang et al. (2024)	Serotonin + acetylcholine
VC04	Yes	Duerr et al. (2001), Wang et al. (2024) & this study	Serotonin + acetylcholine
VC05	Yes	Duerr et al. (2001), Wang et al. (2024) & this study	Serotonin + acetylcholine

**Determined with threshold of 1*

Table 4 – List of neurons inconsistent across studies to suggest co-transmission capacity

Previously suggested:	Co-transmitter combination suggested	Reported by:	*cha-1*	*unc-17*	*unc-25*	*unc-47*	*unc-46*
RIB	GABA + acetylcholine	Gendrel et al. (2016)			X	X	X
AVB	GABA + acetylcholine	Gendrel et al. (2016)	X	X			X
AVA	GABA + acetylcholine	Gendrel et al. (2016)	X	X			

	Maximum CenGEN threshold that shows expression of each gene
4	X
3	X
2	X
1	X

1015 **FIGURE LEGENDS**

1016

1017 **Figure 1 - Endogenous fluorescence labeling of synaptic vesicle transporters**

1018 (Left) FLP-on and (Right) split GFP strategies to endogenously label synaptic vesicle transporters.
1019 **(A)** Cartoon representation of the CRISPR-engineered worm in the endogenous locus of the
1020 target synaptic vesicle gene. **(B)** Cell-specific driver that expresses (Left) Flippase or (Right)
1021 GFP1-10. **(C)** Resulting tagged synaptic vesicle proteins with a (Left) full-length GFP or mRuby3
1022 or (Right) by reconstituting GFP in the cell of interest. **(D)** Schematic of the resulting toolkit to label
1023 and eliminate the endogenous machinery that packages or synthesizes glutamate, GABA,
1024 acetylcholine and monoamines.

1025

1026 **Figure 2 – Probing glutamatergic transmission in *C. elegans***

1027 **(A)** Predicted protein structure (using AlphaFold Protein Structure Database) of EAT-4 (cyan)
1028 tagged with GFP (green) (Abramson et al., 2024). The last amino acid in the C-terminus end
1029 (W576) corresponds to the tagged residue. **(B)** Schematic of the Vesicular Glutamate Transporter
1030 (VGLUT/*eat-4*) gene structure, loss of function allele (*ky5*) and endogenously tagged versions
1031 built for this study and by others. *eat-4* (*ky5*) mutants lack the first three exons. For cell-specific
1032 knock-in (KI) tools, GFP (*syb8568*) and mRuby (*syb9193*) FLP-ON cassettes (Schwartz &
1033 Jorgensen, 2016) were inserted before the STOP codon. To cell-specifically knock out (KO) *eat-*
1034 *4*, two FRT sites flank the coding sequence of the *eat-4* gene (*kySi76 kySi77*) (Lopez-Cruz et al.,
1035 2019). When recombination takes place, the *eat-4* coding sequence is removed and cytosolic
1036 mCherry is inserted in-frame to be expressed as a proxy for *eat-4* sequence removal. **(C)**
1037 Mutations in the *che-1* (prevents ASE development (Uchida et al., 2003)) (17.42 ± 7.7 mm) or *eat-*
1038 *4* gene (13.15 ± 4 mm) results in disrupted migration across the salt gradient. Wild-type animals
1039 (7.76 ± 5.2 mm) migrate across the salt gradient similarly to EAT-4::GFP FLP-on (*syb*8568)
1040 animals that express (7.6 ± 3.6 mm) or not (4.9 ± 4.3 mm) flippase pan-cellularly (*sybIs9614*).
1041 Animals that express flippase in all cells (5.61 ± 3.9 mm) migrate across the salt gradient as a
1042 wild-type animals. Results represent the mean distance of each worm from the salt peak,
1043 averaged across the final minute of the assay, with each dot representing a single animal. Plots
1044 are overlaid with Mean ± Standard Deviation. Kruskal-Wallis test with Dunn's multiple comparison
1045 post hoc test. **** represents $p<0.0001$; *** represents $p<0.001$ and NS means "not significant".
1046 **(D)** (Top) Fluorescent image of an adult worm expressing endogenously labeled EAT-4 with GFP
1047 in all cells (P*eft-3*::Flippase). Scale Bar = 50μm. (Bottom) Zoom-in area of the head shows EAT-

1048 4 expressed predominantly in the nerve ring. Scale Bar = 10μm. **(E)** (Left) Electron microscopy
1049 rendering of ASE synapses in an L4 wild-type animal (White et al., 1986) (image generated with
1050 NeuroSC (Koonce et al., 2025). (Right) Fluorescent image of endogenously tagged EAT-4 protein
1051 cell-specifically in the ASE axons (P*flp-6*::Flippase). Scale Bar = 10μm.
1052
1053 **Figure S1**
1054 **(A)** Graphical representation of conservation of the amino acid predicted structure for the
1055 Vesicular Glutamate Transporter across common model organisms (named in Figure S1B). Dark
1056 colors denote the least conserved region, while clear colors denote the highest conservation. Note
1057 the C-terminus end, where we introduced the GFP, is one of the darkest (least conserved) regions
1058 in the structure. **(B)** Sequence alignment of the amino acid sequences for the Vesicular Glutamate
1059 Transporter across common model organisms. Blue letters indicate conservation of the amino
1060 acid properties (basic, acid, neutral) but not identities. Gray represents columns with gaps and no
1061 conservation.
1062 **(C)** Schematic of chemotaxis assay. (Top) A concentration gradient of NaCl (~60-85 mM) is
1063 established on assay plates (blue rim) by adding high concentration NaCl drops to the outer point
1064 of the assay plate at pre-determined times (See Methods). (Bottom) Larva stage 4 animals are
1065 picked, and twenty-four hours later, the young adult animals are transferred to NaCl 100mM
1066 training plates (red rim) for five hours. Animals are transferred to NGM buffer drops to wash off
1067 bacteria, before being placed on the assay plates (blue rim, placement at blue dot in schematic),
1068 where animal movement away from the highest [NaCl] is recorded (towards red dot in schematic).
1069 **(D)** Displacement of trained wild type animals on a sham gradient (13.92 ± 5.3 mm) or untrained
1070 wild-type animals on a gradient of NaCl (13.84 ± 5.4 mm). Wild-type animals (7.76 ± 5.2 mm)
1071 migrate across the salt gradient like EAT-4::GFP FLP-on (*syb8568*) animals that express (8.36 ±
1072 5.8 mm) flippase in ASE neurons (*sybIs9606*). Animals that only express flippase in ASE neurons
1073 (7.61 ± 5.3 mm) migrate across the salt gradient similar to wild-type animals. Results represent
1074 the mean distance of each worm from the salt peak, averaged across the final minute of the assay,
1075 with each dot representing an individual animal. Plots are overlaid with Mean ± Standard
1076 Deviation. Kruskal-Wallis test with Dunn's multiple comparison post hoc test. **** represents
1077 $p<0.0001$; *** represents $p<0.001$; * represents $p<0.05$; and NS means "not significant".
1078
1079 **Figure S2**
1080 Endogenous RAB-3::GFP synaptic vesicle clusters in the axonal process of ASER and ASEL.
1081

1082 **Figure 3 – Probing GABAergic transmission in *C. elegans***
1083 **(A)** UNC-47 predicted protein structure from AlphaFold Protein Structure Database. GFP11 tag
1084 (red) was added between amino acids E145 and N146. Complementary GFP1-10 (green) was
1085 modeled as bound to GFP11. **(B)** Schematics of the Vesicular GABA Transporter (VGAT/*unc-47*)
1086 loss of function allele and endogenously tagged versions built for this study. *unc-47(e307)* mutant
1087 animals have a single base pair substitution (G to A in the first nucleotide of exon 6) that results
1088 in a splicing acceptor mutant. Fluorescent tags GFP (*syb6990*) and mKate2 (*syb7358*) were
1089 inserted between amino acids E145 and N146. For cell-specific endogenous labeling, UNC-47
1090 was tagged with one (*syb7313*) or three copies (*syb7849*) of GFP11. To silence GABA
1091 transmission, we flanked the Glutamic Acid Decarboxylase/*unc-25* coding sequence with two FRT
1092 sites (*syb5949 syb6275*). Upon recombination, the *unc-25* coding sequence is removed and
1093 nuclear (black) mCherry (purple) is designed to be in-frame and expressed as a proxy for *unc-25*
1094 sequence removal. **(C)** (Top) Fluorescent image of an adult worm expressing endogenously
1095 labeled UNC-47 with reconstituted split-GFP in all cells (P*eft-3*::GFP1-10). Scale Bar = 50μm.
1096 (Bottom) Zoom-in area of the head shows UNC-47 expressed in the nerve ring and nerve cords.
1097 Scale Bar = 10μm. **(D)** (Left) Electron microscopy renderings of RIB synapses in an L4 wild-type
1098 animal (White et al., 1986) (image generated with NeuroSC (Koonce et al., 2025)). (Right) RIB-
1099 specific UNC-47 puncta (green) *in-vivo* using the UNC-47:GFP11 with reconstituted split-GFP in
1100 RIB (P*sto-3b*::GFP1-10) Scale Bar = 10μm. **(E)** *unc-47(e307)* mutant animals thrash significantly
1101 less per minute (30.8 ± 17) than wild-type animals (94.5 ± 10). Animals with non-reconstituted
1102 UNC-47::GFP11X3 (82.2 ± 9) (*syb7849*) thrash slightly less than wild-type animals (94.5 ± 10),
1103 while animals that express pan-cellular GFP1-10 (100.5 ± 9) (*muIs253*) are no different than wild-
1104 type animals. UNC-47::GFP11x3 animals that express Pan-cellular::GFP1-10 (with reconstituted
1105 GFP) (88.6 ± 7) thrash similarly to wild-type animals. FRT-flanked *unc-25* animals (*syb5949*
1106 *syb6275*) that do not express Flippase (95.8 ± 12) thrash similarly to wild-type animals (91 ± 8).
1107 Cell-specific *unc-25* knockout animals (*syb5949 syb6275*) that express Flippase in every neuron
1108 (*bqSi506*) (49.36 ± 19) thrash to the same extent as *unc-25* (*e156*) mutant animals (40.2 ± 19).
1109 Plots are overlaid with Mean ± Standard Deviation. Kruskal-Wallis test with Dunn's multiple
1110 comparison post hoc test. **** represents p<0.0001; *** represents p<0.001; and NS means "not
1111 significant".
1112
1113 **Figure S3**

1114 **(A)** Graphical representation of conservation of the Vesicular GABA Transporter amino acid
1115 predicted structure across common model organisms (named in Figure S2B). Dark colors denote
1116 the least conserved region, while clear colors denote the highest conservation. **(B)** Sequence
1117 alignment of the cytosolic loop between transmembrane domains 2 and 3 of the vesicular GABA
1118 transporter across common model organisms. Red letters indicate highly conserved columns
1119 (conservation of amino acid identity), and blue letters indicate conservation of the amino acid
1120 properties (basic, acid, neutral) but not identities. Gray represents columns with gaps. **(C)**
1121 Schematic of thrashing assay. "One thrash cycle" is scored when the animal bends as indicated
1122 in the schematic (from elongated-to-bent-to-elongated). We measured the number of thrashes
1123 per minute. **(D)** *unc-47(e307)* mutant animals thrash significantly less (41.5 ± 21.35) than wild-
1124 type animals (109.2 ± 23), while over-expression of UNC-47::GFP (100.2 ± 16), CRISPR knock-
1125 in UNC-47::GFP (107.9 ± 29) and UNC-47::mKate2 (103.1 ± 18) CRISPR-tagged animals thrash
1126 similarly to wild-type animals. Plots are overlaid with Mean ± Standard Deviation. Kruskal-Wallis
1127 test with Dunn's multiple comparison post hoc test. **** represents p<0.0001; *** represents
1128 p<0.001; ** represents p<0.01; * represents p<0.05; and NS means "not significant". **(E-F)**
1129 Fluorescent image of endogenously tagged **(E)** UNC-47::GFP (*syb6990*) and **(F)** UNC-
1130 47::mKate2 (*syb7358*). DNC = Dorsal Nerve Cord, VNC = Ventral Nerve Cord. Scale Bar = 10 μm.
1131
1132 **Figure S4**
1133 **(A)** All presynaptic sites from known GABAergic neurons in the *C. elegans* nerve ring (RIS, RME,
1134 and RIB), according to 3D electron microscopy of a Larva stage 4 (L4) wild-type animal (White et
1135 al., 1986) (image generated with NeuroSC (Koonce et al., 2025)). **(B)** 3D-rendering of UNC-
1136 47::GFP (green) puncta in the *C. elegans* nerve ring. A-P denotes anterior-posterior axis. Scale
1137 bar = 10 μm. **(C)** Addition of RIB::BFP into Figure S3B. Green arrowheads point to UNC-47::GFP
1138 puncta that overlap with RIB::BFP. Yellow arrowheads point to the synapses we interpret, based
1139 on our labeling and distribution, to belong to the RME neurons. **(D)** Endogenous mScarlet::RAB-
1140 3 in RIB highlight the characteristic shape of the RIB axon. **(E)** *In-vivo* reconstitution of UNC-
1141 47::GFP11x3 in DD neurons when tagged with (Top) one or (Bottom) three copies of GFP11 (P*flp-*
1142 *13*::GFP1-10) (He et al., 2019). **(F-G) (F)** Line scans and **(G)** quantification of reconstituted GFP
1143 fluorescence intensity with one (11.3 ± 6) or three copies (38.3 ± 28) of GFP11 in DD neurons.
1144 Scale bar = 10 μm. Plots are overlaid with Mean ± Standard Deviation. Mann-Whitney test. ****
1145 represents p<0.0001.
1146

1147 **Figure 4 – Probing cholinergic transmission in *C. elegans***

1148 **(A)** Predicted UNC-17 protein structure (magenta) tagged with GFP (green) on the last amino
1149 acid in the C-terminus end (W532). **(B)** Schematics of the Vesicular Acetylcholine Transporter
1150 (VACHT/*unc-17*) loss-of-function allele and endogenously tagged versions tested in this study
1151 (and built by others). *unc-17(e245)* mutant animals have a single base pair substitution in the third
1152 exon which leads to an amino acid change (arrowhead). Full-body knock-in animal labels UNC-
1153 17 with mKate (*ot907*). For cell-specific labeling, the N-terminus GFP FLP-ON cassette (*syb7251*)
1154 was inserted between amino acids P6 and V7 (See Methods). Similarly, the C-terminus GFP FLP-
1155 ON cassette (*ola503*) and mRuby FLP-on cassette (*syb7882*) were inserted before the STOP
1156 codon. **(C)** *unc-17(e245)* mutant animals (1.9 ± 2) thrash significantly less than wild-type animals
1157 (93 ± 10). UNC-17::GFP FLP-on (*ola503*) animals that express pan-cellular::Flippase (88 ± 1)
1158 (*sybIs9614*) or animals that only express pan-cellular::Flippase (94.8 ± 12) are indistinguishable
1159 from wild-type animals in their thrashing behavior. UNC-17::GFP FLP-on animals (98.7 ± 8) thrash
1160 significantly more than wild-type animals. Mean ± Standard Deviation. Brown-Forsythe ANOVA
1161 test with Dunnett's T3 multiple comparisons post hoc test. **** represents $p<0.0001$; * represents
1162 $p<0.05$; and NS means "not significant". **(D)** (Top) Fluorescent image of an adult worm expressing
1163 endogenously labeled UNC-17::GFP in all cells (P*eft-3*::Flippase). Scale Bar = 50μm. (Bottom)
1164 Zoom-in area of the head shows UNC-17 expressed in the nerve ring, nerve cords and sub-lateral
1165 cords. DNC = Dorsal Nerve Cord, VNC = Ventral Nerve Cord. Scale Bar = 10μm. **(E)** (Left)
1166 Electron microscopy rendering of ADF synapses in an L4 wild-type animal (White et al., 1986)
1167 (image generated with NeuroSC (Koonce et al., 2025). (Right) Fluorescence image of
1168 endogenously tagged UNC-17::GFP protein specifically in the ADF neuron. . Scale Bar = 10μm.
1169

1170 **Figure S5**

1171 **(A)** Graphical representation of the amino acid conservation of the Vesicular Acetylcholine
1172 Transporter (VAChT) across common model organisms. Dark colors denote the least conserved
1173 region, while clear colors denote the highest conservation. Note the C-terminus end is one of the
1174 darkest regions in the structure, where the fluorophore was added. **(B-C)** Amino acid sequence
1175 alignment of VAChT across model organisms. Black arrowhead points to insertion site of
1176 fluorescent tag. **(B)** Sequences between transmembrane domains 6 and 7, which was tagged in
1177 *olaEx5704* array (See panel E). **(C)** Sequence at the C-terminus end. Red letters indicate highly
1178 conserved columns (exact conservation of the amino acid identity), and blue indicates
1179 conservation of the amino acid properties (basic, acid, neutral) but not identities. Gray represents

areas of no conservation. **(D)** Fluorescence image of CRISPR-tagged UNC-17::mKate2 (*ot907*) animal. Scale Bar = 10μm. **(E)** Schematic of UNC-17 predicted topology (magenta) along the membrane (gray). Green represents the locations of fluorescent tags tested for thrashing assays. Alleles, either extrachromosomal arrays expressed in *unc-17* (*e245*) mutants or CRISPR knock-in strains in the *unc-17* locus, are listed based on where the fluorescent tag was inserted. **(F)** *unc-17(e245)* mutant animals barely swim (1.7 ± 2). Over-expression of untagged P*unc-17*::UNC-17 (*olaEx5703*) (114.8 ± 18) and N-terminus-tagged UNC-17::GFP (*olaEx5400*) (91.1 ± 22) swim like wild-type animals (99.4 ± 20). GFP-tag between TM6-7 (*olaEx5704*) (34.3 ± 19) or CRISPR-insertion of C-terminus mKate2 tag (*ot907*) (77.7 ± 17) leads to reduced swimming behavior when compared to wild-type animals. Insertion of GFP-FLP-on cassette at the N-terminus end (s*yb7251*) (82.9 ± 16) or insertion of the GFP-FLP-on cassette at the C-terminus (*ola503*) (101.9 ± 16) thrash as well as wild-type animals (109 ± 25). We are unsure as to the phenotypic differences of *ola503* allele and *ot907* in our thrashing assays, but note that in addition to the use of different fluorescent proteins, each allele also employs distinct linker sequences between UNC-17 and the fluorescent protein (new Figure S6). *syb7882* allele, which employes mRuby3 with a similar linker to *ola503*, also does not display defects in the thrashing assay (Figure S6). Mean ± Standard Deviation. Kruskal-Wallis test with Dunn's multiple comparison post hoc test. **** represents p<0.0001; ** represents p<0.01; * represents p<0.05; and NS means "not significant".

Figure S6

(A) (Top) Fluorescent image of an adult worm expressing endogenously labeled UNC-17::mRuby3 in all cells (P*eft-3*::Flippase). Scale Bar = 50μm. (Bottom) Zoom-in area of the head shows UNC-17 expressed in the nerve ring. DNC = Dorsal Nerve Cord, VNC = Ventral Nerve Cord. Scale Bar = 25μm. **(B)** *unc-17(e245)* mutant animals (3 ± 4.1) thrash significantly less than wild-type animals (94 ± 7.8). UNC-17::mRuby3 FLP-on (*syb7882*) animals that express pan-cellular::Flippase (99 ± 6.6) (*sybIs9614*) or animals that only express pan-cellular::Flippase (95 ± 6.2) are indistinguishable from wild-type animals in their thrashing behavior. UNC-17::mRuby FLP-on animals (100 ± 6.1) thrash significantly more than wild-type animals. Mean ± Standard Deviation. Kruskal-Wallis ANOVA test with Dunn's multiple comparisons post hoc test. **** represents p<0.0001; * represents p<0.05; and NS means "not significant".

1212 **Figure 5 – Probing Monoaminergic transmission in *C. elegans***
1213 **(A)** Predicted CAT-1 protein structure (blue) labeled with GFP11 (red) at C-terminus end (E145).
1214 Complementary GFP1-10 (green) was modeled with bound GFP11. **(B)** Schematic of the
1215 Vesicular Monoamine Transporter (VMAT/*cat-1*) loss-of-function allele and endogenously tagged
1216 versions used to monitor monoaminergic transmission. *cat-1(ok411)* mutant animals have a
1217 deletion that spans exons 7 and 8 (black line) of the *cat-1* gene. For cell-specific labeling, three
1218 copies of GFP11 (*syb7239*) were inserted before the STOP codon. For cell-specific silencing of
1219 *cat-1* activity, two FRT sites (*ky1101 ky1118*) flank the coding sequence of the *cat-1* gene. Upon
1220 recombination, expression of cytosolic mCherry (magenta) is used as a proxy for deletion of the
1221 *cat-1* coding sequence. **(C)** (Top) Fluorescence image of reconstituted CAT-1::GFP11x3 with
1222 expression of complementary GFP1-10 in the whole animal (P*eft-3*::GFP1-10). Scale Bar = 50μm.
1223 (Bottom) Zoom-in of the (Left) head and (Right) vulva area of an adult worm shows CAT-1
1224 expressed in the nerve ring and pharyngeal neurons as well as in the vulva. Scale Bar = 10μm.
1225 **(D)** (Top) A well-fed day-1 adult animal is placed on NGM plates covered with a thin layer of
1226 bacteria, allowed to roam for 16 hours and the number of squares traveled was recorded. (Bottom)
1227 Wild-type animals (43.6 ± 10) roam less than *cat-1(ok411)* mutants (87.5 ± 12). CAT-1::GFP11x3
1228 (*syb7239*) animals with GFP reconstituted (43.3 ± 20) (or not (56.8 ± 14)) roam similar to wild-
1229 type animals. Animals with pan-cellular expression of GFP1-10 (*muIs253*) (53.3 ± 20) also roam
1230 like wild-type animals. **(E)** (Top) A well-fed day-1 adult animal is placed on NGM plates covered
1231 with a thin layer of *E. coli*, allowed to roam for 20 hours and the aversion ratio was calculated.
1232 (Bottom) Wild-type animals (0.12 ± 0.07) display less aversion to *E. coli* lawns than ADF-specific
1233 *cat-1* conditional KO animals (*ky1101 ky1118; syb9159*) (0.4 ± 0.1), consistent with previous
1234 reports using serotonin-depletion mutants (Feng et al., 2025). *cat-1* conditional KO animals that
1235 do not express Flippase in ADF neurons (0.07 ± 0.03) are indistinguishable from wild-type. Mean
1236 ± Standard Deviation. Kruskal-Wallis test with Dunn's multiple comparison post hoc test. ****
1237 represents $p<0.0001$; ** represents $p<0.01$; * represents $p<0.05$; and NS means "not significant".
1238

1239 **Figure 6 – Mapping of co-transmitter neurons in the *C. elegans* nervous system**
1240 **(A)** Schematic of the approach used to find co-expression of two vesicular transporters in the
1241 same cells. Flippase drivers (Element #1, blue) and Flippase-dependent cassettes that result in
1242 fluorescence (Element #2, orange) are used. Magenta cells are seen when both elements are co-
1243 expressed (in green box). **(B)** Strategy to track the co-expression of the vesicular glutamate and
1244 acetylcholine transporter in combination with the 4 most common neurotransmitters in *C. elegans*:

1245 Acetylcholine, GABA, Serotonin and Dopamine. “Elements #1” or “Element #2” refers to the
1246 genetic elements in the schematic in Fig 6A. **(C-D)** Specific example of the genetic strategy
1247 outlined in Fig 6A, for the vesicular transporters of glutamate (EAT-4) and acetylcholine (UNC-
1248 17). **(C)** We repurposed the *eat-4* conditional KO strain (*kySi76 kySi77*) (Figure 1B) (Lopez-Cruz
1249 et al., 2019) in which the *eat-4* gene coding sequence is flanked by two FRT sites and followed
1250 by cytosolic mCherry (Element #1). We crossed this line with a strain that has an endogenously
1251 inserted self-cleaving peptide sequence (T2A) followed by Flippase before the STOP codon in
1252 the *unc-17* gene locus (Table 1). **(D)** (Top) Co-expression of EAT-4 and UNC-17 results in
1253 cytosolic mCherry. (Bottom) Cytosolic mCherry was detected in the head of three neurons: (i)
1254 AFDR, AFDL and M5; and in two neurons in the tail region: (ii) PVN, and DVA. **(E)** Fluorescence
1255 microscopy shows neurons with co-expression of **(E)** VGLUT/EAT-4 and VGAT/UNC-47; **(F)**
1256 VGLUT/EAT-4 and dopamine synthesis gene DAT-1; **(G)** VAChT/UNC-17 and VGAT/UNC-47;
1257 and **(H)** VAChT/UNC-17 and the serotonin synthesis gene TPH-1. All scale bars = 10μm.
1258
1259 **Figure S7**
1260 **(A)** To track glutamate-involved co-transmission, we repurposed the *eat-4* conditional KO strain
1261 (*kySi76 kySi77*) (Lopez-Cruz et al., 2019) where the *eat-4* gene coding sequence is flanked by
1262 two FRT sites and followed by cytosolic mCherry (Element #2, orange box). Crossing this line
1263 with a panel of flippase drivers (Element #1, blue box) results in activation of cytosolic mCherry
1264 only in cells were both elements were co-expressed (Readout, green box). P*dat-1*::Flippase and
1265 P*tph-1*::Flippase driver strains were made available from (Muñoz-Jiménez et al., 2017). **(B)** To
1266 track acetylcholine-involved co-transmission, we repurposed the unc-17::GFP conditional KI
1267 strain (*ola503*) (Figure 3B) for which, after the *unc-17* gene coding sequence, there are FRT sites
1268 flanking the STOP codon and 3’ UT, followed by GFP (Element #2, orange box). Crossing this
1269 line with a panel of flippase drivers (Element #1, blue box) results in the protein fusion of UNC-17
1270 with GFP in cells where both elements were co-expressed (Readout, green box). **(C-D)**
1271 Systematic mapping shows neurons with co-transmission of **(C)** glutamate in combination with
1272 acetylcholine, GABA, and dopamine. **(D)** Co-transmission of acetylcholine is found in combination
1273 with GABA and serotonin.
1274
1275 **Figure S8**
1276 Live-imaging of co-expression strategy of the *eat-4* conditional knockout strain (*kySi76 kySi77*)
1277 with **(A)** endogenous P*unc-47*::UNC-47::T2A::Flippase and **(B)** P*dat-1*:: Flippase driver. Live-
1278 imaging of co-expression strategy of the *unc-17* conditional GFP knock-in strain (*kySi76 kySi77*)

1279 with **(C)** P*tph-1*:: Flippase driver, and with **(D)** endogenous P*unc-47*::UNC-47::T2A::Flippase.
1280 (Top) DIC images. (Bottom) Fluorescence imaging. All scale bars = 10μm.
1281
1282 **Figure S9**
1283 Our results (bold) are consistent and extend findings from previous studies in the field (See Table
1284 3 and numbered references below). Here, we present an atlas of co-transmission in the *C.*
1285 *elegans* nervous system. Co-transmitter neurons are present in the (i) head, mid-body region and
1286 (ii) tail of the animal.
1287 *Note that I2L, M4 and SDQR express UNC-47/VGAT but do not stain positive for GABA staining
1288 (Gendrel et al., 2016) nor express genes required for GABA synthesis or uptake.
1289 [1] Jafari et al. (2011), Serrano-Saiz et al. (2013), and Wang et al. (2024)
1290 [2] Serrano-Saiz et al. (2013), and Wang et al. (2024)
1291 [3] Reilly et al. (2022), and Wang et al. (2024)
1292 [4] Jafari et al. (2011), and Wang et al. (2024)
1293 [5] Alkema et al. (2005), Serrano-Saiz et al. (2013), and Wang et al. (2024)
1294
1295 **Figure 7 – Visualizing the distribution of cholinergic and serotonergic vesicles in ADF**
1296 **neurons.**
1297 **(A)** Dual-labeling of the endogenous acetylcholine (UNC-17, magenta) and serotonin (CAT-1,
1298 green) vesicular transporters in ADF neurons. **(B)** UNC-17::mRuby and CAT-1::GFP overlap
1299 along the ADF axon. White arrowheads denote overlap of both signals. **(B')** UNC-17::mRuby and
1300 CAT-1::GFP intensity profile. **(C)** Example of UNC-17::mRuby and CAT-1::GFP when they
1301 partially do not overlap along the ADF axon, green arrowheads point to CAT-1-only puncta. **(C')**
1302 UNC-17::mRuby and CAT-1::GFP intensity profile. Scale bar = 10μm. **(D-D')** Endogenous UNC-
1303 17::mRuby and CAT-1:::GFP are absent from the axon of *unc-104* mutant animals. Line scan of
1304 axon **(D)** and fluorescent images **(D')**. **(E)** Schematic of the dual-labeling of endogenous CAT-
1305 1::GFP or UNC-17::GFP with endogenous active zone protein UNC-13::mScarlet along the ADF
1306 axon. **(F)** Live imaging of the ADF axon reveals UNC-13::mScarlet puncta that lack CAT-1::GFP.
1307 Scale bar = 10 μm. **(F'- F'')** Zoom-in region of E. White arrowheads show overlapping vesicular
1308 transporter tagged (green) with the active zone protein UNC-13 (magenta) in individual puncta.
1309 Magenta arrowhead points to UNC-13::mScarlet puncta that do not overlap with CAT-1::GFP. **(G)**
1310 Live imaging of the ADF axon reveals UNC-13::mScarlet puncta that lack UNC-17::GFP. Scale
1311 bar = 10 μm. **(G'- G'')** Zoom-in region of F. White arrowheads show overlapping vesicular
1312 transporter tagged (green) with the active zone protein UNC-13 (magenta) in individual puncta.

1313 Magenta arrowhead points to UNC-13::mScarlet puncta that do not overlap with CAT-1::GFP.
1314 Scale Bar = 2 μm. **(H)** AiryScan imaging of dual-labeled UNC-17::mRuby and CAT-1::GFP along
1315 the ADF axon show localization in the same synaptic bouton but with distinct enrichment areas.
1316 Green arrowhead head points to CAT-1 enrichment and magenta arrowhead points to UNC-17
1317 enrichment. Scale Bar = 2 μm**.**
1318
1319 **Figure S10**
1320 **(A)** Schematic of genes required for serotonergic identity. Mammalian (bold) and *C. elegans*
1321 (italics) homologue genes are listed. Detectable expression of **(A')** *tph-1,* **(A'')** *bas-1* and **(A''')**
1322 *mod-5* in ADF neuron (blue). Scale Bar = 5 μm**.**
1323 **(B)** Schematic of genes required for cholinergic identity. Mammalian (bold) and *C. elegans* (italics)
1324 homologue genes are listed. Detectable expression of **(B')** *cho-1* in ADF neuron (blue). Scale Bar
1325 = 10 μm**.**
1326 **(C)** Presynaptic densities (green) on ADF axons as determined by serial electron microscopy
1327 reconstructions (White et al., 1986) (image generated with NeuroSC (Koonce et al., 2025). **(C')**
1328 3D rendering of live fluorescence imaging of endogenous UNC-17::GFP and **(C'')** CAT-1::GFP
1329 specifically in ADF neurons. Scale bar = 10 μm**.**
1330
1331 **Table 1 – List of alleles for neurotransmitter examination in vivo**
1332 **Table 2 – List of potential co-transmitter neurons by neuronal type**
1333 **Table 3 – List of potential co-transmitter neurons reported by at least more than one study**
1334 **Table 4 – List of neurons inconsistent across studies to suggest co-transmission capacity**
1335 **Table 5 – List of all molecular locations tested for labeling each synaptic vesicle**
1336 **transporter**

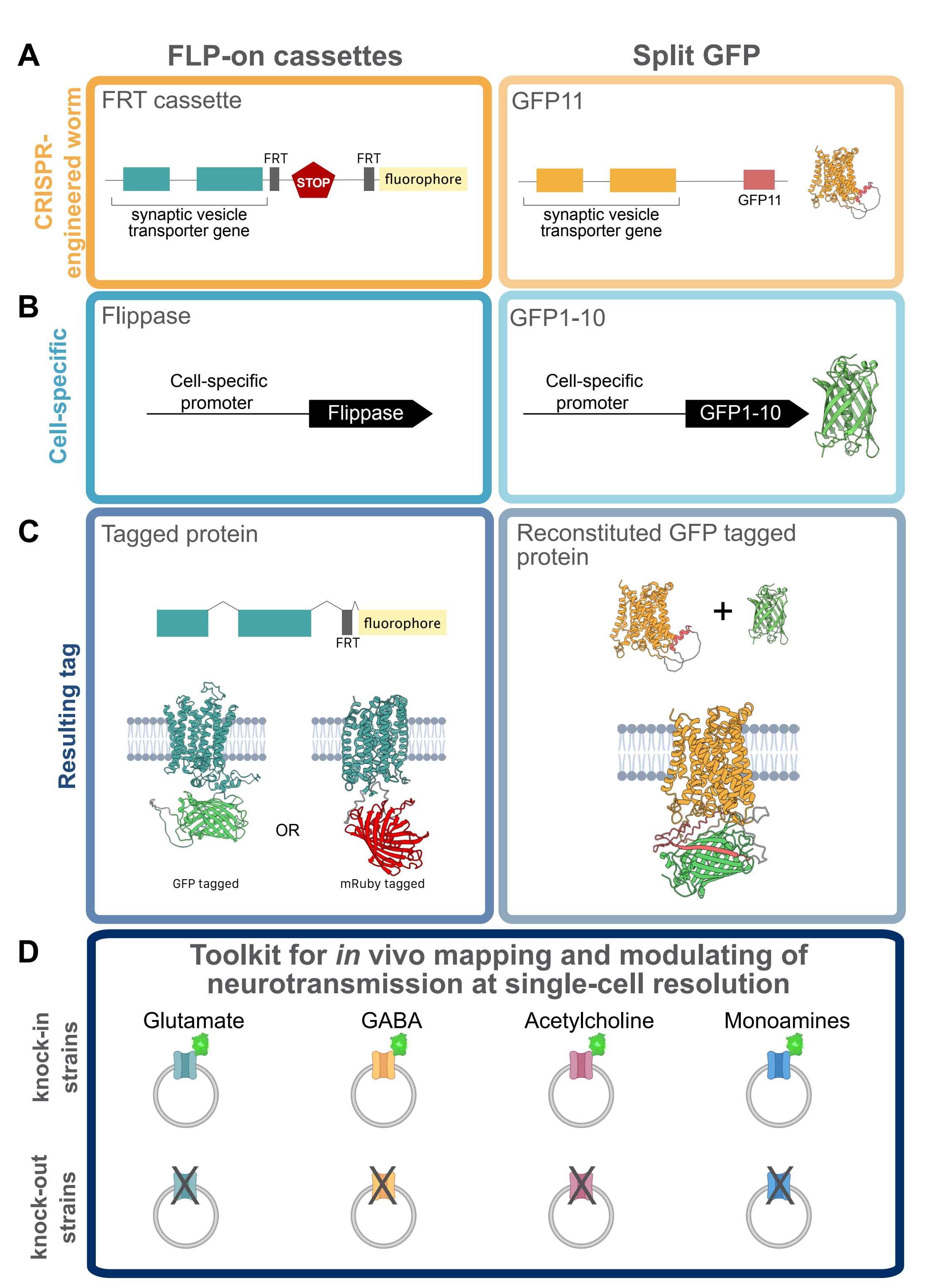
A
FLP-on cassettes
Split GFP
CRISPR-engineered worm
FRT cassette
FRT
STOP
FRT
fluorophore
synaptic vesicle transporter gene
GFP11
synaptic vesicle transporter gene
GFP11
B
Cell-specific
Flippase
Cell-specific promoter
Flippase
GFP1-10
Cell-specific promoter
GFP1-10
C
Resulting tag
Tagged protein
fluorophore
FRT
OR
GFP tagged
mRuby tagged
Reconstituted GFP tagged protein
+
D
Toolkit for in vivo mapping and modulating of neurotransmission at single-cell resolution
knock-in strains
knock-out strains
Glutamate
GABA
Acetylcholine
Monoamines

Figure 2

A Tagged Vesicular Glutamate Transporter/EAT-4

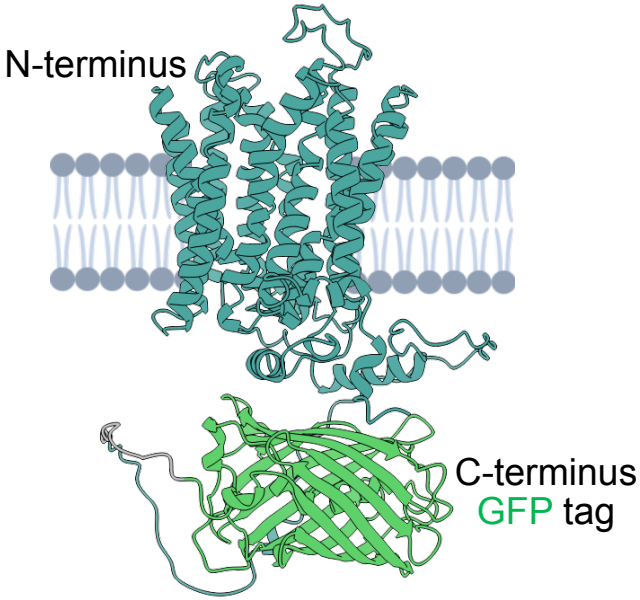

B Resources for the study of glutamatergic transmission

Tool	Allele	Sequence representation	Reference
eat-4 loss of function	*ky5*		Mori et al. (1993)
eat-4::GFP FLP-on knock in	*syb8568*	FRT STOP FRT	This study
eat-4::mRuby FLP-on knock in	*syb9193*	FRT STOP FRT	This study
FRT-flanked *eat-4*	*kySi76* *kySi77*	FRT STOP FRT	Lopez-Cruz (2019)

C Chemotaxis Assay

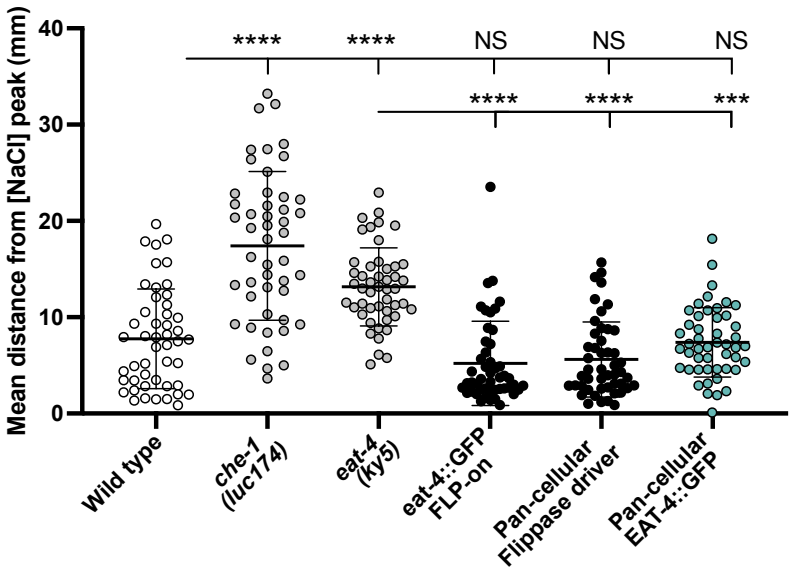

D EAT-4::GFP FLP-on (*syb8568*) + Pan-cellular::Flippase (*sybIs9614*)

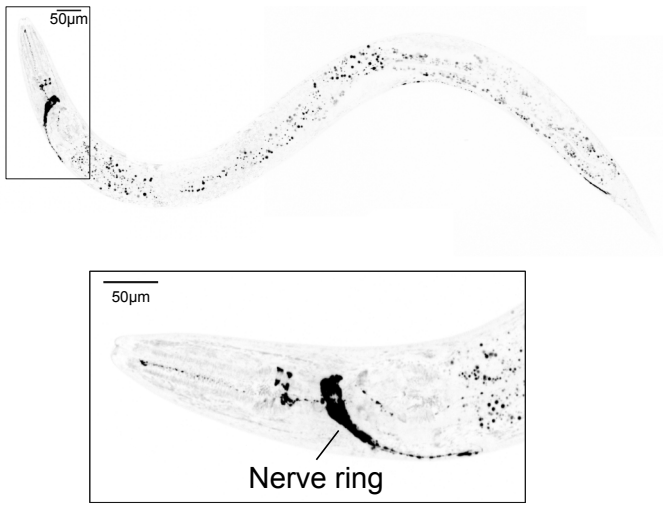

E ASE-specific Flippase

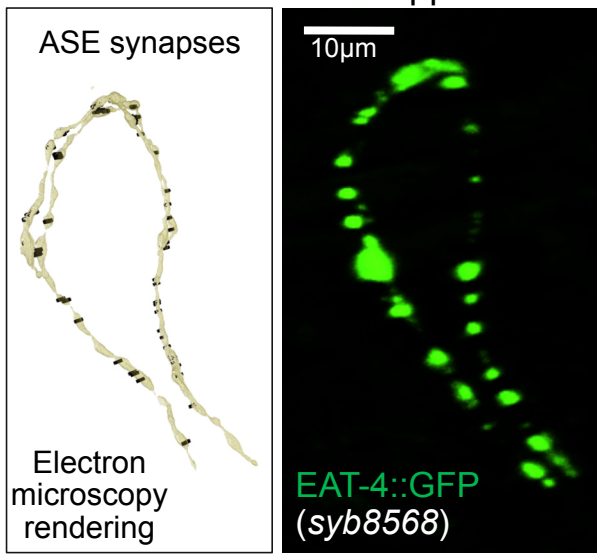

Figure S1

A Vesicular Glutamate Transporter conservation

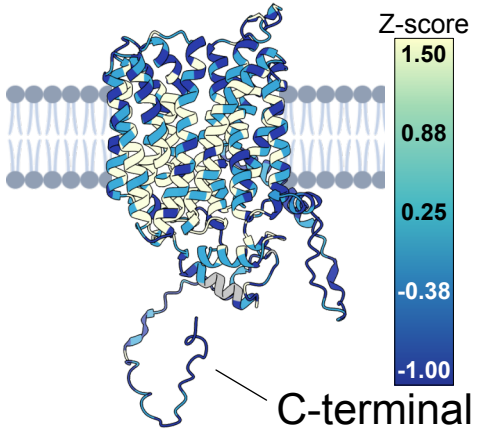

B Vesicular Glutamate Transporter C-terminus sequence

Tag insertion site ▼

```
C. elegans     549  ------------APGTNP[ 5]---------   DEHGSSGVVENPHYQQW---  576
M. musculus    534  PPAPPPSYGATHSTVQPP    RPPPPVRDY   --------------------  560
H. sapiens     534  PPAPPPSYGATHSTFQPP    RPPPPVRDY   --------------------  560
D. rerio       541  LATRQKTYGTTDNSSGRK    QGWKKKRGV[4]EDDHESNHYENGEYQTQyq-  590
D. melanogaster 571 --STAISYGATGHVANNP[13]DAPPTYGDV[4]QYGYTQGQMPSYDPQGYqqq  632
```

C Chemotaxis Assay set up

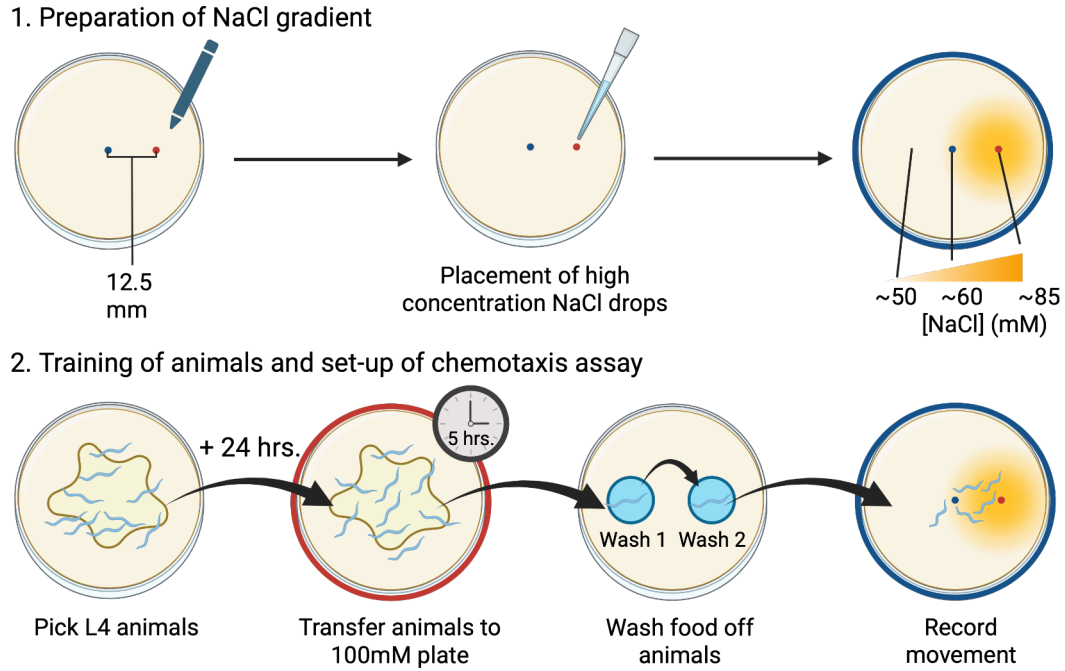

D Chemotaxis Assay Controls

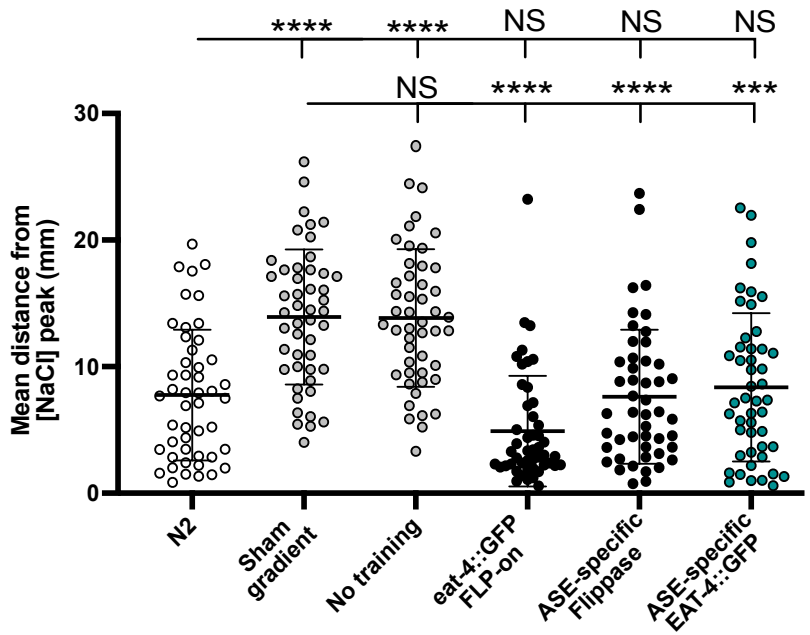

Figure S2

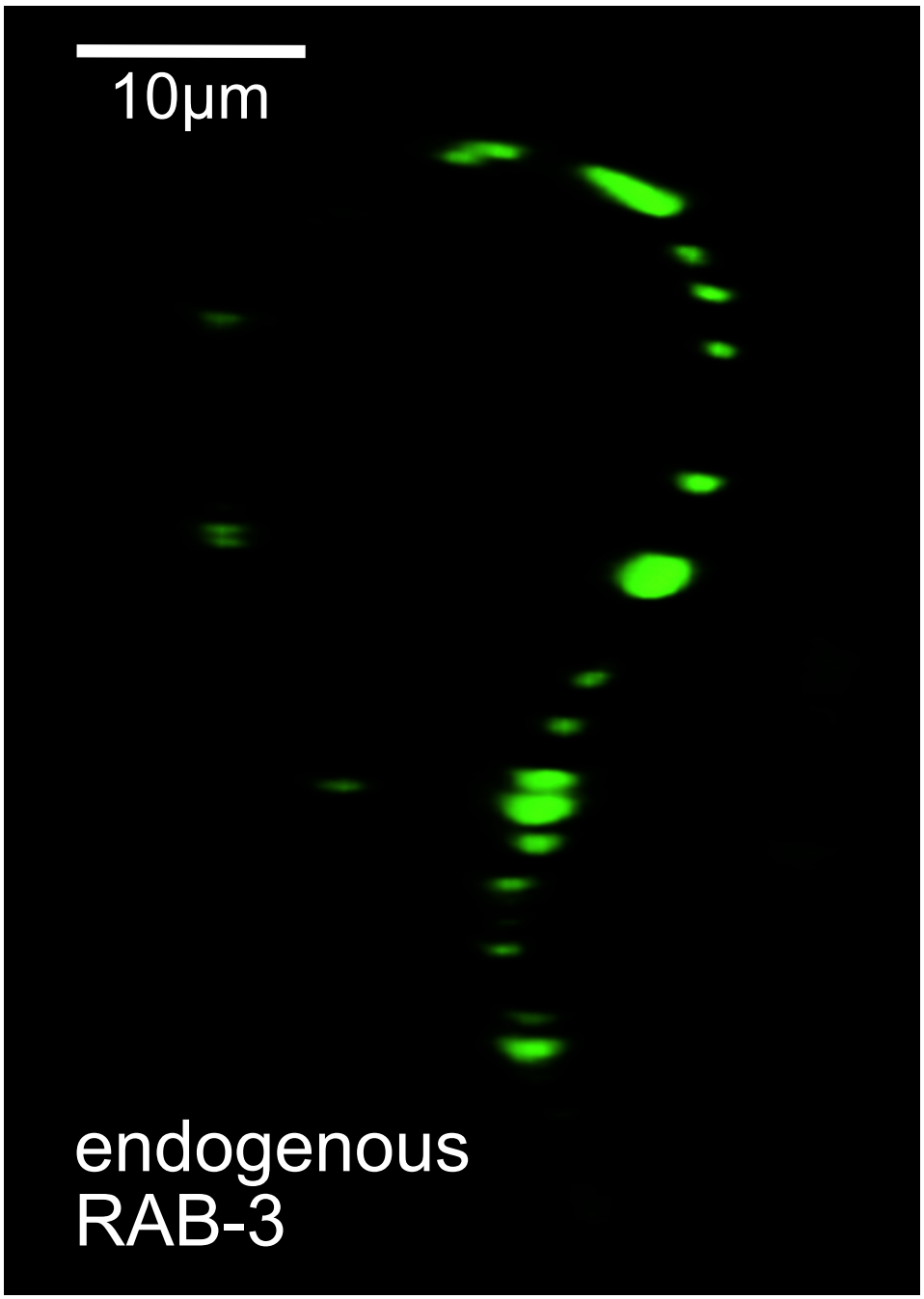

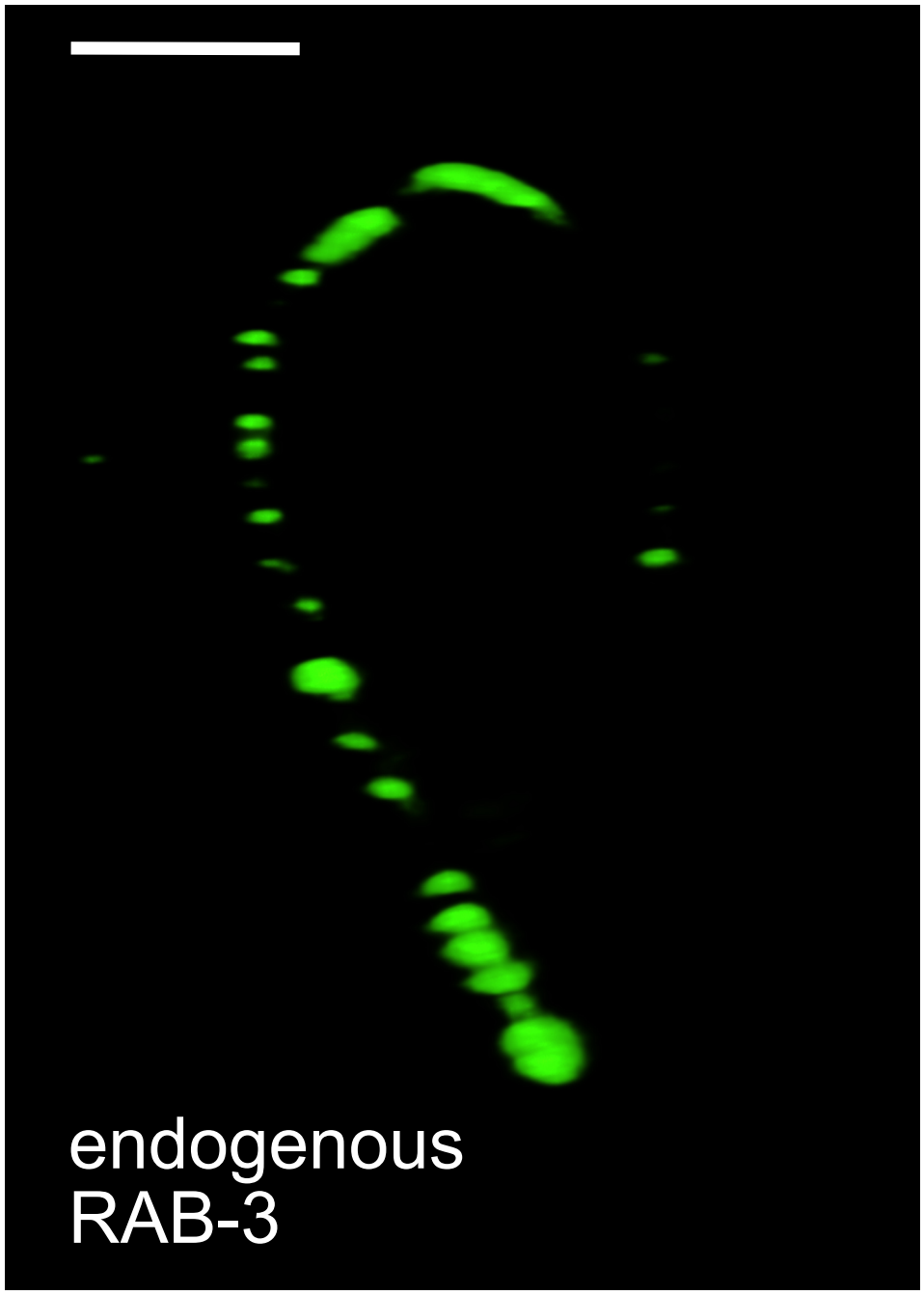

Figure 3

A

Tagged Vesicular GABA Transporter/UNC-47

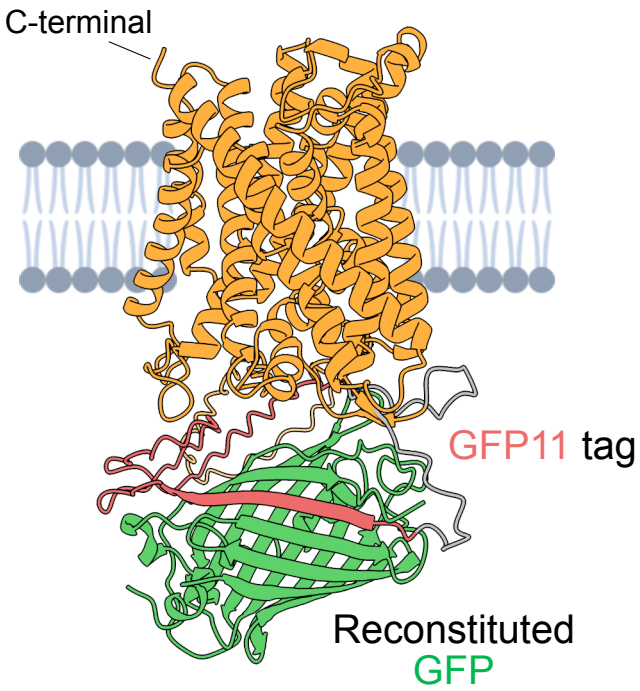

B

Resources for the study of GABAergic transmission

Tool	Allele	Sequence representation	Reference
unc-47 loss of function	*e307*	Splicing acceptor mutant	Brenner (1974)
unc-47::GFP full-body knock in	*syb6990*		This study
unc-47::mKate full-body knock in	*syb7358*		This study
unc-47::GFP11 cell-specific labeling	*syb7313*		This study
unc-47::GFP11x3 cell-specific labeling	*syb7849*		This study
FRT-flanked *unc-25*	*syb5949* *syb6275*	FRT STOP FRT	This study

C

UNC-47::GFP11x3 (*syb7849*) + Pan-cellular::GFP1-10 (*muIs253*)

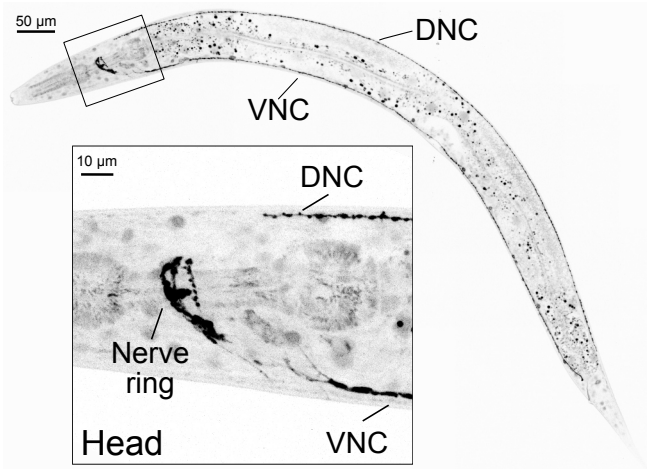

D

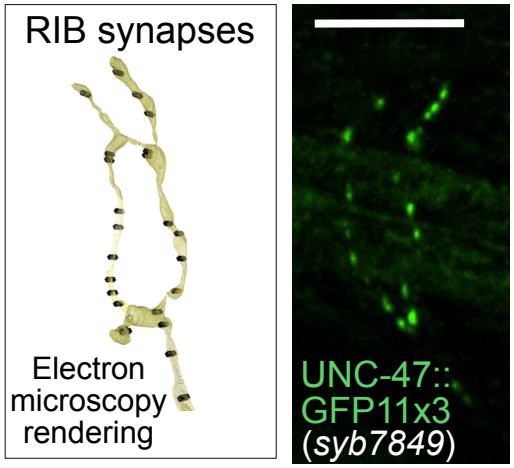

E

Thrashing Assay

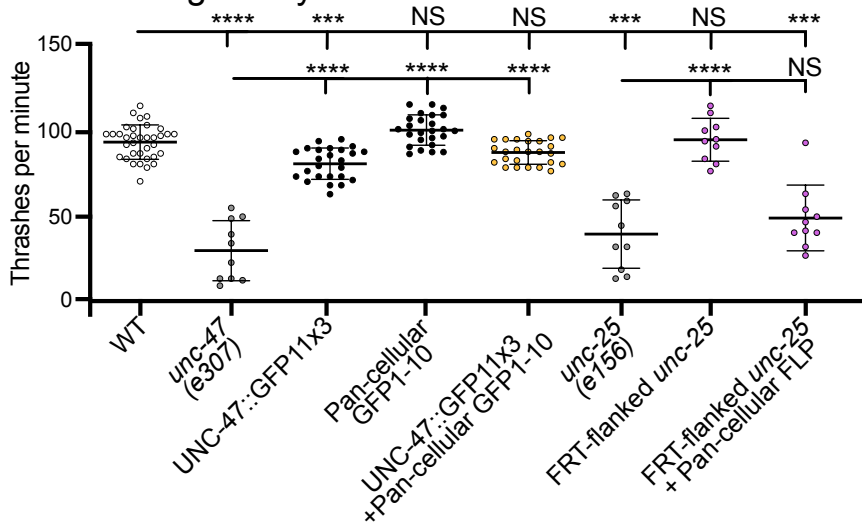

Figure S3

A Vesicular GABA Transporter conservation

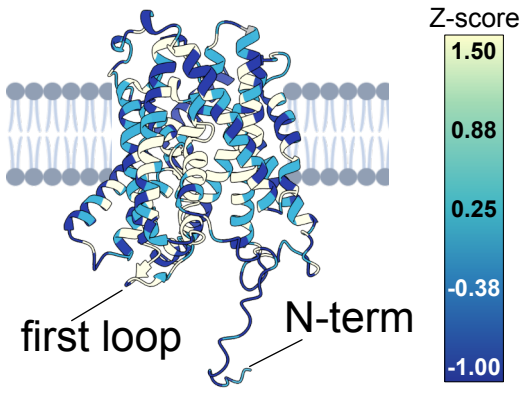

B Vesicular GABA Transporter sequence

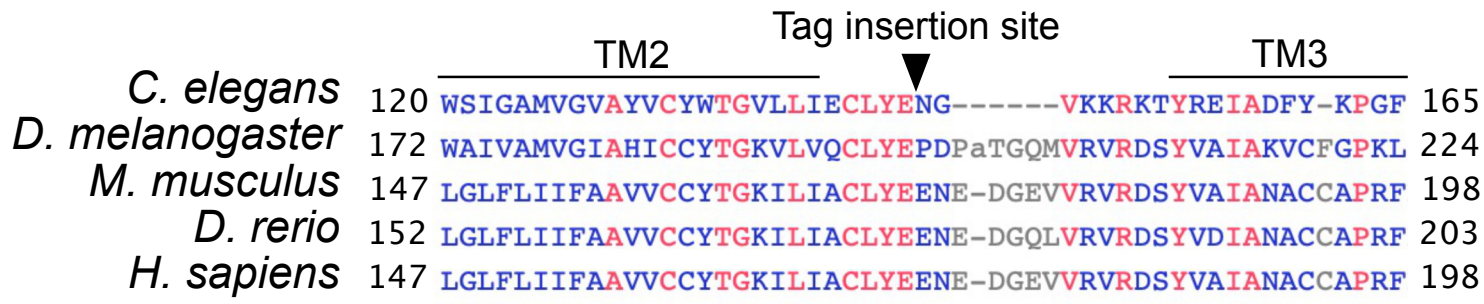

C Thrashing assay

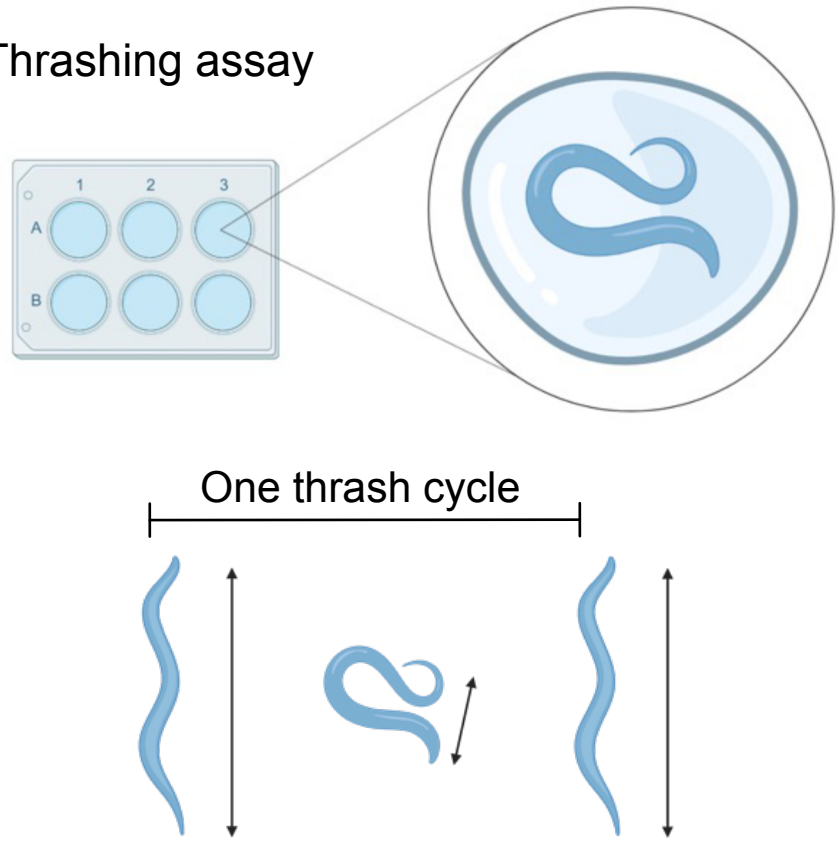

D

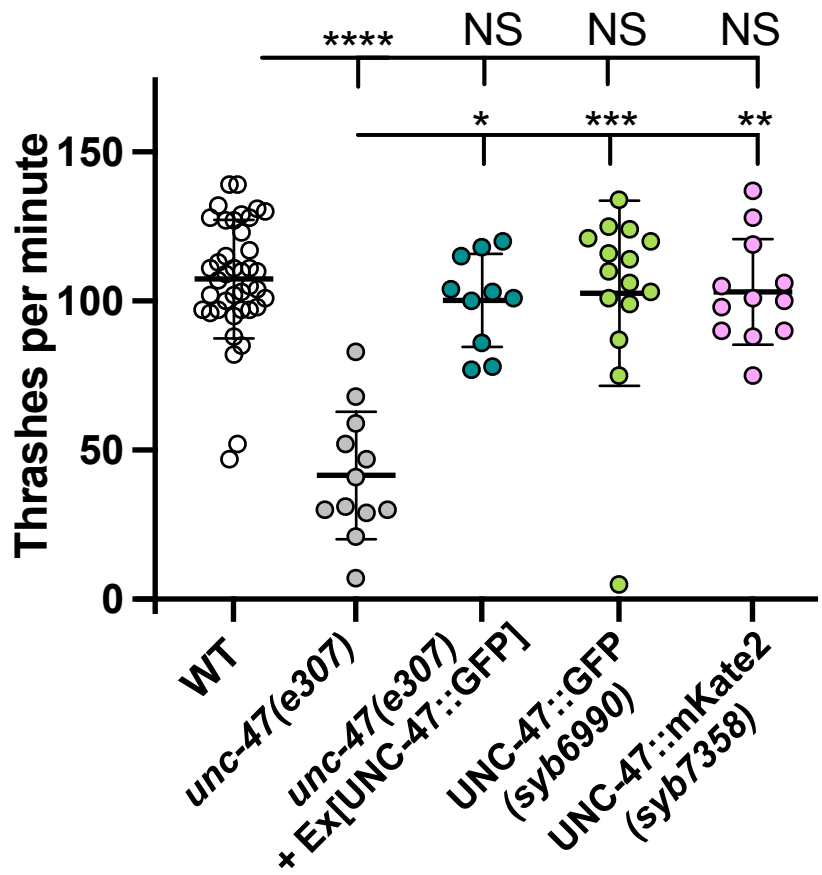

E

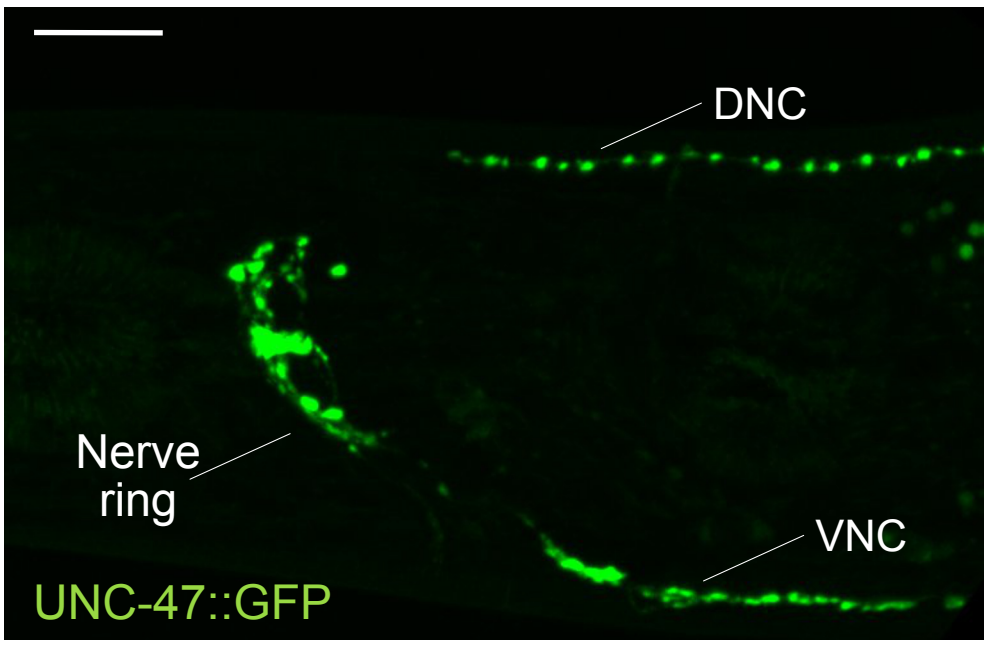

F

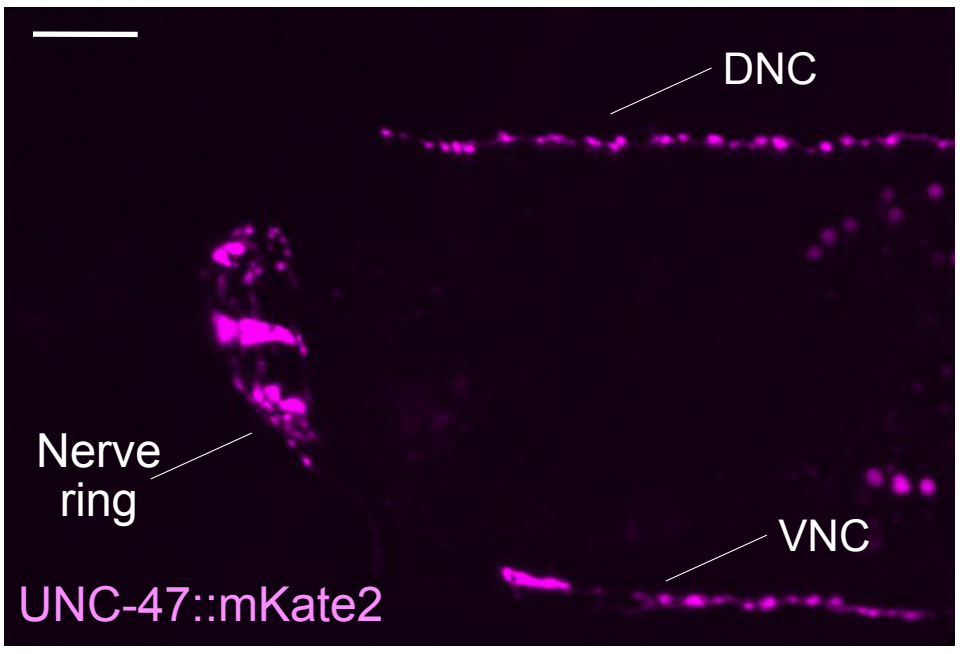

Figure S4

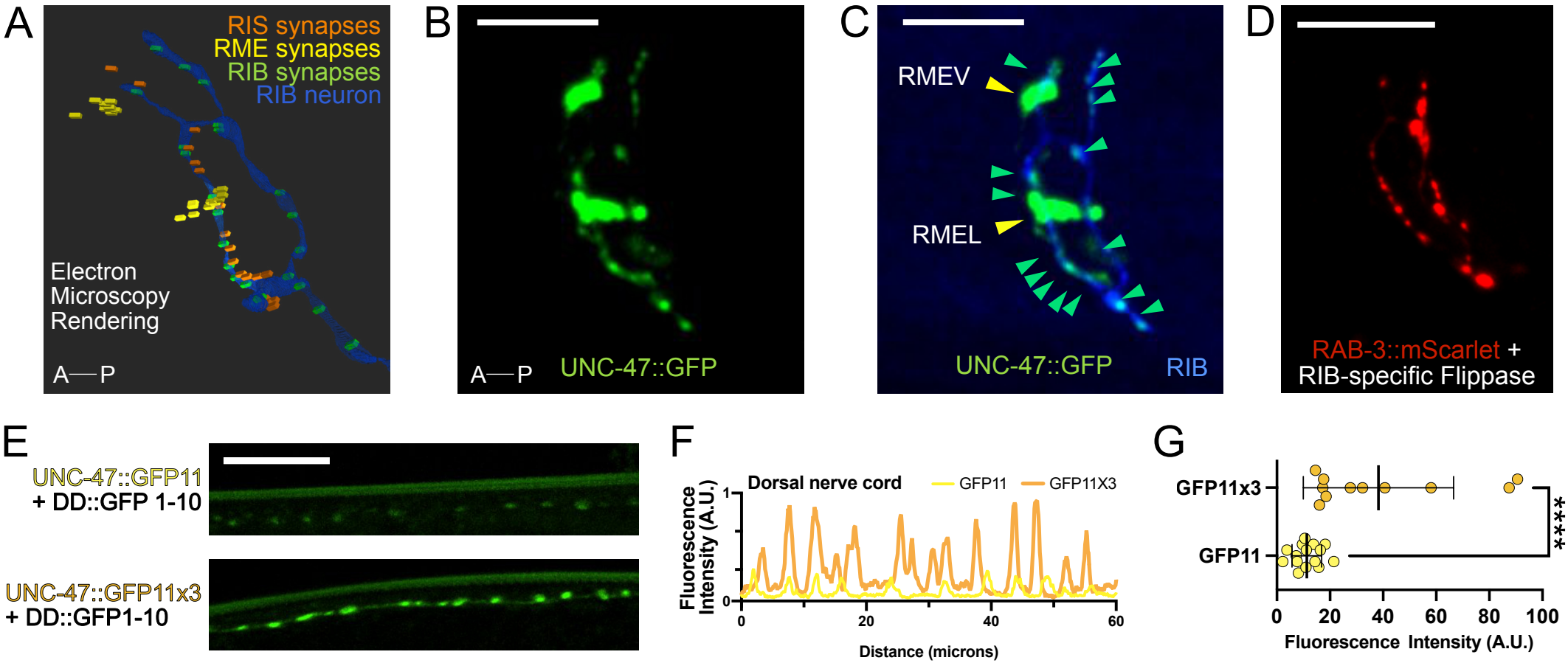
A
RIS synapses
RME synapses
RIB synapses
RIB neuron
Electron
Microscopy
Rendering
A—P
B
A—P
UNC-47::GFP
C
RMEV
RMEL
UNC-47::GFP
RIB
D
RAB-3::mScarlet +
RIB-specific Flippase
E
UNC-47::GFP11
+ DD::GFP 1-10
UNC-47::GFP11x3
+ DD::GFP1-10
F
Dorsal nerve cord
GFP11
GFP11X3
Fluorescence Intensity (A.U.)
1
0
0
20
40
60
Distance (microns)
G
GFP11x3
GFP11
****
0
20
40
60
80
100
Fluorescence Intensity (A.U.)

Figure 4

A Tagged Vesicular Acetylcholine Transporter/UNC-47

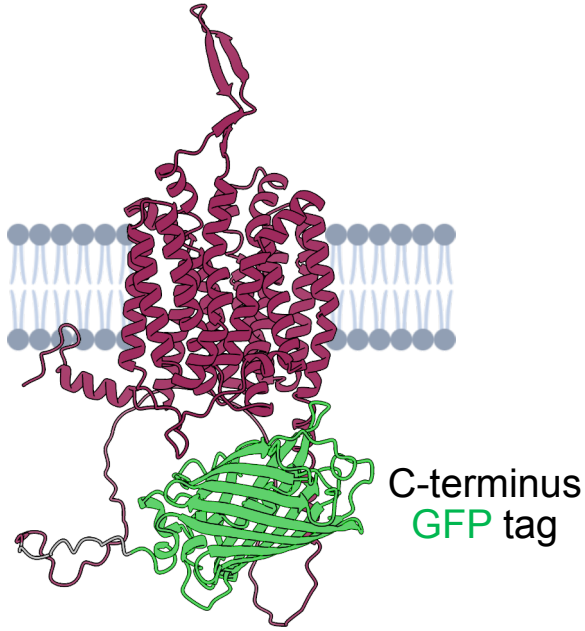

B Resources for the study of cholinergic transmission

Tool	Allele	Sequence representation	Reference
unc-17 loss of function	*e245*	G347R	Brenner (1974)
unc-17::mKate full-body knock in	*ot907*		Pereira et al. (2019)
GFP::*unc-17* FLP-on knock in	*syb7251*	SL2, FRT, FRT	This study
unc-17::GFP FLP-on knock in	*ola503*	FRT, STOP, FRT	This study
unc-17::mRuby FLP-on knock in	*syb7882*	FRT, STOP, FRT	This study
LoxP-flanked *unc-17*	*syb5779* *syb5987*	LoxP, LoxP	Huang et al. (2023)

C Thrashing Assay

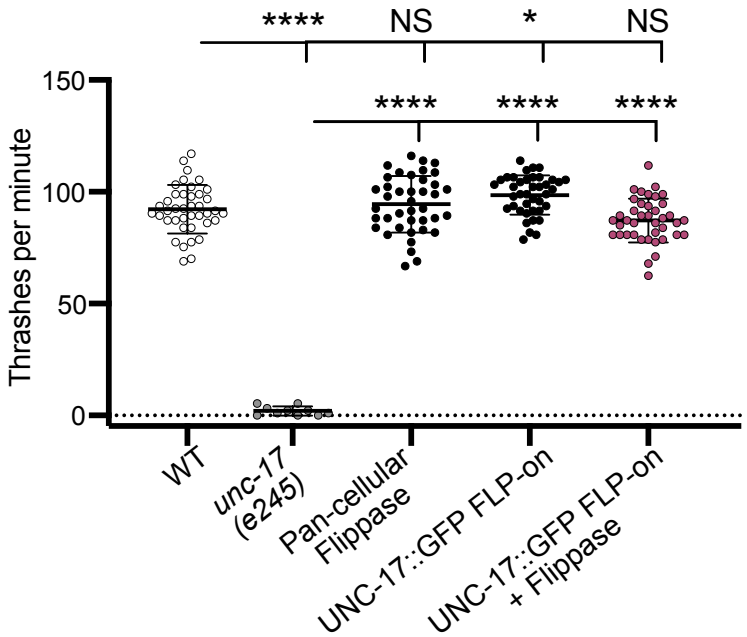

D UNC-17::GFP FLP-on (*ola503*) + Pan-cellular::Flippase (*sybIs9614*)

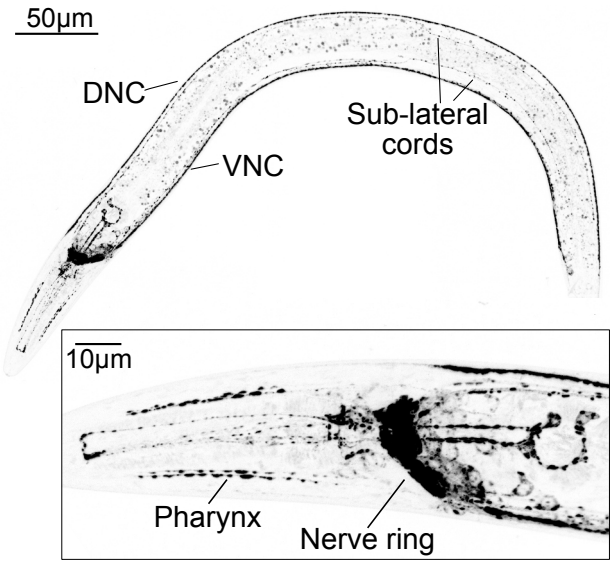

E ADF-specific Flippase

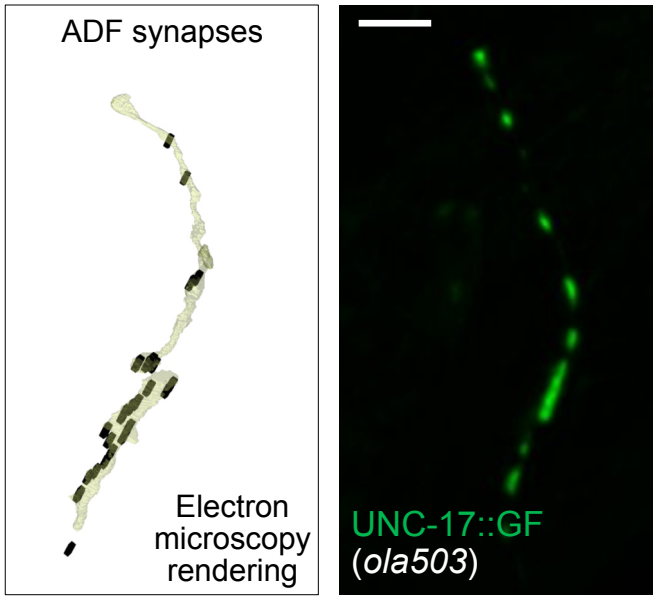

Figure S5

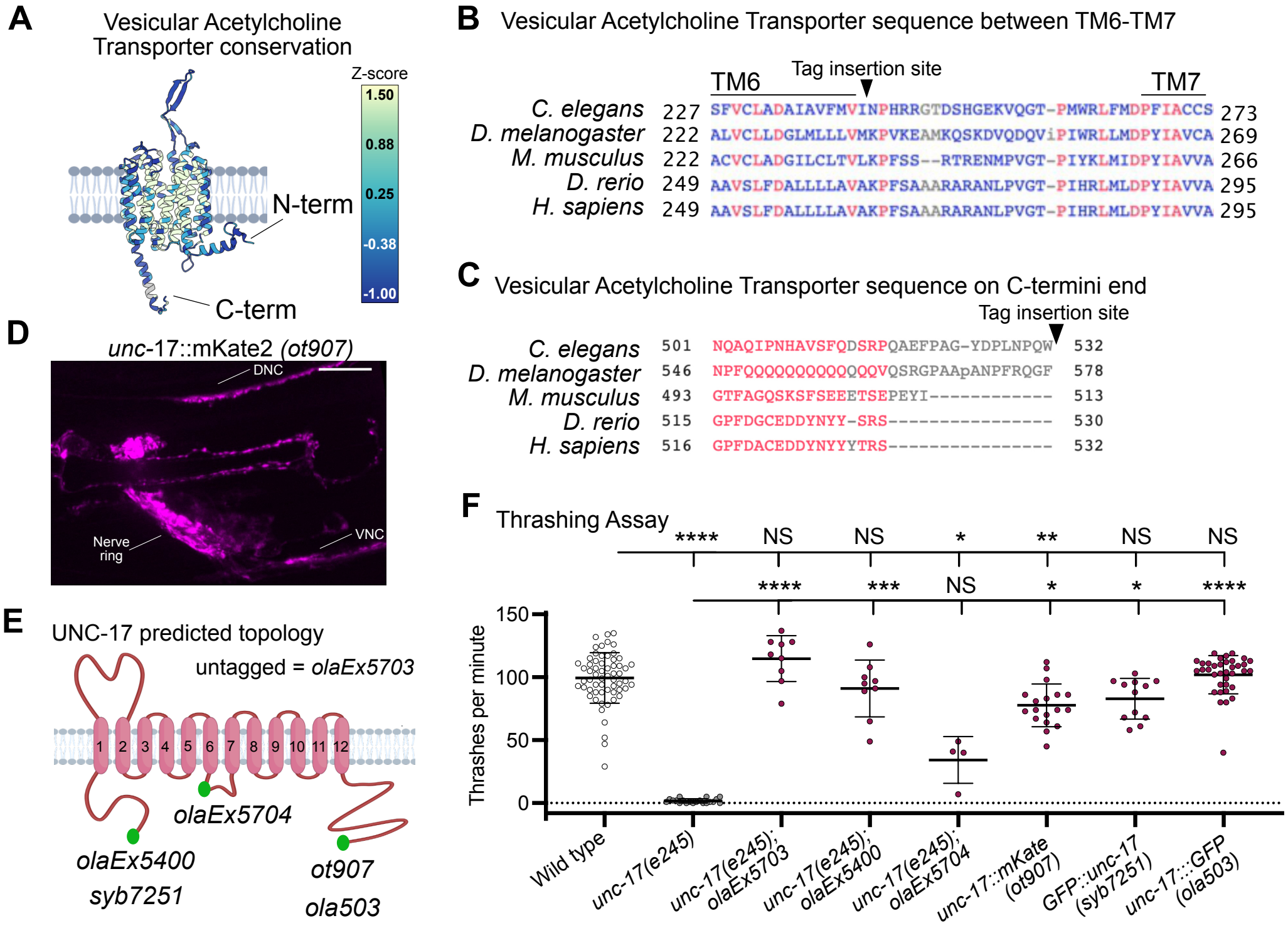

A
Vesicular Acetylcholine Transporter conservation
Z-score
1.50
0.88
0.25
-0.38
-1.00
N-term
C-term
B
Vesicular Acetylcholine Transporter sequence between TM6-TM7
Tag insertion site
TM6
TM7
C. elegans 227 SFVCLADAIAVFMVINPHRRGTDSHGEKVQGT-PMWRLFMDPFIACCS 273
D. melanogaster 222 ALVCLLDGLMLLLVMKPVKEAMKQSKDVQDQViPIWRLLMDPYIAVCA 269
M. musculus 222 ACVCLADGILCLTVLKPFSS--RTRENMPVGT-PIYKLMIDPYIAVVA 266
D. rerio 249 AAVSLFDALLLLAVAKPFSAAARARANLPVGT-PIHRLMLDPYIAVVA 295
H. sapiens 249 AAVSLFDALLLLAVAKPFSAAARARANLPVGT-PIHRLMLDPYIAVVA 295
C
Vesicular Acetylcholine Transporter sequence on C-termini end
Tag insertion site
C. elegans 501 NQAQIPNHAVSFQDSRPQAEFPAG-YDPLNPQW 532
D. melanogaster 546 NPFQQQQQQQQQQQQVQSRGPAApANPFRQGF 578
M. musculus 493 GTFAGQSKSFSEEETSEPEYI---------- 513
D. rerio 515 GPFDGCEDDYNYY-SRS---------- 530
H. sapiens 516 GPFDACEDDYNYYYTRS---------- 532
D
unc-17::mKate2 (ot907)
DNC
Nerve ring
VNC
E
UNC-17 predicted topology
untagged = olaEx5703
1 2 3 4 5 6 7 8 9 10 11 12
olaEx5704
olaEx5400
syb7251
ot907
ola503
F
Thrashing Assay
**** NS NS * ** NS NS
**** *** NS * * ****
Thrashes per minute
150
100
50
0
Wild type
unc-17(e245)
unc-17(e245); olaEx5703
unc-17(e245); olaEx5400
unc-17(e245); olaEx5704
unc-17::mKate (ot907)
GFP::unc-17 (syb7251)
unc-17:::GFP (ola503)

Figure S6

A. UNC-17::mRuby3 (*syb7882*) + Pan-cellular::Flippase (*sybIs9614*)

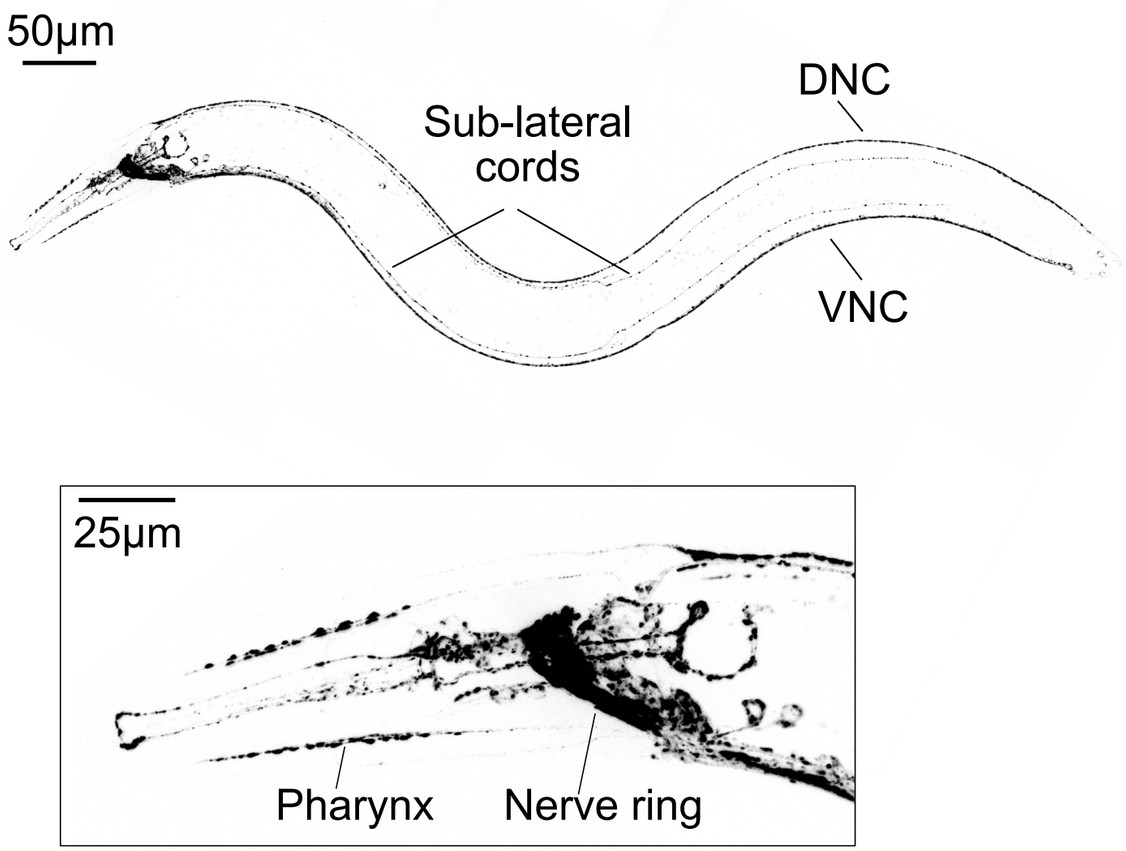

B. Thrashing Assay

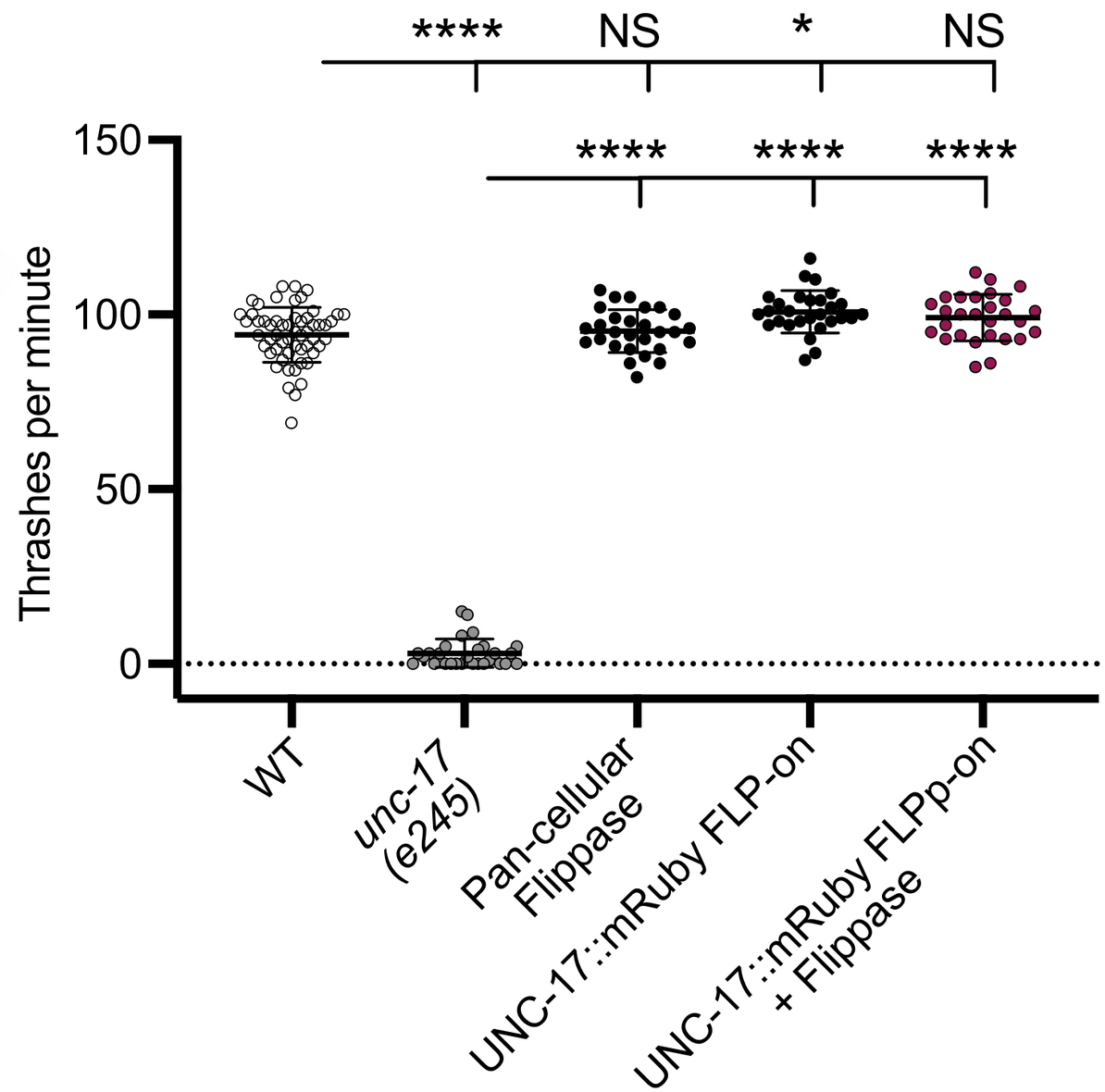

Figure 5

A Tagged Vesicular Monoamine Transporter/CAT-1

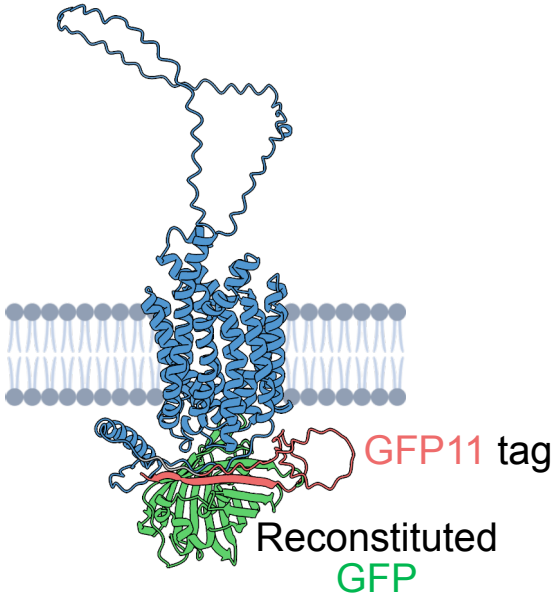

B Resources for the study of monoaminergic transmission

Tool	Allele	Sequence representation	Reference
cat-1 gene	*ok411*		Hukema et al. 2008
cat-1::GFP11x3 knock in	*syb7239*		Huang et al. 2023
FRT-flanked *cat-1*	*ky1101* *ky1118*	FRT STOP FRT	This study

C CAT-1::GFP11x3 (*syb7239*) + Pan-cellular::GFP1-10 (*muIs253*)

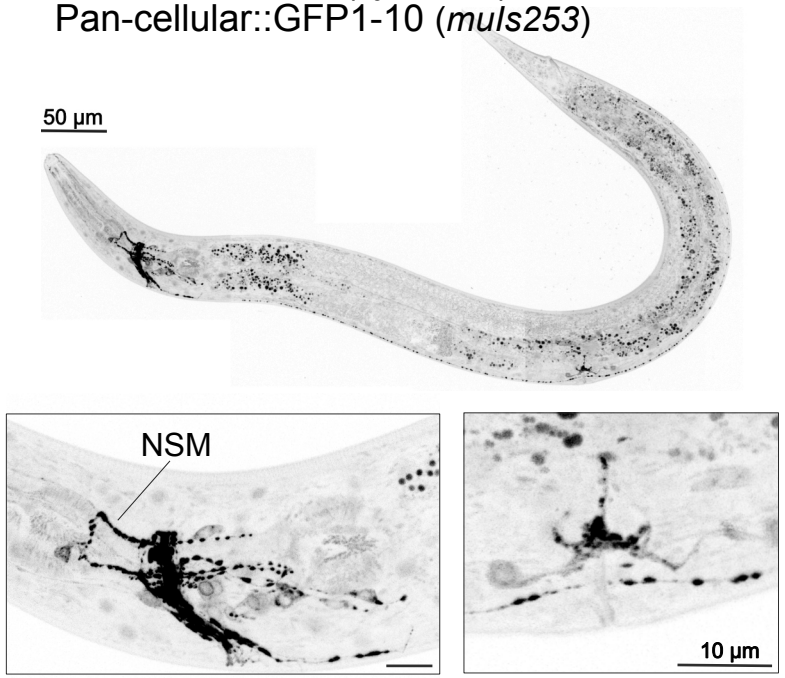

D On-food exploration assay

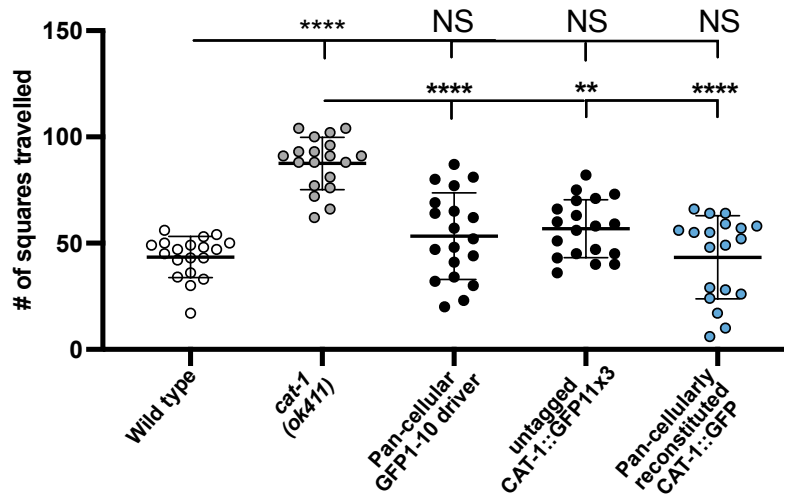

E Aversion assay

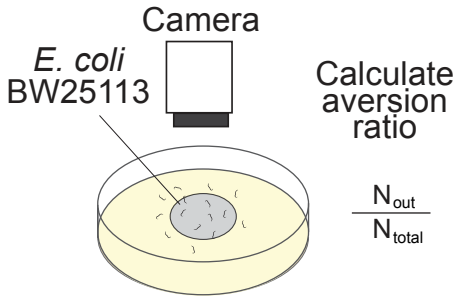

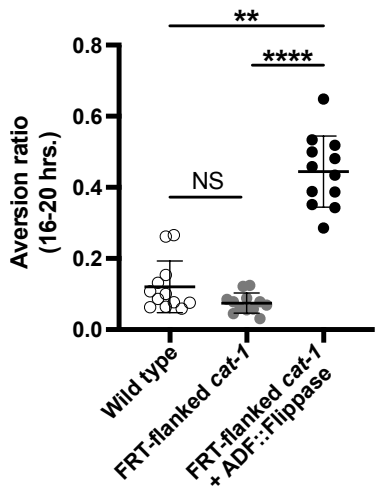

Figure 6

A

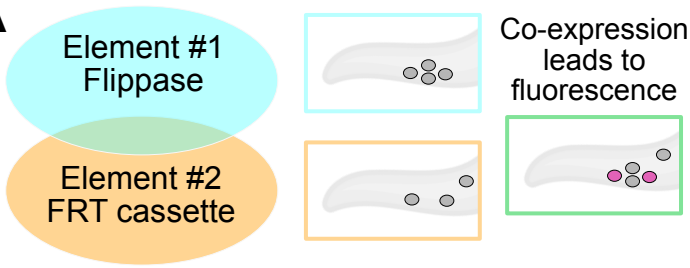

B

Element #2	Element #1: Acetylcholine *unc-17*	Element #1: GABA *unc-47*	Element #1: Serotonin *tph-1*	Element #1: Dopamine *dat-1*
Glutamate *eat-4*	X	X	X	X
Acetylcholine *unc-17*		X	X	X

C *eat-4*-based co-transmission

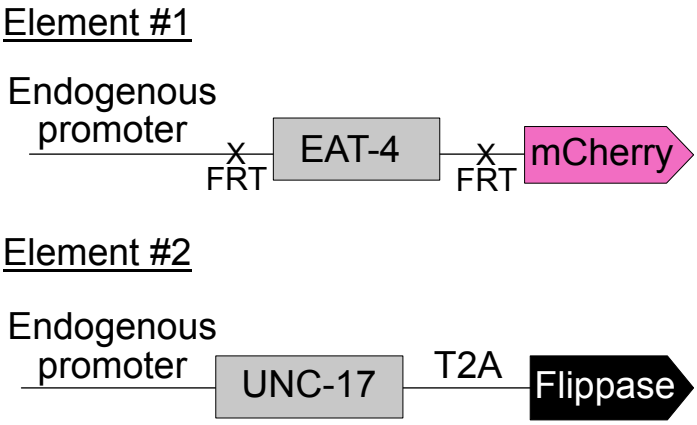

D Readout:

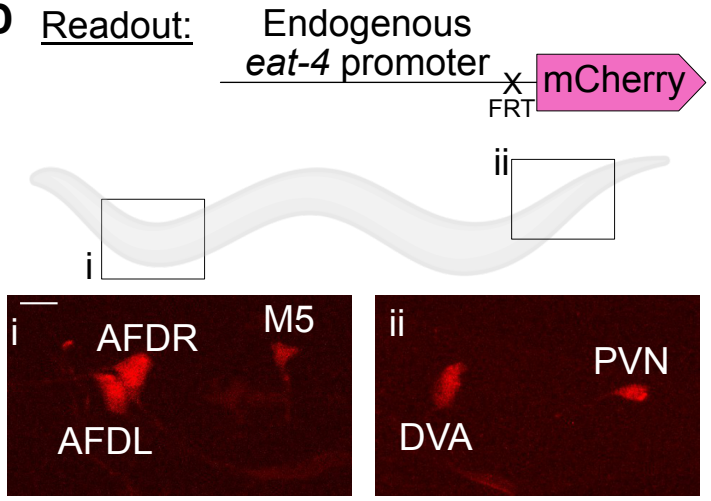

E *eat-4* FLP-on + P*unc-47*::Flippase

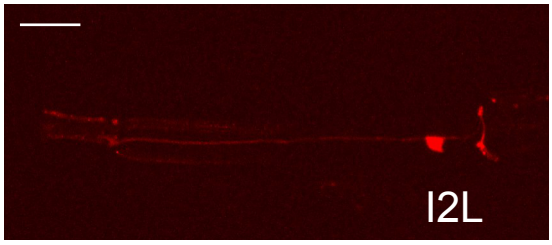

G *unc-17* FLP-on + P*unc-47*::Flippase

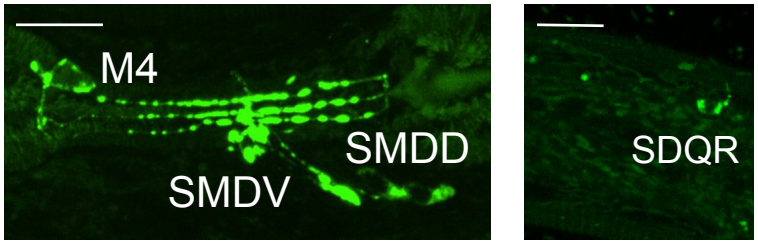

F *eat-4* FLP-on + P*dat-1*::Flippase

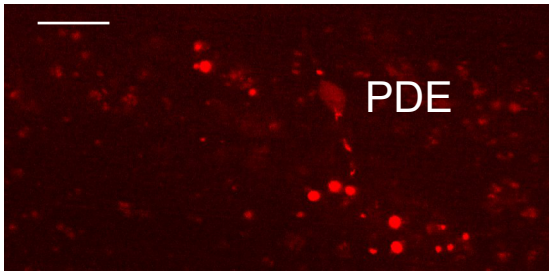

H *unc-17* FLP-on + P*tph-1*::Flippase

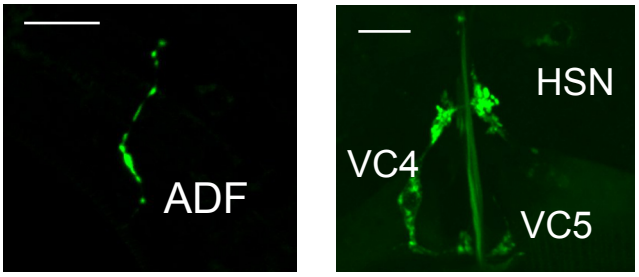

Figure S7

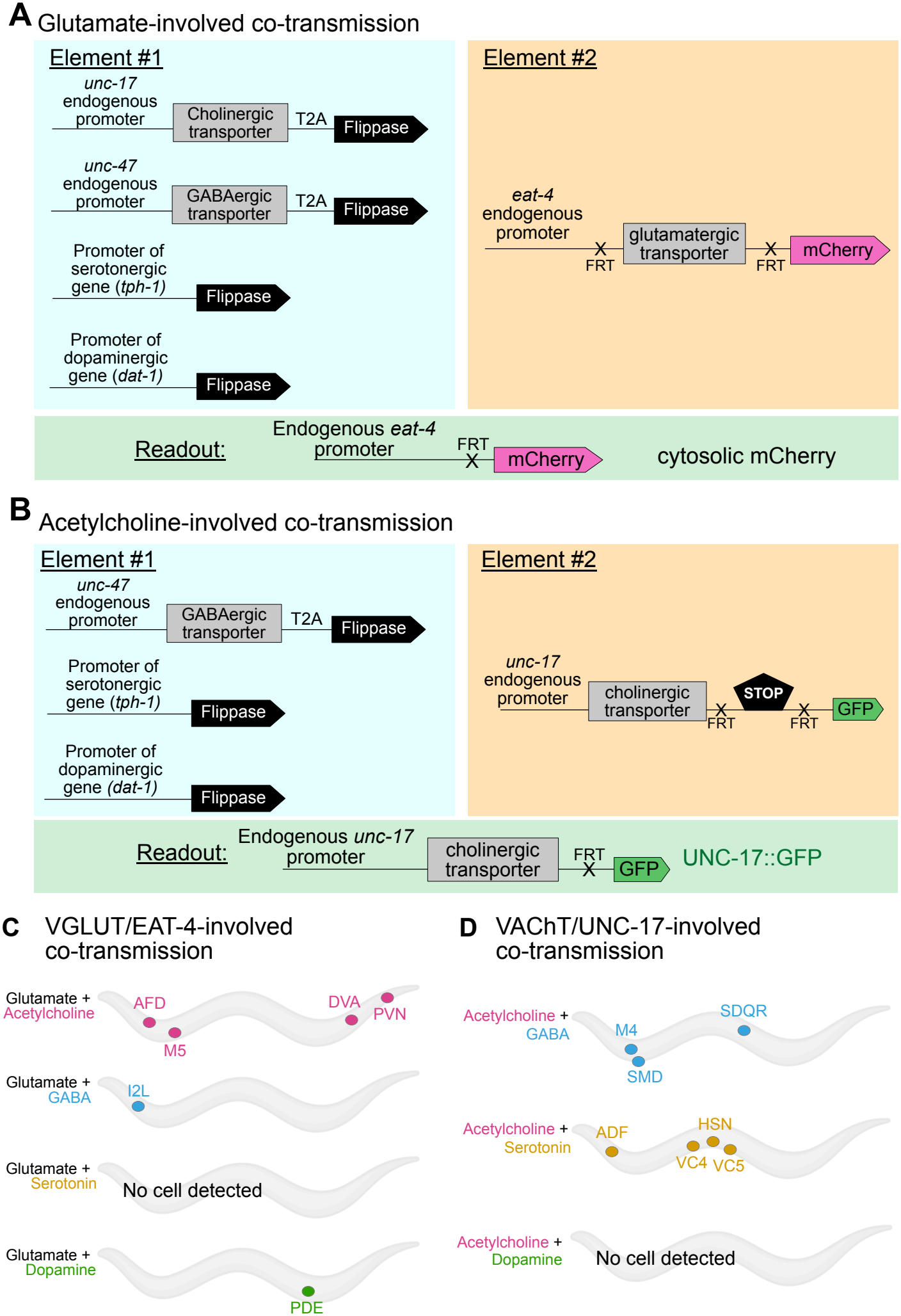
A Glutamate-involved co-transmission
Element #1
unc-17 endogenous promoter
Cholinergic transporter
T2A
Flippase
unc-47 endogenous promoter
GABAergic transporter
T2A
Flippase
Promoter of serotonergic gene (tph-1)
Flippase
Promoter of dopaminergic gene (dat-1)
Flippase
Element #2
eat-4 endogenous promoter
FRT
glutamatergic transporter
FRT
mCherry
Readout:
Endogenous eat-4 promoter
FRT
mCherry
cytosolic mCherry
B Acetylcholine-involved co-transmission
Element #1
unc-47 endogenous promoter
GABAergic transporter
T2A
Flippase
Promoter of serotonergic gene (tph-1)
Flippase
Promoter of dopaminergic gene (dat-1)
Flippase
Element #2
unc-17 endogenous promoter
cholinergic transporter
STOP
FRT
FRT
GFP
Readout:
Endogenous unc-17 promoter
cholinergic transporter
FRT
GFP
UNC-17::GFP
C VGLUT/EAT-4-involved co-transmission
Glutamate + Acetylcholine
AFD
M5
DVA
PVN
Glutamate + GABA
I2L
Glutamate + Serotonin
No cell detected
Glutamate + Dopamine
PDE
D VAChT/UNC-17-involved co-transmission
Acetylcholine + GABA
M4
SMD
SDQR
Acetylcholine + Serotonin
ADF
HSN
VC4
VC5
Acetylcholine + Dopamine
No cell detected

Figure S8

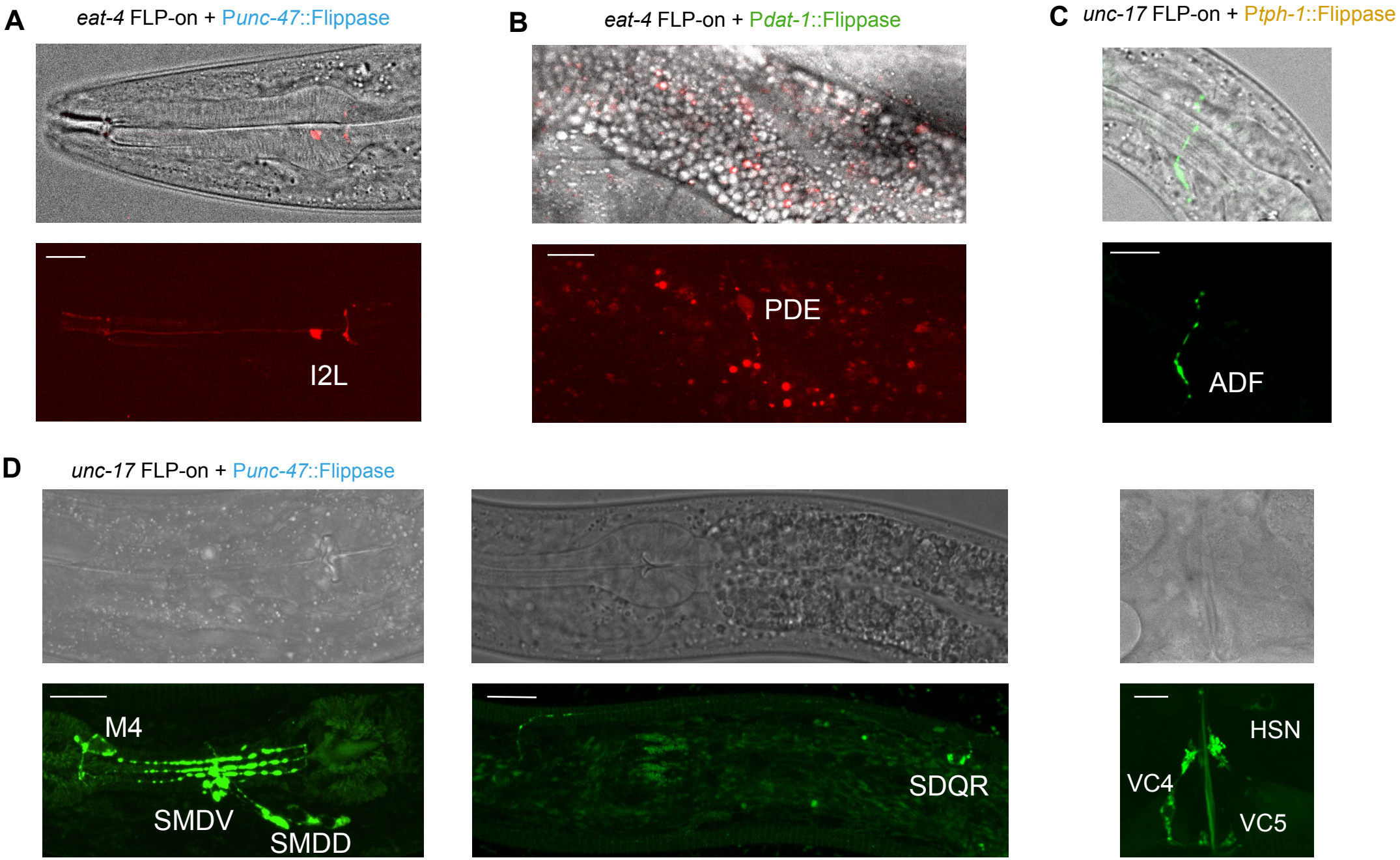
A
eat-4 FLP-on + Punc-47::Flippase
I2L
B
eat-4 FLP-on + Pdat-1::Flippase
PDE
C
unc-17 FLP-on + Ptph-1::Flippase
ADF
D
unc-17 FLP-on + Punc-47::Flippase
M4
SMDV
SMDD
SDQR
HSN
VC4
VC5

Figure S9

Co-transmission atlas of the *C. elegans* nervous system

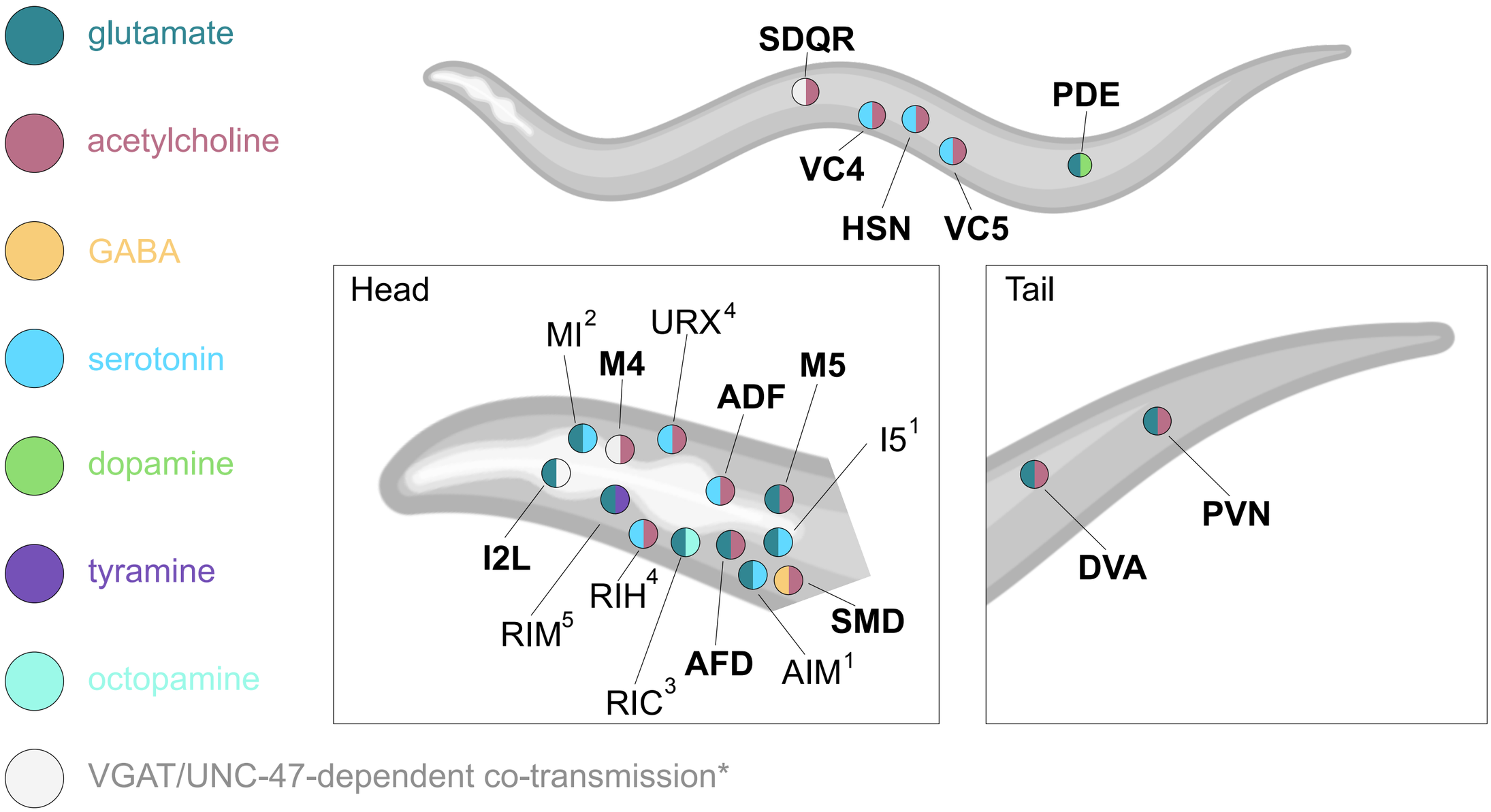

Figure 7

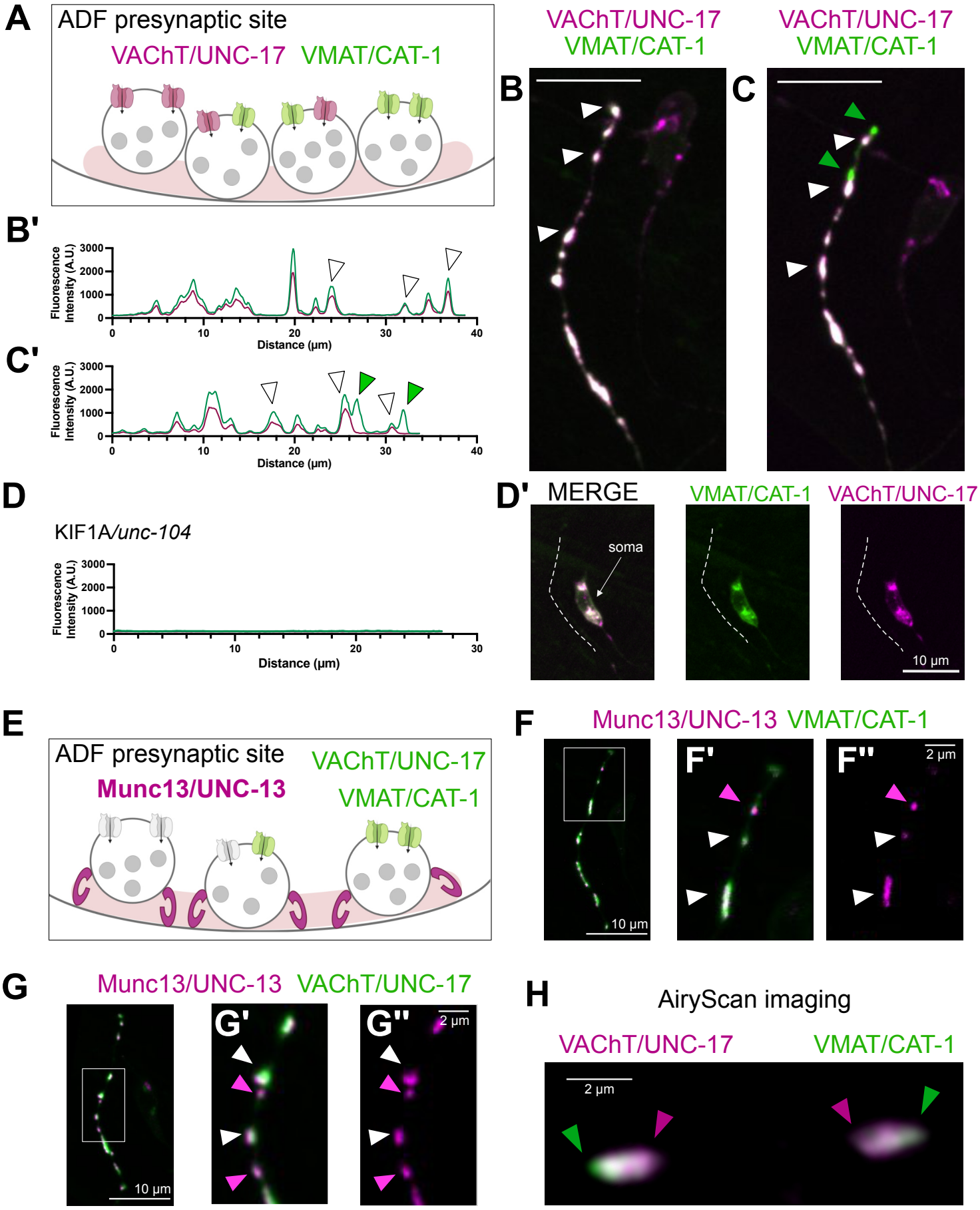
A
ADF presynaptic site
VAChT/UNC-17 VMAT/CAT-1
B'
Fluorescence Intensity (A.U.)
Distance (µm)
C'
Fluorescence Intensity (A.U.)
Distance (µm)
VAChT/UNC-17
VMAT/CAT-1
B
C
D
KIF1A/unc-104
Fluorescence Intensity (A.U.)
Distance (µm)
D'
MERGE
VMAT/CAT-1
VAChT/UNC-17
soma
10 µm
E
ADF presynaptic site
Munc13/UNC-13
VAChT/UNC-17
VMAT/CAT-1
F
Munc13/UNC-13 VMAT/CAT-1
F'
F''
2 µm
10 µm
G
Munc13/UNC-13 VAChT/UNC-17
G'
G''
2 µm
10 µm
H
AiryScan imaging
VAChT/UNC-17
VMAT/CAT-1
2 µm

Figure S10

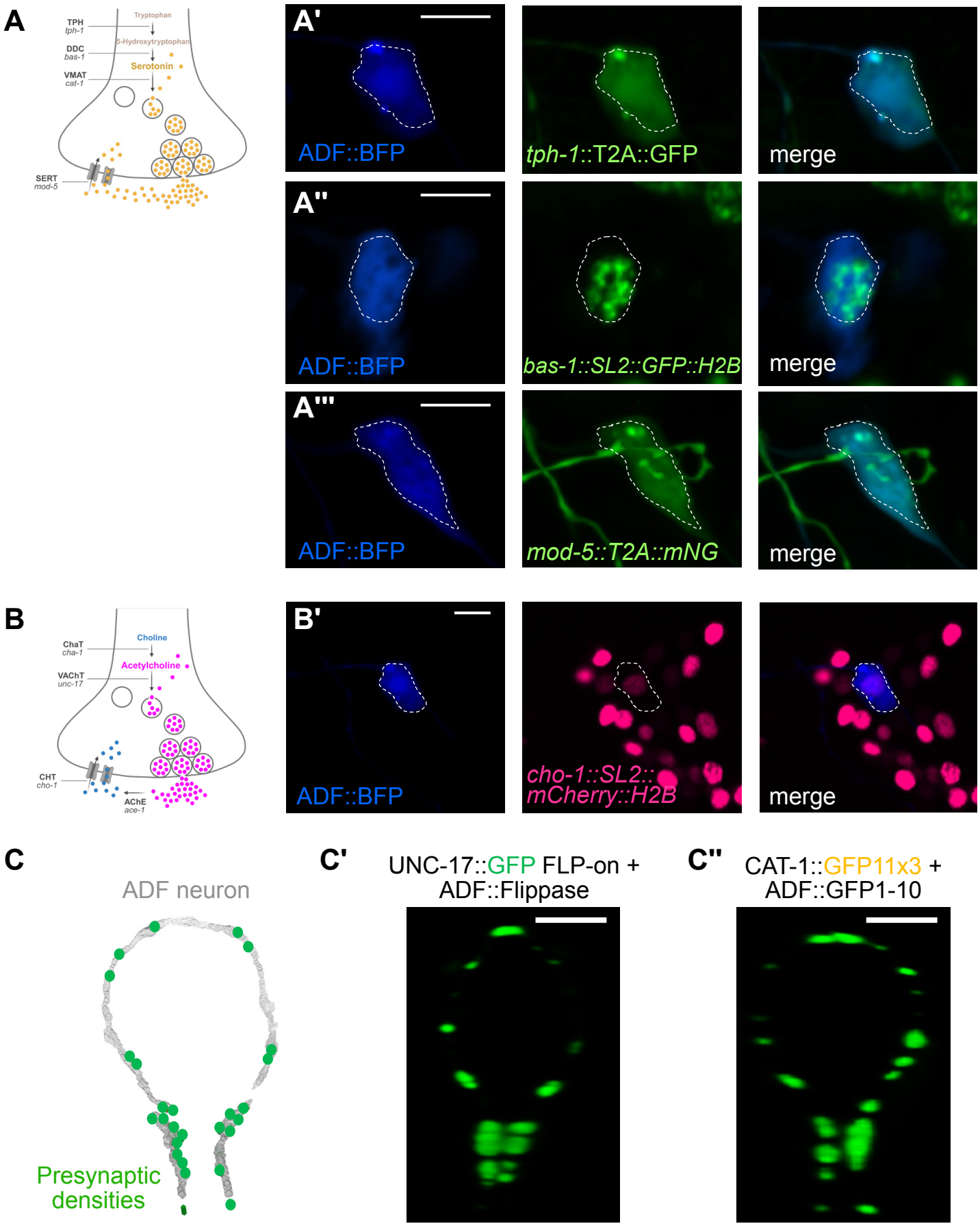
A
TPH
tph-1
Tryptophan
5-Hydroxytryptophan
DDC
bas-1
Serotonin
VMAT
cat-1
SERT
mod-5
A'
ADF::BFP
tph-1::T2A::GFP
merge
A''
ADF::BFP
bas-1::SL2::GFP::H2B
merge
A'''
ADF::BFP
mod-5::T2A::mNG
merge
B
ChaT
cha-1
Choline
Acetylcholine
VAChT
unc-17
CHT
cho-1
AChE
ace-1
B'
ADF::BFP
cho-1::SL2::
mCherry::H2B
merge
C
ADF neuron
Presynaptic
densities
C'
UNC-17::GFP FLP-on +
ADF::Flippase
C''
CAT-1::GFP11x3 +
ADF::GFP1-10